To the Graduate Council:

I am submitting herewith a thesis written by Martha A. Jones entitled "Processing and Characterization of Poly(ester-amide)s and Poly(ester-amide) Copolymer Monofilaments." I have examined the final copy of this thesis for form and content and recommend that it be accepted in partial fulfillment of the requirements for the degree of Master of Science, with a major in Polymer Engineering.

J. E. Spruiell, Major Professor

We have read this thesis
and recommend its acceptance:

Edward S. Clark

Roberta Benson

Accepted for the Council:

Associate Vice Chancellor
and Dean of the Graduate School

STATEMENT OF PERMISSION TO USE

In presenting this thesis in partial fulfillment of the requirements for a Master's degree at The University of Tennessee, Knoxville, I agree that the Library shall make it available to borrowers under rules of the Library. Brief quotations from this thesis are allowable without special permission, provided that accurate acknowledgment of the source is made.

Permission for extensive quotation from or reproduction of this thesis may be granted by my major professor, or in his absence, by the Head of Interlibrary Services when, in the opinion of either, the proposed use of the material is for scholarly purposes. Any copying or use of the material in this thesis for financial gain shall not be allowed without my written permission.

Signature Martha A Jones

Date August 4, 1994

PROCESSING AND CHARACTERIZATION OF POLY(ESTER-AMIDE)S AND POLY(ESTER-AMIDE) COPOLYMER MONOFILAMENTS

A Thesis

Presented for the

Master of Science

Degree

The University of Tennessee, Knoxville

Martha A. Jones

December 1994

ACKNOWLEDGMENTS

The author would like to express her sincere gratitude to her major advisor, Professor Joseph E. Spruiell, for his advise, guidance, and encouragement throughout the course of this work.

She would also like to offer her sincere thanks to Professors R. S. Benson and E. S. Clark for serving on her committee and for their many helpful discussions.

The author would like to thank the 3M company for providing the materials used in this study. Special thanks are extended to Dr. Thomas H. Barrows at 3M for his cooperation and collaboration.

The author would also like to thank the members of the mechanical and electronic systems groups for their assistance throughout this work. Furthermore, she would like to thank her fellow graduate students and friends for their help and friendship, with special mention to Deepak Agrawal.

The author would finally like to express her appreciation to her family and friends for their support and love through this endeavor.

ABSTRACT

The introduction of synthetic polymers in the 1940's has revolutionized the field of biomaterials. Currently, applications for polymeric biomaterials include surgical implants, prosthetic devices, artificial ligaments, synthetic blood vessels, and controlled drug release systems. A great deal of work has been focused on developing surgical suture implants, which will provide adequate strength while the tissues heal and will be absorbed in the body over a reasonable amount of time. Several synthetic absorbable sutures are currently on the market, but improvements over the properties observed for these materials is desired. The 3M company has recently developed a new class of bioabsorbable polymers for potential surgical suture applications, known as the "poly(ester-amide)s". It is the purpose of the present research to obtain preliminary information on these materials and conduct experimental and analytical studies on its processing into fibers.

The melting and glass transition temperatures of these materials were determined. Additionally, attempts were made to estimate the values of amorphous and crystalline densities for PEA 6,2. These values were used to estimate the crystallinity of PEA 6,2 fibers and films by measuring their densities. A PEA 6,2 copolymer was also studied in relation to the PEA 6,2 homopolymer.

Melt spinning studies were performed on PEA 6,2 and a copolymer of PEA 6,2. These melt spun fibers were drawn under several drawing conditions to study the effect of different processing variables on the structure and properties of these fibers. Previously reported information on the processing and properties of PEA 10,2 are included for comparison purposes only.

In previous studies, a large drop in molecular weight was observed during processing, which adversely affected the properties of the final fibers. Improvements in the molecular weight retention were achieved by reducing the polymer's residence time using the Maxwell extruder. Further improvements in molecular weight retention achieved by redrying the polymer prior to processing to remove any moisture absorbed. Many difficulties were encountered with the processing of these materials; many of these problems appear to result from problems in the synthesis of these polymers and in their basic properties. For example, additional cooling devices were required to expedite the solidification of PEA 6,2 and PEA 6,2 copolymer monofilaments, resulting from the materials glass transition temperature, which is close to room temperature, and its sluggish crystallization kinetics.

It was observed from x-ray studies on PEA 10,2, PEA 6,2 and the PEA 6,2 copolymer that they all form the same basic crystal structure with annealing. The crystallographic

repeat distance for PEA 10,2 is higher than that observed for PEA 6,2 and the PEA 6,2 copolymer, which is attributed to the four additional methylene groups present in PEA 10,2. The crystallographic repeat distance for PEA 6,2 and the PEA 6,2 copolymer were not significantly different from each other. Furthermore, little difference between crystals formed from these two materials was observed, indicating that they are essentially the same material.

TABLE OF CONTENTS

CHAPTER		PAGE
1	INTRODUCTION	1
2	BACKGROUND	6
	2.1 Biomaterials	6
	2.1.1 Biomedical Polymers	7
	2.1.1.1 Bioabsorbable and Biodegradable Polymers	9
	2.1.1.2 Poly(ester-amide)s	14
	2.2 Fiber Formation Processes	18
	2.2.1 Melt Spinning	20
	2.2.1.1 Maxwell Extruder	25
	2.2.2 Drawing	28
	2.3 Characterization Methods	29
	2.3.1 Crystallinity Determination	30
	2.3.2 Orientation	32
	2.3.3 Tensile Properties	34
3	EXPERIMENTAL MATERIALS AND PROCECURES	37
	3.1 Resin Identification	37
	3.2 Fiber Processing	38
	3.2.1 Melt Spinning	38
	3.2.2 Drawing	40
	3.3 Characterization of Fibers and Films	47
	3.3.1 Sample Preparation for Films	47

CHAPTER PAGE

3.3.2 Mechanical Testing 48

3.3.3 Orientation 49

3.3.3.1 Birefringence 49

3.3.3.2 Wide Angle X-ray Scattering 50

3.3.4 Density 52

3.3.5 Differential Scanning Calorimetry 52

3.3.6 Dynamic Mechanical Analysis 53

4 RESULTS AND DISCUSSION 54

4.1 Preliminary Information 55

4.1.1 Thermal Transitions 55

4.1.1.1 Melting Temperature 55

4.1.1.2 Glass Transition Temperature 59

4.1.2 Enhancement of Crystallinity 66

4.1.2.1 Qualitative Interpretation of X-ray Data 67

4.1.2.2 Quantitative Interpretation of X-ray Data 77

4.1.2.3 Oriented Fibers 80

4.1.3 Determination of Crystalline and Amorphous Densities 91

4.1.3.1 Crystalline Density 92

4.1.3.1.1 Pseudo-hexagonal Interpretation 93

4.1.3.1.2 Pseudo-orthorhombic Interpretation 95

CHAPTER PAGE

4.1.3.2 Amorphous Density 96
4.2 Processing of Poly(ester-amide)s 98
4.2.1 Initial Processing of PEA 10,2 99
4.2.2 Thermal Degradation Studies 100
4.2.3 Gel Spinning 100
4.2.4 Melt Spinning Using the Maxwell Extruder 102
4.2.4.1 PEA 10,2 104
4.2.4.2 PEA 6,2 106
4.2.4.3 PEA 6,2 Copolymer 108
4.3 Characterization of PEA Monofilaments 110
4.3.1 PEA 10,2 Fibers Extruded on Maxwell Extruder 111
4.3.2 PEA 6,2 Fibers Extruded on Maxwell Extruder 119
4.3.3 PEA 6,2 Copolymer Extruded on Maxwell Extruder 127
5 CONCLUSIONS AND RECOMMENDATIONS 134
5.1 Conclusions 134
5.2 Recommendations 138
REFERENCES 140
VITA 147

LIST OF TABLES

TABLE		PAGE
2.1	Various polymeric materials and their biomedical uses.	8
2.2	Examples of biodegradable and bioabsorbable polymers.	12
3.1	Summary of experimental processing conditions for melt spinning of poly(ester-amides).	39
3.2	Legend for identification of PEA 6,2 fibers.	41
3.3	Legend for identification of PEA 6,2 copolymer fibers.	42
3.4	Legend for identification of PEA 10,2 fibers.	43
4.1	Results of glass transition studies on PEA polymers using dynamic mechanical analysis.	65
4.2	PEA 6,2 water annealed film crystalline reflections obtained from diffractometer scan and flat plate film patterns.	78
4.3	Water annealed PEA 6,2 copolymer d-spacings obtained from diffractometer scan and flat plate film patterns.	79
4.4	PEA 6,2 water annealed fiber d-spacings obtained from flat plate film patterns and equatorial diffractometer scans.	84
4.5	Crystallographic repeat distance for oriented PEA 6,2 fibers.	87

TABLE PAGE

4.6 Crystallographic repeat distance for oriented PEA 6,2 copolymer fibers. 90

4.7 Effect of solvent content on the melting of PEA polymers. 103

4.8 Extrusion conditions for PEAs. 105

4.9 Properties of PEA 10,2 as-spun fibers. 112

4.10 Strength and orientation of fibers drawn at 65° C. 113

4.11 Comparison of tensile strength (<>) and Young's modulus ([]) of fiber MA119 after drawing under different conditions. 114

4.12 Strength and orientation in as-spun and in-line drawn fibers. 116

4.13 Strength and orientation in the in-line drawn fibers after redrawing at 65° C. 117

4.14 Comparison of strength and orientation after heat setting. 118

4.15 Properties of PEA 6,2 as-spun fibers. 120

4.16 Properties of as-spun and drawn PEA 6,2 fibers. 124

4.17 Properties of as-spun and drawn PEA 6,2 copolymer fibers using a crosshead speed of 50 mm/min. 128

TABLE PAGE

4.18 Properties of selected PEA 6,2 copolymer fibers using a crosshead speed of 100 mm/min. 129

LIST OF FIGURES

FIGURE		PAGE
1.1	Classification of sutures.	4
2.1	The effect of diacid methylene chain length on melting temperature of poly(ester-amide)s.	16
2.2	Schematic of melt spinning equipment.	22
2.3	Principle process variables in melt spinning.	24
2.4	Cross-sectional view of the Maxwell extruder.	26
3.1	X-ray diffraction camera designed by W. O. Statton.	51
4.1	DSC plot of first and second heating ramps of Pro1252 fiber.	56
4.2	Tan delta and storage modulus as a function of temperature for air cooled PEA 6,2 unoriented film.	61
4.3	Tan delta and storage modulus as a function of temperature for water cooled PEA 6,2 unoriented film.	62
4.4	Tan delta and storage modulus as a function of temperature for air cooled PEA 6,2 copolymer unoriented film.	63

FIGURE PAGE

4.5 Tan delta and storage modulus as a function of temperature for water cooled PEA 6,2 copolymer unoriented film. 64

4.6 DSC cooling curves for PEA 6,2 and PEA 6,2 copolymer unoriented films. 68

4.7 WAXD scan (a) and flat plate film pattern (b) of PEA 6,2 amorphous film. 69

4.8 WAXD scan (a) and flat plate film pattern (b) of PEA 6,2 thermally annealed film. 70

4.9 WAXD scan (a) and flat plate film pattern (b) of PEA 6,2 water annealed film. 71

4.10 WAXD scan (a) and flat plate film pattern (b) of PEA 6,2 copolymer amorphous film. 72

4.11 WAXD scan (a) and flat plate film pattern (b) of PEA 6,2 copolymer thermally annealed film. 73

4.12 WAXD scan (a) and flat plate film pattern (b) of PEA 6,2 copolymer water annealed film. 74

4.13 Scaled WAXD pattern of PEA 10,2 amorphous film overlaid on the WAXD pattern of PEA 10,2 slow crystallized film. 76

4.14 Cylindrical coordinates of the point *hkl* in reciprocal space. 81

4.15 WAXD equatorial scan (a) and flat plate film pattern (b) of PEA 6,2 water annealed fiber. 83

FIGURE PAGE

4.16 Flat plate film patterns of PEA 6,2 fibers. (a) 715 (5 cm) drawdown ratio 23.3, (b) 715 (17 cm), (c) 71580 (5 cm) fiber 715 drawn 4.05X at 80° C, (d) 71580 (17 cm). 86

4.17 Flat plate film patterns of PEA 6,2 copolymer fibers taken at 5 cm. (a) Pro1255, drawn 2.71X at 25° C, (b) Pro1451, drawn 2.71X at 45° C, (c) Pro1802, drawn 2.63X at 80° C. 89

4.18 Plot showing the effect of residence time on the molecular weight degradation of PEA 10,2 polymer. 101

4.19 5 cm flat plate film patterns of PEA 6,2 as-spun fibers. (a) 714 drawdown ratio 23.3, (b) 711 drawdown ratio 79. 122

4.20 Flat plate film patterns of PEA 6,2 as-spun and drawn PEA 6,2 fibers taken at 5 cm. (a) 715 drawdown ratio 23.3, (b) 71525 drawn 2.79X at 25° C, (c) 71562 drawn 2.13X at 60° C, (d) 71580 drawn 4.05X at 80° C. 125

4.21 Birefringence as a function of draw ratio at various temperatures for PEA 6,2 copolymer fibers. 130

4.22 Tensile strength as a function of draw ratio for PEA 6,2 copolymer fibers. 131

FIGURE PAGE

4.23 Flat plate film patterns of PEA 6,2 copolymer fibers taken at 5 cm. (a) Pro1 as-spun fiber drawdown ratio 9.6, (b) Pro1451 drawn 2.71X at 45° C, (c) Pro1703 drawn 3.71X at 70° C, (d) Pro1802 drawn 2.63X at 80°C. 133

Chapter 1

INTRODUCTION

A fiber is a fundamental unit of fabrics and textiles and is defined as a unit of matter having a length at least 100 times its width or diameter (1). Using this definition a wide range of materials can be classified as fibers, including natural and synthetic, organic and inorganic products.

In the area of polymers, fibers are classified according to their origin in terms of naturally occurring or synthetic materials. Included in the category of natural occurring fibers are cotton, cellulose, and silk. Synthetic fibers are formed from organic or inorganic materials and include naturally occurring organic polymers and man-made ones. Some of the most common synthetic fibers are formed from polyolefins, polyesters, acrylics, polyamides, and polyurethanes (2). Synthetic fibers are spun in the form of continuous filaments of very long length, or they may be chopped up into much shorter lengths, known as staple fiber. Staple fiber can be further processed into a variety of other forms including spun yarn and thread (1).

The introduction of synthetic fibers in the 1940's has revolutionized the textile industry. In addition to the formation of threads and yarns for fabric, fibers are used in

many other areas including the medical industry. For many years, fibers have been used in medical applications ranging from dressings to tapes, and surgical apparel. Additionally, specialty fibers are used for separations and purification in kidney dialysis (3). Because of their large surface to volume ratio, fibers have an advantage in some biomedical applications, such as separations. Additionally, they can be knitted, woven or formed into hollow structures of varying degrees of porosity and strength necessary for several biomedical applications including blood vessels, artificial ligaments, and controlled drug delivery systems.

One of the oldest and most widely used biomedical applications for fibers is the surgical suture. A suture is defined as a strand of either natural or synthetic material used to ligate blood vessels and to approximate tissue together. Suture materials must keep wounds together until collagen is synthesized by the body and woven into a strong scar to hold the tissues. Sutures are classified into absorbable and nonabsorbable categories, in which they are distinguished from each other by the time frame in which they lose their strength. Absorbable sutures lose their entire tensile strength in two to three months. Sutures which retain their strength longer than two to three months are non-absorbable (4).

Earlier materials used for ligatures and surgical sutures included: iron wire, silver, dried gut, horse hair,

silk, linen and tendon. Prior to the 1940's, catgut and silk dominated the suture market. Since the introduction of synthetic fibers, the number of suture materials with various chemical, physical, mechanical, and biological properties available to surgeons has increased (4). In the early 1970's, the first synthetic absorbable sutures based on bioabsorbable polyesters were introduced under the trade names of Dexon® and Vicryl®. In addition to the differences in chemical structure, sutures are available in many configurations, including monofilament, multifilament, and braids. A summary of the types and configurations of sutures, along with the desired properties is shown in Figure 1.1.

The Life Sciences Research Laboratories at 3M have developed a promising class of bioabsorbable polymers for potential biomedical applications. These polymers combine the amide and ester linkages and are known as poly(ester-amides) or PEA. PEA's are synthesized from a highly water soluble diamidediol and a diacid chloride under controlled conditions to yield PEA y,x polymers. They offer an advantage over bioabsorbable polyesters in that lower molecular weights are adequate to achieve comparable fiber strength. Additionally, the PEA exhibit lower modulus, greater toughness and durability compared to the bioabsorbable polyesters (5). The 3M Life Sciences Research Laboratories have evaluated the degradation behavior and

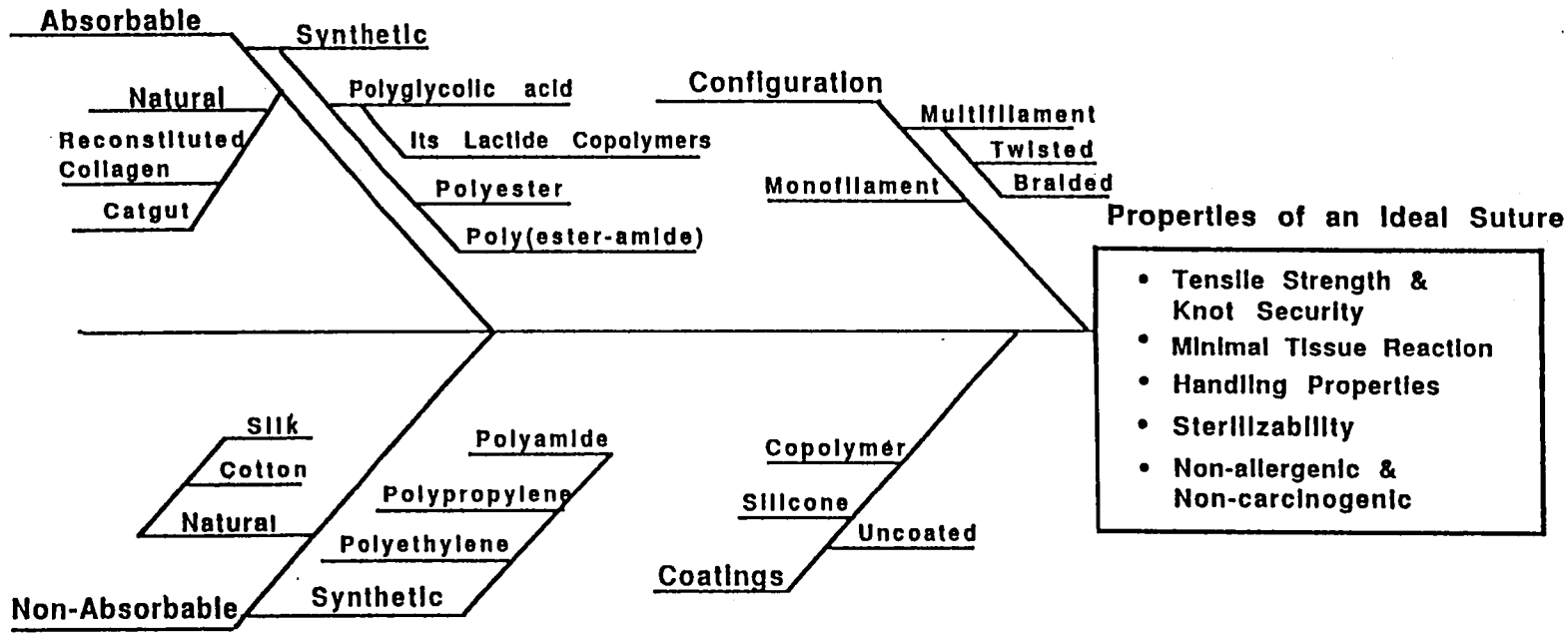


Figure 1.1 Classification of sutures.

strength retention of these homopolymer and copolymer materials and have found these material offer promise for biomedical applications.

The fiber research group at The University of Tennessee has shown that PEA 10,2 and PEA 6,2 polymers can be melt spun and drawn into monofilaments. Additionally, the mechanical properties of these straight monofilaments have been evaluated (6). In the present research, experimental and analytical studies on the PEA 6,2 and a PEA 6,2 copolymer synthesized with 20 mole % of a proprietary diacid were conducted. The purpose of these studies was to establish and determine the appropriate melt spinning and drawing conditions for these polymers to achieve the most desirable end use properties for the fibers. Experimental studies include establishing processing conditions and evaluating the effect of various processing variables on final fiber properties. Only the mechanical properties from a straight monofilament configuration were evaluated. Analytical studies include examining the effect of orientation, molecular weight, and crystallinity of the fiber on its mechanical properties. Additionally, an effort will be made to determine the glass transition temperatures of unoriented PEA 6,2 and the PEA 6,2 copolymer. Furthermore, a proposal for the crystal structure for the PEAs will be made.

Chapter 2

BACKGROUND

2.1 BIOMATERIALS

Biomaterials are defined as "materials which are used in contact with tissue, blood, cells, protein, and any other living substances" (7). Their goal is to restore the function of natural living tissues and organs within the body, fulfilling a temporary or permanent need. Consequently, biomaterials must possess certain physical, chemical, and mechanical properties that will enable them to perform a desired function at a specific location in the body (8). Through collaborative efforts of chemists, biologists, material scientists, engineers, and surgeons, biomaterials have been developed to fulfill the requirements of various medical applications (9). Materials such as metals, ceramics, polymers and their composites are used for these biomedical applications (10). Recently, focus has turned to developing new polymers for use as biomaterials because their properties can be tailored to meet desired end uses.

2.1.1 Biomedical Polymers

The use of polymers in medicine has increased rapidly since the 1950's, when the first polymeric vascular grafts were fabricated. Today, polymeric materials are used in nearly all areas of medicine including drug formulation and delivery systems, long-term and temporary therapeutic devices, aids in improvement of diagnostic examinations, and devices for bioengineering (8-10). Examples of these polymers and their end uses are given in Table 2.1 (12, 13).

In order for a polymer to be used in a biomedical application, certain requirements must be fulfilled including (9, 10):

- The polymer must possess the required chemical, physical, and mechanical properties for its desired use.
- It should be free of all impurities such as residual monomer, catalysts, solvents, additives, etc., which may change its performance.
- It must be non toxic to prevent adverse reactions in the body; it should not induce thrombus formation, inflammatory reaction, cell changes, tumor formation, immune response, etc.

Table 2.1 Various polymeric materials and their biomedical uses.

Polymer	Uses
Polyacrylates	Contact lens, dentures, orthopaedics, tissue replacement, macrocapsules, repair of brain lesions
Polyamides	Sutures, wound dressing, dentures
Polydioxanone	Sutures, surgical fastener
Polyesters (biostable)	Orthopaedics, tissue flaps
Polyesters (bioabsorbable)	Sutures, drug delivery systems, prostheses, orhopaedics, ligating clips
Polyethylene	Orthopaedics, cardiovasular devices
Polyglycolic acid and its copolymers	Controlled delivery systems, sutures
Polypropylene	Sutures, reconstruction surgery
Polytetrafluoroethylene	Cardiovascular devices, sutures, tissue flap
Polyurethanes	Prostheses, wound dressings, conceptives, liver support systems

Adapted from J. Paul and P. Gita Ph. D. dissertations, I.I.T. Delhi, India, April (1991) and July (1992), respectively.

- The polymer must be able to withstand sterilization procedures without adversely affecting its properties.
- It should be able to withstand the biological environment of the body for the desired time period.

Polymeric biomaterials can be divided into three categories based on their behavior in living tissue: biostable, bioabsorbable and biodegradable. Biostable polymers retain their properties for very long time periods, are physiologically inert and cause minimal response to surrounding tissue (14). However, in most cases tissues need only temporary assistance from a biomaterial (15, 16). In these situations, bioabsorbable or biodegradable polymers are better options.

2.1.1.1 Bioabsorbable and Biodegradable Polymers

Bioabsorbable and biodegradable polymers act in a temporary manner, supporting, covering or filling damaged tissue until it is able to heal. Bioabsorbable polymers are distinguished from biodegradable polymers by the mechanism of absorption in the body. In general, the absorption of these materials can be divided into two stages, decomposition and absorption. The decomposition stage involves bond breaking along the polymer's main chain, causing a decrease

in its molecular weight, and producing non-toxic monomeric and oligomeric compounds, via hydrolysis. Hydrolysis can occur in the presence or absence of an enzyme, and it is the mechanism of hydrolysis which distinguishes biodegradable polymers from bioabsorbable ones (17). Only enzymatically degradable polymers are truly biodegradable, while nonenzymatically degradable polymers are decomposed by water hydrolysis. In the second stage of bioabsorption, the low molecular weight compounds formed during decomposition are eliminated from the body through natural pathways.(17, 18). Therefore, in designing polymers for biomedical applications, the decomposition products should be involved in the metabolic cycles of the organism.

Bioabsorbable and biodegradable polymeric and composite surgical materials maintain their tissue supporting properties for various lengths of time ranging from days to months. These materials are the best choice in applications requiring temporary internal fixation from both a medical and economic standpoint. Initially, the implants approximate healing tissues gradually they degrade into low molecular weight compounds, transferring stresses to the healing tissue (19). Since the surgical implants degrade and absorb in the body, a separate removal operation is not required, which is a substantial benefit both economically and to the patient involved.

A variety of naturally occurring and synthetic polymers are biodegradable or bioabsorbable. A list of these materials is summarized in Table 2.2 (17). Biologically synthesized biodegradable polymers include the polypeptides, polysaccharides, polynucleotides, and bacterial polyesters. Synthetic polymers and copolymers formed from aliphatic polyesters and α-hydroxy acid derivatives contain hydrolyzable linkages and are reported to be bioabsorbable. However, aromatic polyesters are not susceptible to biological attack (20, 21).

Recently, focus has increased on developing polymers formed from multi-functional hydroxyacids and aminoacids (11). Several hydroxyacids are reported as bioabsorbable, but there have been few reports of degradable or absorbable polyamides. In fact, nylon 6 and nylon 6,6 are generally considered to be non-degradable although partial degradation and loss of tensile strength over a long period of time have been reported (22-25). Recently, Vanderbilt et al. have reported that polyamides based on 4,4'- spirobibutyrolactone are degradable and compatible with tissues (26, 27).

A new approach for obtaining additional improvements in the properties of synthetic absorbable polymers is to synthesize polymers containing both amide and ester linkages. The reasoning for designing these polymers is to combine the absorbability of polyesters with the high performance of polyamides. Several attempts to join these functional groups

Table 2.2 Examples of biodegradable and bioabsorbable polymers.

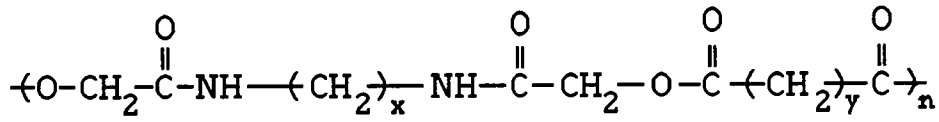
Polymer	Examples	Decomposition Mechanism
Polypeptides	Collagen, Gelatin	Enzyme
Polyamino acids	Poly-L-glutamic acid	Enzyme
Polysaccharides	Amylose, Dextran	Enzyme
Polyesters (bacterial)	Poly(beta-hydroxybutyrate)	Enzyme
Nucleic acids	Synthetic DNA	Enzyme
Poly(alpha-hydroxy acids)	Polyglycolide, Polylactide and its copolymers	Water Hydrolysis
Poly(omega-hydroxyl acids)	Poly- -caprolactone	Water Hydrolysis
Poly(ester-ethers)	Polydioxanone	Water Hydrolysis
Poly(amide-ester)	Polydepsipeptide	Water Hydrolysis

Adapted from Y. Kimura in "Biomedical Applications of Polymeric Materials", ed. T. Tsuruta et al., CRC Press (1993).

have been reported (28-43). T. H. Barrows et al. (28-30) have reported the synthesis of absorbable poly(ester-amides) using *bis*-hydroxyacetamides and a diacid, preferably succinic acid. Shalaby and Jamiolkowski (31) have formed absorbable poly(ester-amides) by reacting *bis*-oxamidodiols and oxalic acid. Bezwada, Jamiolkowski, and Shalaby have also formed segmented copolymers of ε-caprolactone/glycolide by a two stage polymerization process. This copolymer has been shown to be absorbable and is used in monofilament suture applications (32, 33). Gonsalves, Chen and Cameron have reported synthesizing degradable poly(ester-amides) from a two step polycondensation reaction of hexanediol-1,6 and adipoyl chloride (34, 35). Goodman et al. have synthesized poly(amide-ester)s containing alternating residues of α-amino acids and α-hydroxy acids (36-39). Copolyamide-esters (CPAE) have also been synthesized through an amide-ester interchange reaction by Y. Tokiwa et al.(40, 41). Regular block/segmented (amideester)-ester copolymers have been reported by Bera and Jedlinski by reacting oligo(amideester) and oligo ester (42). Biodegradable poly(ester-amide)s with pendant protected functional groups have been obtained from a ring opening copolymerization of either ε-caprolactone or DL-lactide with morpholine-2,5-dione derivatives (43).

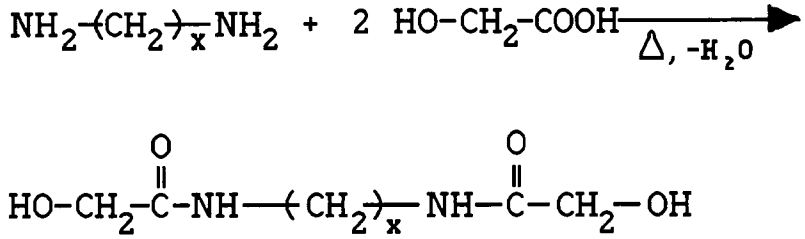
The polymers studied in the present research are the poly(ester-amide)s formed from the reaction of diamidediols with a dicarboxylic acid or a bischloroformate (44). The

general formula for the polymers in this family can be represented by the following formula:



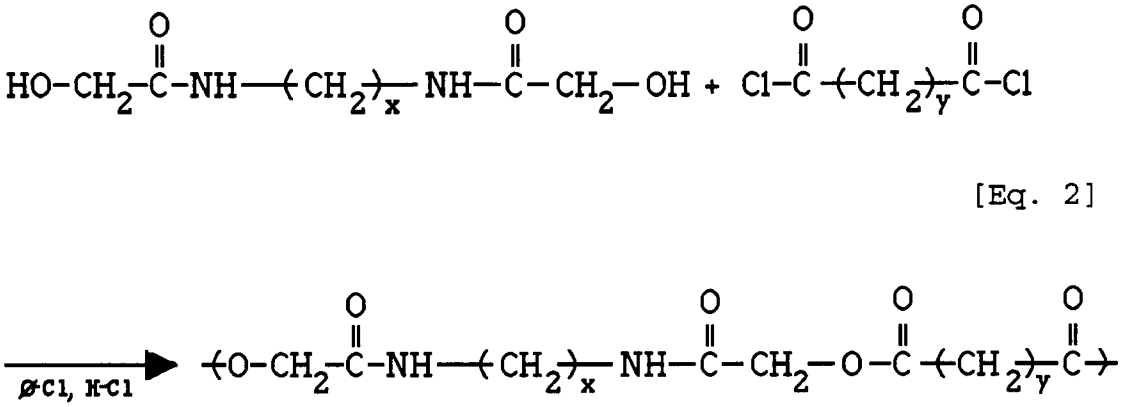
2.1.1.2 Poly(ester-amide)s

Poly(ester-amide)s are synthesized through a two stage condensation reaction. In the first stage, two moles of glycolic acid are reacted with one mole of a linear, aliphatic diamine to form a diamidediol monomer (equation 1).



[Eq. 1]

In the second stage, the diamidediol is polyesterified, preferably with a diacid chloride under controlled conditions in chlorobenzene to produce a regularly, alternating copolymer.



[Eq. 2]

Using this method of chemical synthesis, a variety of poly(ester-amide) polymers can be achieved. For example, the x and y can be varied independently or together by changing the diamine and/or diacid used in the reaction. Additionally, mixtures of different monomers with different values of x and y can be copolymerized in various ratios, allowing the formation of even more polymers. Furthermore, aromatic or heteroatomic substituents can also be present in the diamine or the diacid, offering additional possibilities.

The effect of the diacid methylene chain length on the polymer's melting temperature has been studied and the results are shown in Figure 2.1. In this study, the number of diamine methylene groups was held at a constant value of 12 (29). Melting temperature of the poly(ester-amide)s with diacid methylene chain length greater than 2 are fairly low (T_m < 100° C). Fibers produced from these polymers exhibited low strength and rapid *in vivo* strength loss. It has been shown that the use of succinic acid as the diacid comonomer

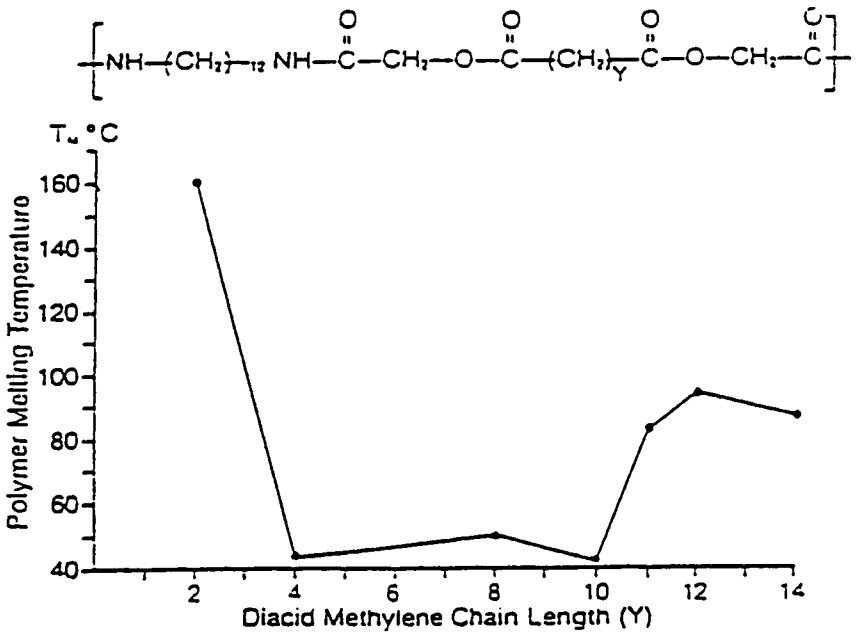


Figure 2.1 The effect of diacid methylene chain length on melting temperature of poly(ester-amide)s.

Source: T. H. Barrows, et al., "The Design and Synthesis of Poly(ester-amide)s", private communication.

maximizes the polymer's melting point. Fibers formed from these materials yield high strengths and exhibit a more prolonged rate of strength retention (29). Life Sciences Research Laboratories at 3M have evaluated the degradation behavior and strength retention of the poly(ester-amide)s.

In this research, fibers formed from polymers with y=6 and x=2 will be characterized. Also, fibers formed from an 80/20 molar mixture of PEA 6,2 and another PEA formed with a proprietary diacid will be examined. The rationale behind the incorporation of the proprietary diacid is to decrease the *in vivo* absorption time of the polymer. Some confusion may exist when referring to the earlier papers regarding the synthesis of the PEAs, due to a change in the naming scheme. However, the materials studied in this research following the PEA(y,x) naming scheme, where y is the number of methylene groups in the diacid chloride and x is the number of methylene groups in the diamine. Furthermore, the PEA 10,2 polymer mentioned also follows the PEA(y,x) naming scheme.

2.2 FIBER FORMATION PROCESSES

The production of synthetic fibers typically involves the following operations (46):

1.) Preparation of fiber-forming polymer;
2.) Preparation of spinning fluid (i.e. polymer melt, solution, emulsion, etc.);
3.) Spinning, i.e., extrusion of spinning fluid, followed by solidification and deformation of the spin-line and collection of the filaments;
4.) Mechanical, thermal, and chemical treatments.

The first operation refers to chemical operations, such as monomer synthesis and polymerization. The second operation pertains to unit processes including, melting, dissolving, mixing, deaeration and filtration. In the third stage, the polymer fluid is extruded and formed into fiber. Fibers may be extruded as a single strand, known as monofilament, or many single stands may be extruded simultaneously through a multi-hole spinneret. In order to improve the fiber's properties, mechanical, thermal and chemical treatments are employed. Spun fibers may be mechanically deformed with the application of a uniaxial tensile stress. This operation, known as drawing, causes the fiber to elongate to several times its original length,

increasing its degree of molecular orientation and improving the fiber's overall mechanical properties. Fibers can be drawn continuously and either directly following the spinning operation, or in a separate operation beginning with undrawn material previously collected on bobbins. Additionally, the fiber's structure can be stabilized through a heat treatment stage. Thermal treatment is often combined with water or a solvent treatment, which increases the mobility of the polymer chains (46). It also leads to the relaxation of internal stresses, reduces the degree of fiber shrinkage and brings the fiber structure closer to thermodynamic equilibrium (47). The focus of the present research is on the manufacturing operations and mechanical and thermal treatments in synthetic fiber formation.

Depending on the nature of the polymer material and the required fiber properties, several spinning operations may be employed. The three major types of fiber spinning processes are: melt spinning, dry spinning, and wet spinning. The major difference in these operations is based on the solidification process of the spinning fluid. In melt spinning, undiluted polymer melt is extruded into a gaseous or liquid cooling chamber, where it solidifies by liberation of heat. Consequently, there is no mass exchange between the spin line and the surrounding area. In dry spinning, the polymer is dissolved in a volatile solvent and extruded into a heated drying chamber, where the solvent is evaporated and

the fiber solidifies. Wet spinning involves the spinning of a polymer solution into a liquid bath containing a non-solvent. In the bath, the polymer precipitates and the solvent is washed out, resulting in a solid fiber. Other spinning methods include: reaction spinning, phase separation spinning, emulsion spinning, and gel spinning. The fiber forming process is similar in all of the spinning operations. Polymer fluid is extruded through a small hole called a spinneret, shaping it into the fiber form. The material transforms to a solid and is wound up on a bobbin or spool. Fibers may then be subjected to mechanical, thermal, or chemical treatments to improve their properties (46, 48).

2.2.1 Melt Spinning

Melt spinning is the most common and simplest method for forming fiber. The ability to spin fibers at high velocities, the absence of materials such as solvents and precipitation agents, and the simplicity of the spinning apparatus, make melt spinning the most convenient and economical method of fiber processing. However, its application is limited to polymers which are fusible and yield thermally stable, spinnable melts. Examples of melt spinnable polymers include polycondensation polymers like the polyamides and polyesters. Additionally, linear polyolefins

such as, polyethylene and polypropylene can be formed into fibers by melt spinning (48).

In melt spinning with conventional screw extruders (Figure 2.2), polymer pellets or powders enter the extruder from a hopper. The polymer is melted due to thermal conduction and the mechanical action of the screw. The melt flows to a metering gear pump, where it is transported at a constant rate to a filter assembly. Large solid or gel particles are removed from the melt during the filtration process. This step eliminates the possibility of particles blocking the spinneret holes, or filling part of the cross-sectional area of the filament, affecting the processing or tensile properties.

Following the filtration process, the melt passes to a spinneret, containing orifices through which molten polymer is extruded under pressure. Spinnerets may have up to 500 orifices for the production of continuous filament, but 50 to 200 holes are more common. The velocity of the extrudate is determined by the constant mass flow rate of the melt, the diameter of the spinneret orifice and the material's density. Directly below the spinneret, cool air is blown across the spin line to promote uniform cooling and solidification of the fiber. Other cooling devices, such as water baths may be used to increase the rate of solidification and heat transfer of the polymer. As the spin line cools, it is drawn down and attenuated by a force, supplied by the take-up

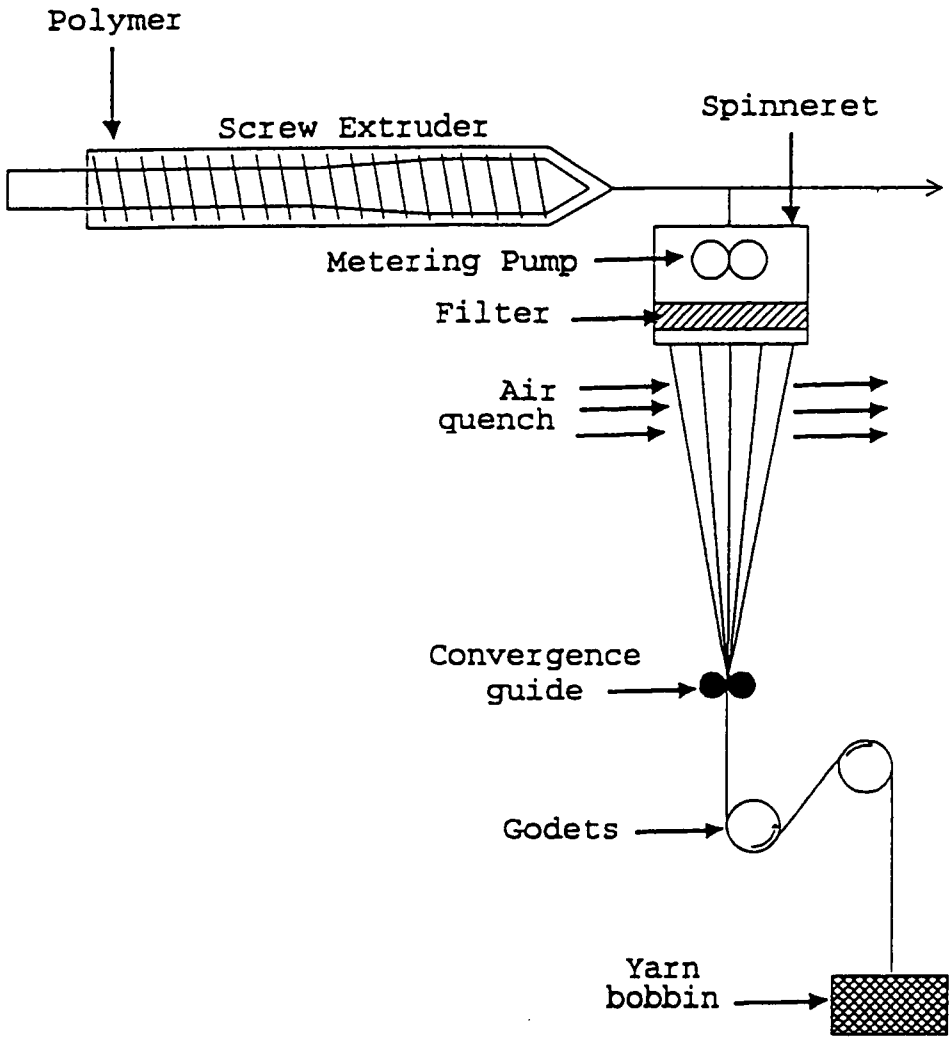


Figure 2.2 Schematic of melt spinning equipment.

Source: "Encyclopedia of Chemical Processing and Design", Marcel Dekker, N. Y. (1984).

device located at some distance, L from the spinneret. It provides the filament with a constant velocity, V_L, which is related to the average spun filament diameter, d_L. During this operation, the fiber diameter decreases and the solid fiber is wound on a bobbin or spool (48).

The melt spinning process can be described quantitatively in terms of several process variables, shown schematically in Figure 2.3. The primary variables are predetermined technical parameters, which act as initial condition for the dynamic equations. These variables include material characteristics, as well as extrusion and take-up conditions. The secondary variables are related to the primary ones by the continuity equation, or similar relationships and include parameters such as the extrusion velocity fiber diameter and draw down ratio. Finally, the resulting variables are determined by the primary variables and the rate of solidification, as well as the phase and structural transformation of the material. All of these factors influence structure development and properties of the final fiber in regards to morphology, orientation, crystallinity and crystal structure. Consequently, the relationship between the processing variables and structure development of the fiber is a crucial factor in understanding the properties developed during fiber processing. In addition to screw extruders, other types of extruders may be employed to melt spin polymers. In particular, a Maxwell extruder

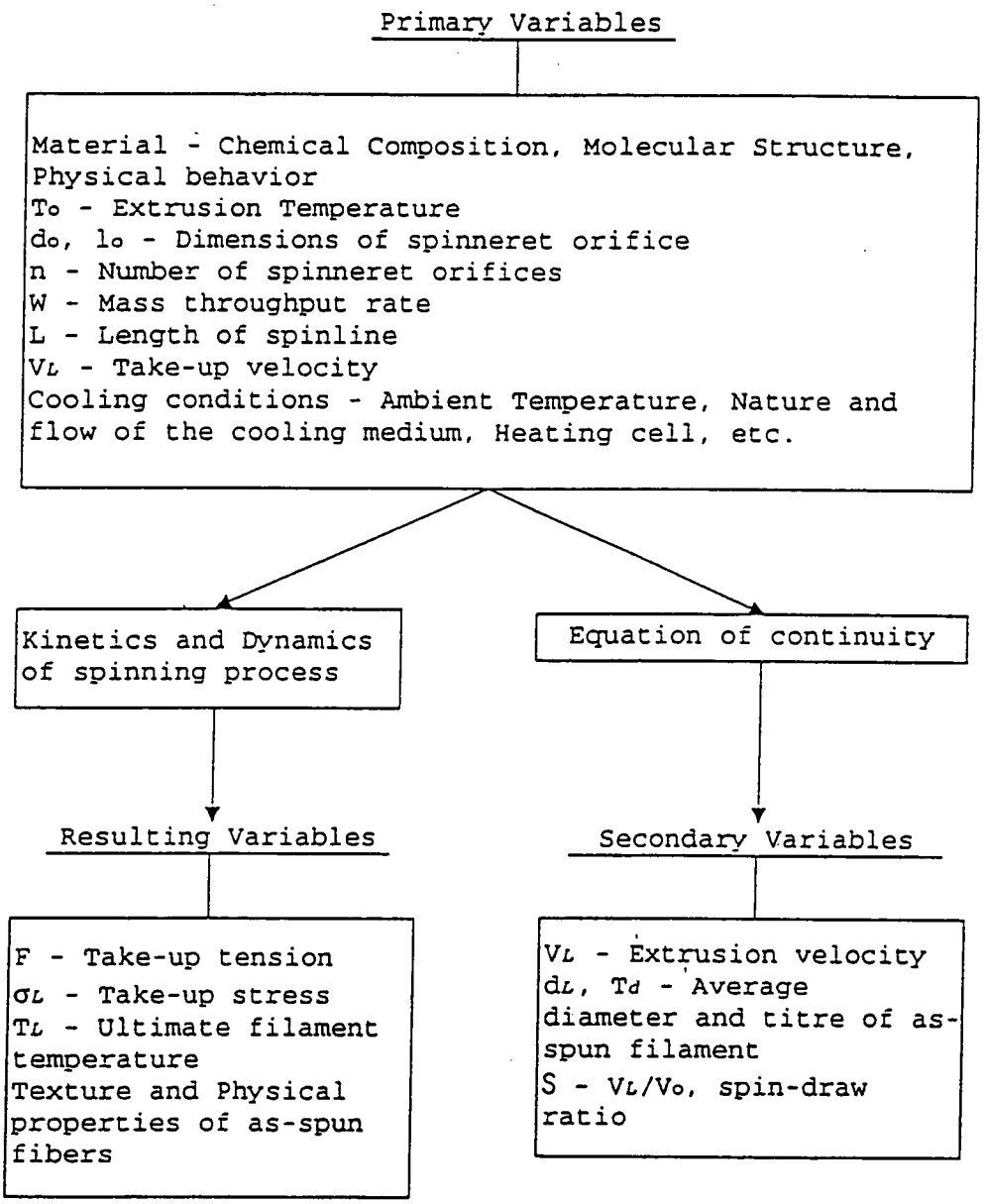


Figure 2.3 Principal process variables in melt spinning.

Source: D. D. Agrawal, "Processing and Characterization of Poly(ester-amide) Monofilaments." Master of Science Thesis in Polymer Engineering, The University of Tennessee at Knoxville, December 1993.

was used to melt spin the poly(ester-amide)s examined in this study. The Maxwell model is a screwless, microscale extruder which utilizes the centripetal pumping action developed from rotational shearing of visco-elastic melts (49-51). It allows very small quantities of polymer to be processed, while also reducing the polymer's residence time. These features are ideal for the PEA family of polymers due to their limited availability and thermal instability. The principle of the extruder's operation is summarized in the following section.

2.2.1.1 Maxwell Extruder

The Maxwell extruder is a screwless extruder and operates on a different principle as compared to conventional screw extruders. Its design is based on the desire to minimize the time hot material is in the extruder and also input as much of the required energy to melt the material by mechanical work instead of thermal energy (51).

A cross-sectional view of the Maxwell extruder is shown in Figure 2.4. During operation, the feed material falls from the hopper and sticks to the hot surface of the cylindrical rotor. The polymer is dragged against the inclined surface of the stationary scroll as the rotor turns, producing a component of axial transport towards the die. The material collects in the radial gap and is compressed by

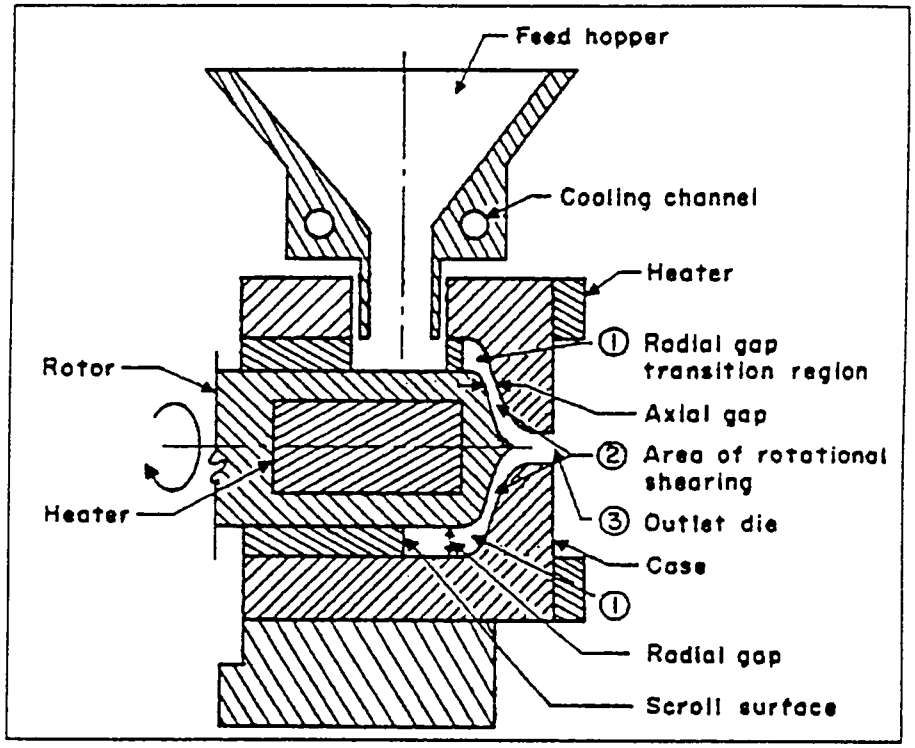


Figure 2.4 Cross-sectional view of the Maxwell extruder.

Source: Bryce Maxwell, Plast. Eng., 40 (1974).

the narrowing space between the scroll surface and the end of the case. New material is continuously supplied to replacethe previous material as rapidly as the axial-gap shear zone pumps material away.

The material is melted by heat conduction from the surfaces of the rotor and case, and also by mechanical work input resulting from the rotor turning with respect to the case. The polymer melt enters the axial gap and is rotationally sheared between the rotor's end and the inside of the case. This action causes mixing and homogenization. In addition, the material is stretched along circular arc, resulting in an elastic tension in the material and producing a radially inward force. This force is developed within the material and causes it to flow to the center and out the die, as in the elastic melt extruder (51). A more detailed description of the Maxwell extruder can be found in references (50, 51).

For the operation of melt spinning, the Maxwell extruder's die was modified with a vertical adapter to permit fiber extrusion. The polymer filament undergoes deformation and solidification along the spin line and is taken up on bobbins as described previously.

2.2.2 Drawing

As-spun filaments characteristically display low tenacity, high plastic deformability, and low moduli. These fibers are usually not suitable for their end use applications until the desired properties are imparted by further processing. In order to improve the fiber's modulus and tensile strength, the filament is subjected to an irreversible elongation process known as drawing. In this process, elongation is accompanied by extension and orientation of the molecules and crystallites with respect to the fiber axis. Crystallization or partial destruction of crystalline regions may also occur during this operation.

Drawing can be performed continuously and either directly following the spinning operation or in a separate stage beginning with the undrawn material previously collected on bobbins. Various drawing operations are available, depending on the characteristics of the undrawn material. For example, melt spun fibers can be drawn in air at room temperature, in a heated air chamber, or in contact with a hot surface. Drawing may also be conducted by submerging the undrawn fibers in a liquid bath, in which the liquid acts as a plasticizer for the fibers (46).

In each case, the drawing apparatus consists of two or more mechanically driven godets, operating at two different velocities. The fiber's draw ratio, R is determined from the

velocity of the feed, V_F and the velocity of the drawing godet, V_R:

$$R = V_R / V_F \qquad \text{(Equation 3)}$$

A major factor influencing the drawability of the fiber is the spinning speed used to form the fiber. Higher spinning speeds result in lower achievable draw ratios, while lower spinning speeds yield higher draw ratios.

The draw ratio affects mechanical properties such as tenacity and elongation. Tenacity increases and elongation decreases with increasing draw ratio. Typically, the maximum tenacity is achieved by drawing the filaments to the greatest extent. During this process, the fiber should maintain good mechanical quality and be free from breaks (52, 53). Consequently, in order to optimize the drawing process, it is important to know how the undrawn material structure, drawing conditions, and the structure and properties of the drawn fibers relate to one another.

2.3 CHARACTERIZATION METHODS

The poly(ester-amide) family of polymers are still in the developmental stages and many of their physical and thermal properties are not known. Much of the basic information necessary for characterization of fibers produced from these materials is not available. Preliminary studies

have been conducted on PEA 10,2 and PEA 6,2 (54). Many of the characterization techniques used in those studies will be employed here for fibers produced from PEA 6,2 and the PEA 6,2 containing 20 mole % of a proprietary diacid, and they are described below.

2.3.1 Crystallinity Determination

The degree of crystallinity is one of the most useful pieces of information used to characterize semi-crystalline polymers. Its basis is founded on the assumption that semi-crystalline polymers consist of two distinct phases, crystalline and amorphous, each having different characteristics. There are several techniques available to estimate crystallinity including (55- 57):

- Density measurement- based on the premise that the density or specific volume of a semi-crystalline polymer varies between the values of a perfectly crystalline and a perfectly non-crystalline sample,
- Infrared spectroscopy- based on the premise that 'amorphous' and 'crystalline' bands are exhibited in an infrared spectra in proportion to their relative amounts,

- Nuclear magnetic resonance- measures the magnetic absorption of a sample. The absorption bands can be resolved into broad and narrow components, relating to mobility of the crystalline and amorphous parts of the polymer,
- Differential Scanning Calorimetry- uses the known heat of fusion for the particular polymer to calculate crystallinity,
- By X-ray diffraction- uses a ratio of the intensity of the amorphous (highly disordered regions) and crystalline (highly ordered regions) peaks.

Density, DSC, and X-ray diffraction are the most common techniques used to determine crystallinity in polymeric materials. Each of these techniques requires some general information about the polymer being examined. In the case of crystallinity determination via density measurement, the densities of the purely amorphous and purely crystalline components are needed. Crystallinity measurements using DSC call for the heat of fusion for the polymer crystal, while the x-ray diffraction method involves resolving diffraction patterns into amorphous and crystalline contributions.

Heat of fusion values are not known for the PEA polymers. Additionally, the PEA polymers undergo some 'annealing' during heating, complicating crystallinity analysis by DSC. Although crystallinity can not be

determined from DSC, other relevant information about the material's thermal behavior may be obtained. As mentioned previously, crystallinity measurements by x-ray diffraction require demarcation of amorphous and crystalline regions, which is difficult. Based on the instrumentation available and the limited supply of material, the density method for estimating crystallinity was chosen. This method also had its limitations when applying it to PEA fibers. PEA 6,2 and the PEA 6,2 with the 20 mole % proprietary diacid took a very long time to reach a stable equilibrium position in the density gradient column. This phenomena was also observed with PEA 10,2 fibers and is believed to be due to hydrogen bonding and additional crystallization of the samples (54). As a result, position measurements were taken five hours after dropping the samples into the DGC.

2.3.2 Orientation

The orientation of polymer chains in formed polymers influences their performance in other areas including mechanical and optical properties. Orientation in polymers can be measured using birefringence, dichroism and x-ray techniques (58-61). In these studies, birefringence and wide angle x-ray diffraction (WAXD) techniques were employed to acquire orientation measurements.

Birefringence is the classical method of assessing the overall state of molecular orientation within polymeric materials and includes both amorphous and crystalline regions. It results because the polarizability, and hence the refractive index of the polymer is different along the chain and perpendicular to it (62). The magnitude and sign of birefringence is determined by the chemical nature of the polymer and the degree and type of orientation present.

Birefringence measurements are easily obtained using a polarizing microscope, which offers the capability of accurate measurements on specimens down to a few micrometers in size (63). In the case of fiber specimens, birefringence is an ideal method for measuring orientation because very little preparation is required. For these reasons, as well as the large number of fibers to be characterized, birefringence was the more attractive option.

Wide angle x-ray diffraction (WAXD) can be used to obtain flat plate film x-ray patterns of fiber and film specimens to get a qualitative idea of their molecular orientation and crystallinity. Depending on the orientation of the crystallites in the fiber, film patterns will range from something similar to a powder pattern to a single crystal rotation pattern. From the positions and intensities of the crystalline diffraction spots, orientation of the crystal and information about its structure is acquired. For example, the magnitude of the azimuthal spread of the

reflections indicates the degree of crystallite orientation, while the breadth of the reflections is related to the crystal size and imperfections (64).

2.3.3 Tensile Properties

Mechanical properties of polymers can be determined by 'static' or 'dynamic' mechanical tests. Static tests are relatively easy to perform and disclose basic information such as modulus, strength and elongation of the material (62). Dynamic tests give information on the viscoelastic nature of the polymer. These tests may be used to describe the time-dependent mechanical properties of polymers when they are subjected to constant stress or constant strain (65).

For the purposes of this study, mechanical property results obtained from static tensile testing are adequate for characterization. Three types of tensile testing machines are normally employed for these tests as described in ASTM D 76 (66):

1. Constant rate of extension (CRE);
2. Constant rate of traverse (CRT);
3. Constant rate of loading (force) (CRL).

In the CRE type machines, the specimen length increases at a uniform rate over time; in CRT type machines, load is applied by a clamp which moves appreciably to actuate a weighing mechanism, resulting in an increase of load or elongation dependent on the extension characteristics of the specimen; in CRL machines, the rate of increasing load applied to the specimen is uniform with time after the first 3 seconds.

Several ASTM test methods suggested for testing fibers in different conformations are contained in ASTM D 76. From this list, ASTM D 2256 (67) was most appropriate and selected for tensile testing PEA monofilaments. The CRE type tensile testing machine was used to perform the tests, although any of the tensile testing machines may be used for this standard. ASTM D 2256 describes the tensile testing and analysis of many fiber shapes, including straight fiber, and "knot-pull" configurations. The straight pull test is self-explanatory, while the knot-pull test examines the behavior of sutures tied with a "Surgeon's knot". However, due to limited supply of fiber, only straight fibers were tested.

Birefringence and x-ray diffraction characterization techniques disclose information on the molecular structure of the fiber, while tensile testing measures properties resulting from its structure. The combination of these three techniques provide a good initial understanding of the structure-property relationships developed during processing.

More specialized characterization methods can be used to obtain additional information relating to structure and properties.

Chapter 3

EXPERIMENTAL MATERIALS AND PROCEDURES

3.1 RESIN IDENTIFICATION

Two different types poly(ester-amides) were supplied by the 3M company for the purposes of this study. They included PEA 6,2 and a PEA 6,2 copolymer synthesized with 20 mole % of a proprietary diacid, which will be referred to as PEA 6,2 copolymer from now on. Two thermally stabilized PEA 6,2s were supplied: 1) 200 grams with an initial intrinsic viscosity of 1.18 dl/g and 2) 800 grams with an initial intrinsic viscosity of 1.56 dl/g. Additionally, 293 grams of the PEA 6,2 copolymer with an initial IV of 1.00 dl/g was supplied. These resins were spun into fiber and/or made into films for characterization experiments. It should also be noted that these studies represent the first experiments ever conducted on the PEA 6,2 copolymer.

Previously, the fiber research group at The University of Tennessee has processed PEA 10,2 on a *Fourne* extruder and a Maxwell extruder. Information included in this section for PEA 10,2 is for reference purposes only and a complete description of the experimental conditions for this material is found in reference 54.

3.2 FIBER PROCESSING

3.2.1 Melt Spinning:

Melt spinning on the Maxwell extruder was conducted for PEA 6,2 and the PEA 6,2 copolymer. Slight modifications were made to the Maxwell extruder to enable the processing of the PEAs. These modifications included enclosing the hopper and adding a purge device to provide a nitrogen environment for the polymer. Furthermore, a vertical die adapter was added to the extruder for fiber spinning purposes. A new take-up and drawing apparatus was designed and constructed to be used with this microscale extruder. It is equipped with two pulleys connected to two variable speed D. C. motors, and a 50 cm long heater. This set-up offers the flexibility of varying processing conditions, such as spin line length and take-up speeds as well as drawing conditions, such as drawing speeds and draw temperatures. Extrusion conditions of PEA 6,2 and the PEA 6,2 copolymer on the Maxwell extruder are listed in Table 3.1. Additional cooling devices were used in some instances due to the tackiness of the filament at the take-up device. Further discussion of the problems associated with spinning these polymers is given in Chapter 4, Results and Discussion.

Different fiber draw down ratios were achieved by changing the pulley's take-up speed. Drawdown ratios are

Table 3.1 Summary of experimental processing conditions for melt spinning of poly(ester-amides).

Spinneret	Circular cross section, single hole, diameter = 2.5 mm.
Spinline length	1.3 m.
Zone Temperatures:	
PEA 6,2 1.18 IV	Rotor- 155° C, Rotor speed = 30%.
	Header- 176° C
PEA 6,2 copolymer 1.00 IV	Rotor- 176° C, Rotor speed = 20%.
	Header- 194° C
Cooling conditions:	
PEA 6,2 1.18 IV	1. Ambient air.
	2. Ambient air and water quench.
PEA 6,2 copolymer 1.00 IV	1. Water quench.

typically determined by the ratio of the velocity of the take-up device to the extrusion velocity. However, the feed to the Maxwell extruder was not constant, resulting in variation in the extrusion velocity. Therefore, the fiber's respective draw down ratio was determined by dividing the die diameter (D_d) squared by the average final fiber diameter squared (D_s), $(D_d)^2/(D_s)^2$.

3.2.2 Drawing

As-spun fibers formed on the Maxwell extruder were drawn on the new melt-spinning and drawing bench. The slack in the feeding fiber was removed by passing it through a tensioner. The filament was drawn between two pulleys, driven by variable speed D. C. motors which rotated at velocities V_1 and V_2, where $V_1<V_2$. By changing the speeds of the motors, different draw ratios were achieved. The fiber's draw ratio was determined by dividing the average initial fiber diameter (D_o) squared by the average final fiber diameter (D_f) squared, $(D_o)^2/(D_f)^2$. Drawing was performed at room temperature and also at elevated temperatures, by running the filament over a heater located between the two pulleys.

The spinning and drawing conditions for the PEA 6,2, and PEA 6,2 copolymer fibers are listed in Tables 3.2-3.3, which also serve as legends. A legend is also provided in Table 3.4 for the PEA 10,2 fibers studied previously and mentioned

Table 3.2 Legend for identification of PEA 6,2 fibers.

Fiber ID	Description
711	As-spun with a drawdown ratio of 79. Air blown countercurrent to spinline.
712	As-spun with a drawdown ratio of 11. Air blown countercurrent to spinline.
713	As-spun with a drawdown ratio of 24.4. Cooled by water quench bath.
714	As-spun with a drawdown ratio of 23.3. Air blown counter to spinline.
71425	714 drawn to 2.79X at 25°C.
71461	714 drawn to 1.62X at 60°C.
71462	714 drawn to 2.97X at 60°C.
71480	714 drawn to 2.74X at 80°C.
715	As-spun with a drawdown ratio of 23.3. Cooled by water quench bath.
71525	715 drawn to 2.05X at 25°C.
71561	715 drawn to 1.84X at 60°C.
71562	715 drawn to 2.13X at 60°C.
71580	715 drawn to 4.05X at 80°C.

Table 3.3 Legend for identification of PEA 6,2 copolymer fibers.

Fiber ID	Description
PRO1	As-spun with a drawdown ratio of 10. Cooled by water quench bath.
PRO1251	PRO1 drawn to 1.27X at 25°C.
PRO1252	PRO1 drawn to 1.56X at 25°C.
PRO1253	PRO1 drawn to 1.92X at 25°C.
PRO1254	PRO1 drawn to 2.39X at 25°C.
PRO1255	PRO1 drawn to 2.71X at 25°C.
PRO1451	PRO1 drawn to 2.71X at 45°C.
PRO1452	PRO1 drawn to 3.97X at 45°C.
PRO165	PRO1 drawn to 2.74X at 65°C.
PRO1701	PRO1 drawn to 2.26X at 70°C.
PRO1702	PRO1 drawn to 2.47X at 70°C.
PRO1703	PRO1 drawn to 3.71X at 70°C.
PRO1801	PRO1 drawn to 1.67X at 80°C.
PRO1802	PRO1 drawn to 2.63X at 80°C.

Table 3.4 Legend for identification of PEA 10,2 fibers.

Reading the Fiber ID
The fiber ID is in the format AB122-3.4H5, where:
A = M. M represents the fibers processed using the Maxwell extruder.
B = A or I. A is used for fibers spun with air cooling, and I is used for the fibers spun with air cooling and in-line drawing.
1 = 1. 1 is used for PEA 10,2 fibers.
22 = ID number or serial number.
3, 3.4 = Numbers representing drawing steps.
H indicates heat setting.
5 = A number representing heat setting steps.

Adapted from D. D. Agrawal, "Processing and Characterization of Poly(ester-amide) Monofilaments." Master of Science Thesis in Polymer Engineering, The University of Tennessee, Knoxville, December, 1993.

Table 3.4 (continued).

Fiber ID	Description
MI110	As-spun with in-line drawing to 3X at 50° C.
MI110-1	MI110 redrawn to 1.76X at 65° C.
MA111	As-spun fiber with a drawdown ratio of 45.
MA111-1	MA111 drawn to 3.19X at 65° C.
MA111-2	MA111 drawn to 3.5X at 65 °C.
MA111-3	MA111 drawn to 7.13X at 65 °C.
MI112	As-spun with in-line drawing to 3X at 60° C.
MI112-1	MI112 redrawn to 1.32X at 65° C.
MI112-2	MI112 redrawn to 1.42X at 65° C.
MI112-3	MI112 redrawn to 1.8X at 65° C.
MA113	As-spun fiber with drawdown ratio of 95.
MA113-1	MA113 drawn to 3.19X at 65° C.
MI114	As-spun fiber with in-line drawing to 3.73X at room temperature, 25° C with steel snubbing pin.
MI114-1	MI114 redrawn to 1.32X at 65° C.
MI114-2	MI114 redrawn to 1.8X at 65° C.

Adapted from D. D. Agrawal , "Processing and Characterization of Poly(ester-amide) Monofilaments." Master of Science Thesis in Polymer Engineering, The University of Tennessee, Knoxville, December, 1993.

Table 3.4 (continued).

Fiber ID	Description
MI115	As-spun fiber with in-line drawing to 3.8X at room temperature, 25° C with steel snubbing pin.
MI115-1	MI115 redrawn to 1.32X at 65° C.
MI115-2.1	MI115 redrawn to 1.22X at 65° C.
MI115-2.1H1	MI115-2.1 heat set at 100° C.
MI116	As-spun fiber with in-line drawing to 3X at room temperature, 25° C with Teflon snubbing pin.
MI116-1	MI116 redrawn to 1.83X at 65°C.
MI116-2	MI116 redrawn to 2.53X at 65°C.
MI116-3	MI116 redrawn to 2.8X at 65°C.
MI116-2.1	MI116 redrawn to 1.22X at 65° C.
MI116-2.1H1	MI116-2.1 heat set at 100° C.
MI116-2.2	MI116 redrawn to 2.33X at 65° C.
MI116-2.2H1	MI116-2.2 heat set at 100° C.
MI116-2.2H2	MI116-2.2 heat set at 105° C.
MI116-2.3	MI116 redrawn to 2.58X at 65° C.
MI116-2.3H1	MI116-2.3 heat set at 100° C.
MI116-2.3H2	MI116-2.3 heat seet at 105° C.

Adapted from D. D. Agrawal , "Processing and Characterization of Poly(ester-amide) Monofilaments." Master of Science Thesis in Polymer Engineering, The University of Tennessee, Knoxville, December, 1993.

Table 3.4 (continued).

MA117	As-spun fiber with drawdown ratio of 138.
MA117-1	MA117 drawn to 3.19X at 65° C.
MA119	As-spun fiber with a drawdown ratio of 22.
MA119-1	MA119 drawn to 3.19X at 65° C.
MA119-2	MA119 drawn to 4.44X at 65° C.
MA119-3	MA119 drawn to 5.15X at 65° C.
MI120	As-spun fiber with in-line drawing to 3X at room temperature, 25° C.
MI120-1	MI120 redrawn to 1.32X at 65° C.
MI120-2	MI120 redrawn to 1.8X at 65° C.
MI120-3	MI120 redrawn to 2.53X at 65° C.
MI120-4	MI120 redrawn to 2.8X at 65° C.
MI120-4H1	MI120-4 heat set at 100° C.
MI120-5	MI120 redrawn to 3.2X at 65° C.

Adapted from D. D. Agrawal , "Processing and Characterization of Poly(ester-amide) Monofilaments." Master of Science Thesis in Polymer Engineering, The University of Tennessee, Knoxville, December, 1993.

in Chapter 4, Results and Discussion. For a more detailed explanation of the processing and characterization of PEA 10,2 fibers see reference 54.

3.3 CHARACTERIZATION OF FIBERS AND FILMS

Fibers and films made from PEA 6,2 and the PEA 6,2 copolymer were examined using several methods. Areas studied include mechanical properties, orientation, density, crystallinity, and thermal properties. The techniques used are explained in the following sections.

3.3.1 Sample Preparation for Films

Polymer pellets were dried overnight in a vacuum oven held at 100° C prior to being pressed into randomly oriented films. Pellets were placed between two thin sheets of Teflon® film and placed in a Wabash 12-ton melt press held at 190° C. The press platens were closed, but no pressure was placed on the polymer pellets. After allowing the pellets to melt for three minutes, pressure was added. The resulting film was quickly removed from the press and quenched in water. Films were also prepared by allowing the polymer melt to air cool.

3.3.2 Mechanical Testing

The mechanical properties of the PEA fibers were examined using the ASTM D2256 standard (67). Fibers were tested using a constant rate of extension (CRE) type tensile testing machine. Prior to subjecting fibers to mechanical testing, diameter measurements were taken along a continuous length of fiber. The average fiber diameter was obtained by taking at least 20 fiber diameter measurements along the length of fiber using a digital micrometer. Sections of fiber with excessive diameter variations above or below 10% of the average diameter values were discarded. Additionally, samples were conditioned for 36 hours at 19° C and 59% relative humidity prior to testing. By allowing the specimens to equilibrate at the same conditions, a better comparison of their properties may be achieved from the tests.

The PEA 6,2 fiber samples produced on the Maxwell extruder were tested on a *United* tensile testing machine using a 10 lb load cell and a crosshead speed to 100 mm/min. Fiber samples made from the proprietary PEA 6,2 were tested on a table model *Instron* using a 20 lb load cell and crosshead speeds of 50 mm/min and 100 mm/min. It was necessary to change machines because the load necessary to break these fibers exceeded the *United* tensile testing machine's 10 lb load cell. In both cases, at least five

specimens were tested. Following the procedures described in ASTM D2256 (67), the ultimate tensile strength, elongation at break, and the Young's modulus were calculated. The overall average values are reported.

3.3.3 Orientation

3.3.3.1 Birefringence

In order to obtain birefringence measurements, fiber samples were mounted on microscope slides. These specimens were examined under white light at 10X magnification using an *Olympus* polarizing microscope at which time fiber diameter measurements were made. A 30 order *Berek* compensator was used to obtain the angle of tilt as outlined in the manual.

The retardation required to center the zero order black line in the plate was measured in both clockwise and counter-clockwise rotations of the plate. From the sum of these two directions, a value relating the tilt of the plate with the amount of retardation was calculated. Retardation values were divided by the respective fiber diameter to obtain birefringence values. The reported birefringence values represent the average value for each sample set.

3.3.3.2 Wide Angle X-ray Scattering

A *Phillips Norelco* X-ray generator, equipped with a *Statton* camera (Figure 3.1), generating nickel filtered CuKα radation at 40 kV and 25 mA was used to obtain wide angle X-ray film patterns of as-spun, drawn fibers, and unoriented films. The camera was aligned and calibrated using highly oriented Spectra® polyethylene fibers. Fibers were mounted as a parallel bundle on a flat collimator with the fiber axis normal to the x-ray beam. PEA film samples were mounted directly onto the collimator. To minimize x-ray scattering due to air, a vacuum pump was connected to the camera to remove the air. Wide angle x-ray scattering fiber and film patterns were obtained for a specimen to film distance of 5 cm. Several fiber patterns were also obtained at a specimen to film distance of 17 cm. The purpose of these patterns was to get more accurate information in the 2-15 degree 2θ range. The exposure time for wide angle patterns at 5 cm distance was 6 hours, while 36 hours was required for the patterns made at 17 cm distance. Following the exposure process, films were developed in *KODAK* industrex developer for six minutes, rinsed in water and fixed in *KODAK* rapidfix for ten minutes. The films were then washed in water and dried.

Wide angle X-ray diffraction scans were obtained for the PEA specimens using a *Rigaku* X-ray diffractometer in the reflection mode. The equipment was run at 40 kV and 35 mA

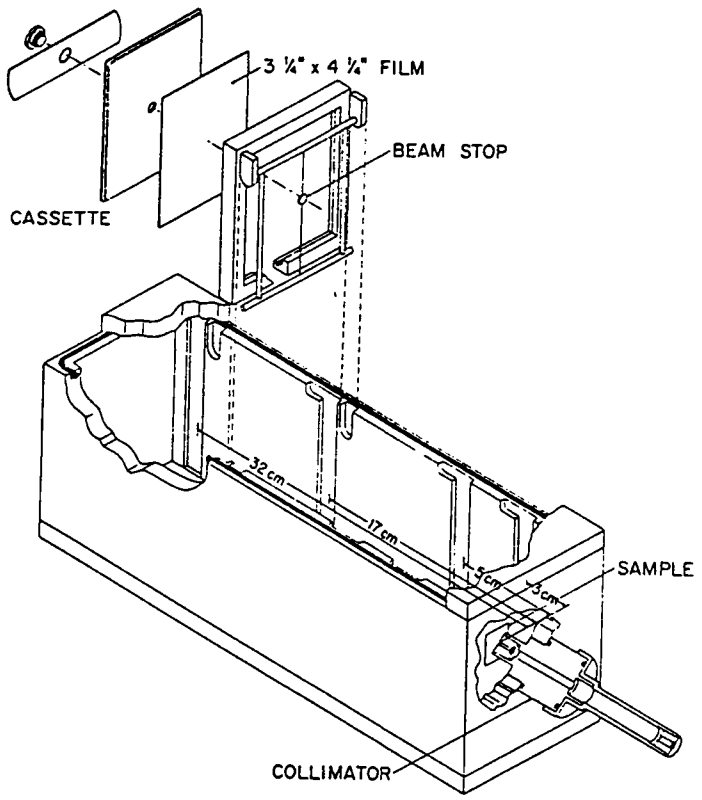


Figure 3.1 X-ray diffraction camera designed by W. O. Statton.

Source: Fred Billmeyer, in Experiments in Polymer Science. John Wiley & Sons, 1973.

over a 2θ range of 3° to 50°. The radiation was monochromated with a graphite crystal monochromator.

3.3.4 Density

The density of PEA 6,2 and PEA 6,2 copolymer films and as-spun and drawn fibers were determined using a sodium bromide density gradient column prepared according to the ASTM standard D1505-68 (68). Two different concentrations of sodium bromide were used to establish a linear density gradient over the range of 1.21 to 1.35 g/cm^3. Glass beads of known density were used to establish a calibration curve for the column. Prior to testing, the samples were immersed in the excess sodium bromide solution and spun in a clinical centrifuge to remove any entrapped air. Specimens were then dropped into the density gradient column and their column height position read after five hours. Using the calibration curve, the density of the fiber sample was calculated from its column height value. PEA 10,2 fibers were tested in a toluene/carbon tetrachloride DGC (54).

3.3.5 Differential Scanning Calorimetry

A *Perkin-Elmer* series 7 thermal analysis differential calorimeter connected to a *Perkin-Elmer* 7500 professional computer and TAS7 instrument controller was used to study

thermal transitions of PEA fibers. An indium standard was used to calibrate the instrument. A baseline was optimized from 0° C to 175° C for the PEA 6,2 samples and from 0° C to 150° C for the samples made from the proprietary PEA 6,2. A sample of 8-10 mg was sealed in hermetic DSC pans and heated at a constant rate of 10° C/min. The PEA 6,2 specimens were heated and cooled twice from 0° C to 175° C. The proprietary PEA 6,2 fibers were heated and cooled twice from 0° C to 150° C. Scans obtained from these tests were plotted on the HP 7470A plotter connected to the DSC7.

3.3.6 Dynamic Mechanical Analysis

Dynamic mechanical analysis studies were conducted on the PEAs to study the thermal relaxation behavior of the polymers. A rheovibron model DDV-II-C manufactured by *Toyo Baldwin Co.* and connected to a *Hewlett Packard* computer was used for these studies. The specimen holder was aligned prior to mounting the film sample. Samples were tested over the temperature range of -100° C to 150° C at a heating rate of 1° C/min under a constant flow of cool, dry nitrogen gas. The sample chamber was cooled to the starting temperature with liquid nitrogen and then covered to prevent rapid heat gain. Data was obtained on the storage modulus E', loss modulus E'', and loss tangent tan δ as a function of temperature at 1.1 Hz, 11 Hz, and 110 Hz.

Chapter 4

RESULTS AND DISCUSSION

The poly(ester-amide) family of polymers are still in their developmental stages and are synthesized in very small quantities. In order to obtain the desired end-use properties, many issues with regard to polymer synthesis need to be resolved. These issues include optimal molecular weight, thermal stability, control of crosslinking, and *in vivo* absorption rate of the polymer. The fiber research group at The University of Tennessee has worked with two types of PEA polymers formed from different diacids, and of different molecular weights, and one PEA copolymer. These polymers include PEA 10,2, PEA 6,2 and a copolymer of PEA 6,2 synthesized with 20 mole % of a proprietary diacid. The PEA 6,2 copolymer was synthesized in hopes of decreasing the absorption time, while maintaining the strength of the PEA 6,2. This chapter includes preliminary information about the PEAs investigated, processing conditions for these materials, and also characterization of resulting fibers. All of the information on PEA 10,2 and some data on PEA 6,2 is taken from reference 54 . This reference should also be referred to for a more in depth discussion of the processing and characterization of PEA 10,2 and its fibers.

4.1 PRELIMINARY INFORMATION

4.1.1 Thermal Transitions

4.1.1.1 Melting Temperature

The melting temperatures of the PEAs were obtained for unoriented films using a Differential Scanning Calorimeter. Peak melting temperatures were 161° C, 145° C, and 130° C for PEA 10,2, PEA 6,2 and the PEA 6,2 copolymer, respectively. The melting temperature at the peak of the endotherm is about 15°C lower for PEA 6,2 than PEA 10,2. Furthermore, the incorporation of 20 mole % of the proprietary diacid into PEA 6,2 lowers the melting point by another 15° C. These differences observed are believed to be associated with the differences in chemical structure of the polymers.

In all cases, the PEA polymers underwent some "annealing" during heating on the DSC. This effect was greatest for the proprietary PEA 6,2 copolymer. Figure 4.1 , displays the first (solid line) and second (dashed line) heating ramps of a PEA 6,2 copolymer fiber drawn 1.56X at 25° C. The first heating ramp for the oriented sample deviates slightly from the baseline above 50° C before melting, indicating additional crystallization during heating. The sample was then cooled from the melt to 0° C at 10° C/min and

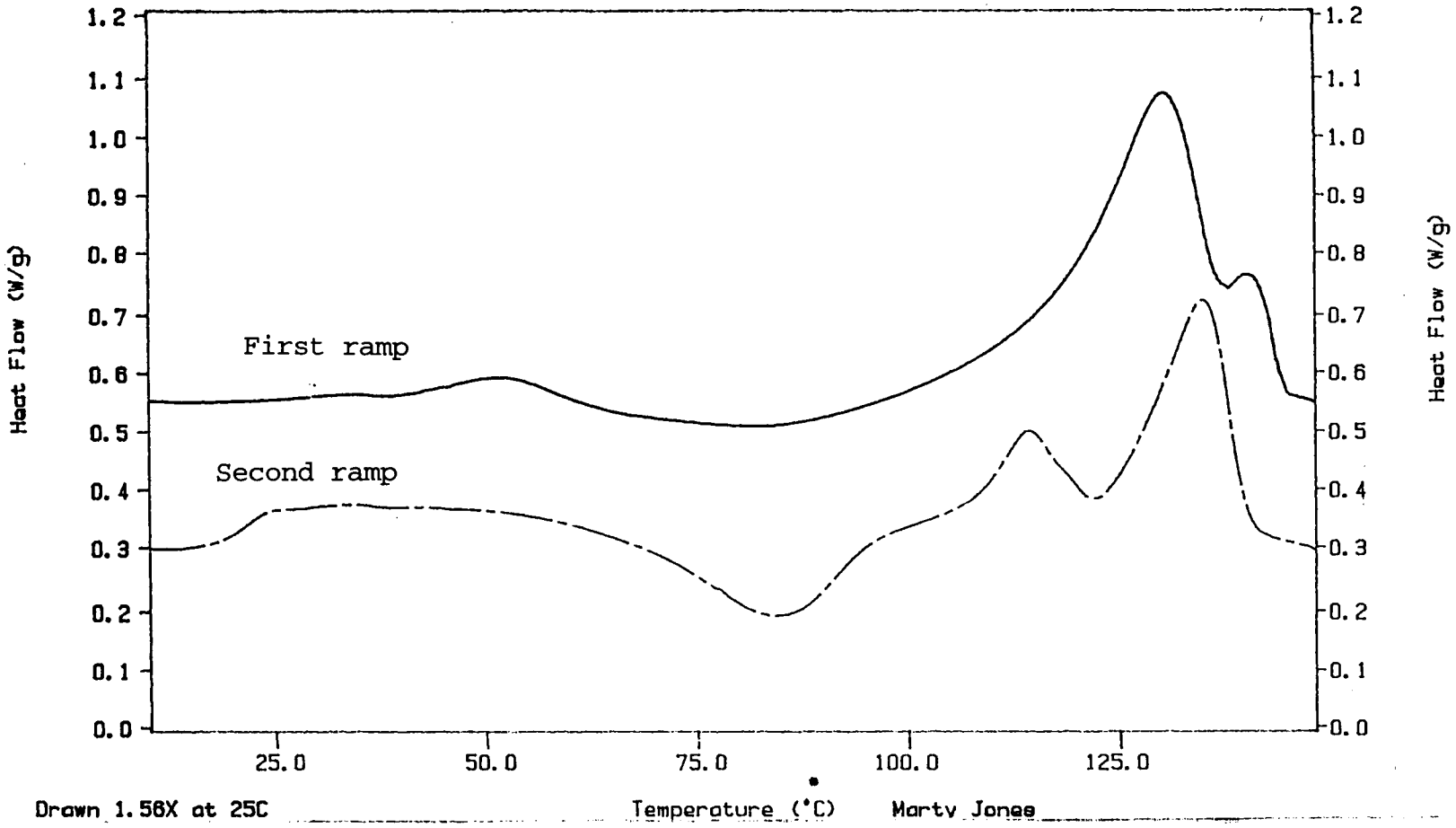


Figure 4.1 DSC plot of first and second heating ramps of Pro1252 fiber.

reheated. Therefore, the second heating is representative of an unoriented sample. A glass transition is clearly seen around 20° C, and then the sample crystallizes during heating as seen by the exotherm around 80° C, prior to remelting. This curve clearly displays the polymer's sluggish crystallization kinetics.

Two melting peaks were also observed for PEA 6,2 and the proprietary PEA 6,2 copolymer fibers and films. PEA 6,2 samples display the first peak temperature between 142-143°C, while the second peak temperature occurs between 153-154°C. For the proprietary PEA 6,2, the first peak temperature occurs around 130°C, while the second peak temperature appears around 141°C. In both cases, the first peak increases with increasing draw ratio, while the second peak diminishes. This could be due to disruption and tearing apart of the crystalline regions during drawing. During the second heating, the second peak is very small or disappears entirely. Possible explanations for the occurrence of the two peaks include:

1.) Phase separation in the polymer.
2.) The material may be crosslinked.
3.) More than one crystal structure is formed during solidification of the polymer.

4.) The morphology of the crystals may exist in two types- one with a greater lamellae thickness than the other.

The first option is not likely for PEA 6,2 because the polymer formed is an alternating copolymer synthesized in two stages. In the first stage, one mole of a diamine is reacted with two moles of glycolic acid to form a diamidediol (an end capping reaction), releasing water in the process. In the second stage, the diamidediol is reacted with a diacid chloride, producing an alternating PEA polymer. Consequently, a block copolymer can not be formed from the reactants involved in the synthesis of PEA homopolymers, although crosslinking of polymer chains through the amide groups is possible if the reaction proceeds too long or at too high of a temperature. However, it is possible for blocks to be formed for the proprietary copolymer. In this case, two diacid chlorides are present and can react with the diamidediol, each forming different repeat units, which can connect with the same repeat unit or the other repeat unit, depending on the concentration of the diacid in that region. Crosslinking can also occur for the proprietary PEA 6,2 copolymer as in the case of the PEA homopolymers. Consequently, the analysis of the proprietary copolymer is very complicated.

Multiple melting peaks have been reported for polyamide 66 and polyamide 6 (69). Magill and Cannon et al. have postulated that the multiple melting peaks observed for polyamide 66 may be due to different types of spherulites present, each type having a different melting point (70, 71). Wunderlich has reported the presence of multiple melting peaks at heating rates lower than 20°C/min for polyamide 6, with increases in magnitude and occurrence of peaks at lower heating rates. These multiple peaks are believed to be due to reorganization or recrystallization of originally, poorly crystallized polymer during the heating (69).

A decision was made not to pursue the cause of the multiple melting peaks, instead focus was turned to establishing processing conditions for these materials. However, it would be helpful to study the crystallization kinetics of the PEA to gain a better understanding of these materials.

4.1.1.2 Glass Transition Temperature

Determination of glass transition temperature was only marginally successful using the DSC. Therefore, the glass transition temperatures (T_g) of the PEAs were determined from dynamic mechanical analysis. The T_g was determined from the peak of the loss tangent curve as a function of temperature for a frequency of 11 Hz. T_g results of oriented PEA 10,2 and

PEA 6,2 fibers have been previously reported (54). In these studies, the T_g was obtained for unoriented films of PEA 6,2 and the PEA 6,2 copolymer cooled in air or a water quench bath. For PEA 6,2 and PEA 6,2 copolymer specimens, three peaks in the loss tangent curve were observed below the polymer's respective melting point. These tan delta and storage modulus curves as a function of temperature are shown in Figures 4.2-4.5. Table 4.1 lists the temperatures corresponding to these peaks and the T_gs reported previously for oriented fibers.

The first peak, γ, occurs at very low temperatures and is associated with the methylene groups present in the polymer. The second peak, corresponding to the β transition has two maxima. This phenomena has also been reported for polyamide 66. It is believed that the first peak is associated with the presence of water, which breaks up the hydrogen bonding between the polymer chains, resulting in the lower transition. The other one is related to a structural characteristic present in quenched specimens, but not in slow cooled or annealed specimens (72, 73). The two β peaks may also be explained in terms of two amorphous regions, unrigid amorphous and rigid amorphous. For this interpretation, the unrigid amorphous corresponds to the β_1 peak, and the rigid amorphous represents the β_2 peak. For either interpretation, the maxima of the β_1 peak is believed to be the T_g, and this temperature corresponds well with the observed drop in the

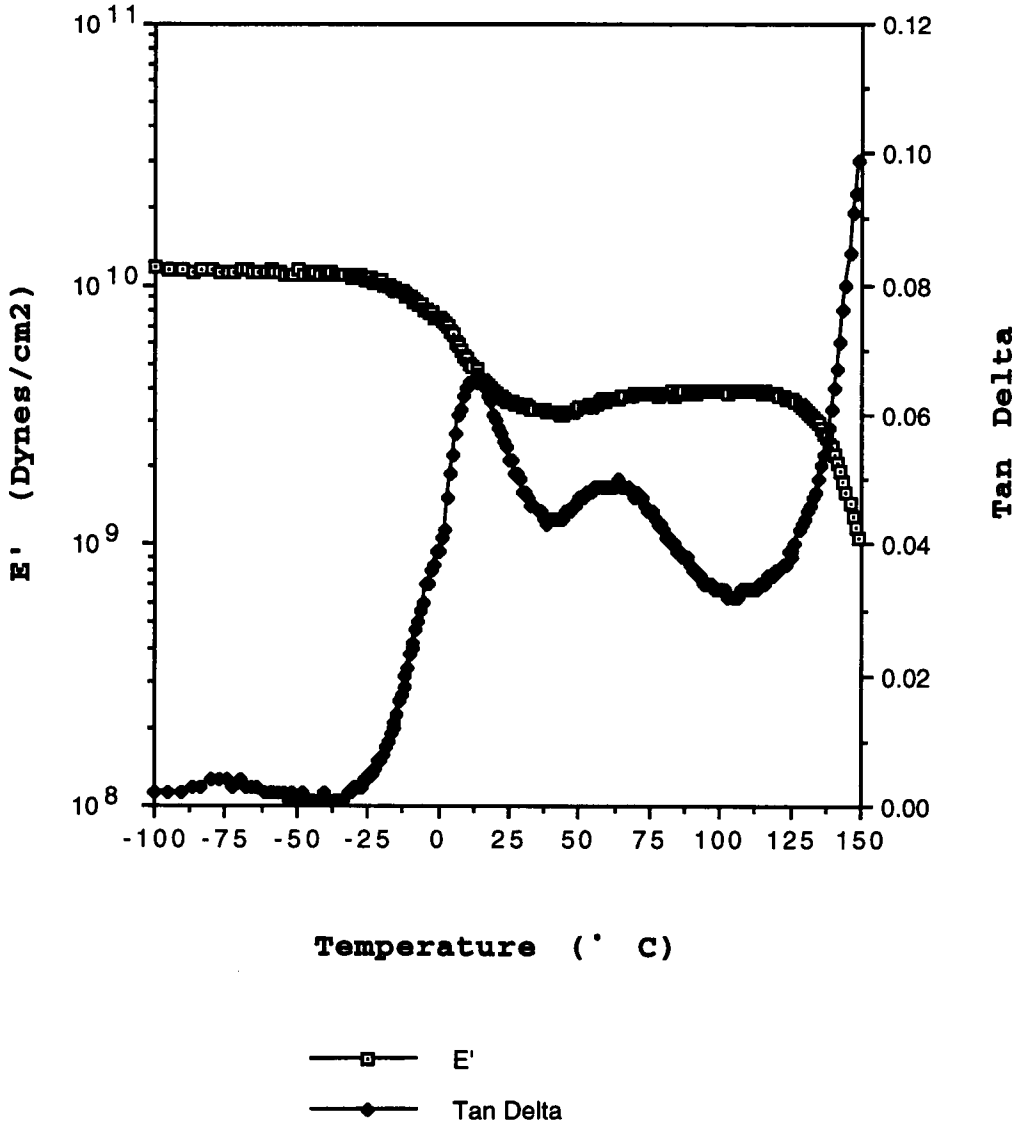


Figure 4.2 Tan delta and storage modulus as a function of temperature for air cooled PEA 6,2 unoriented film.

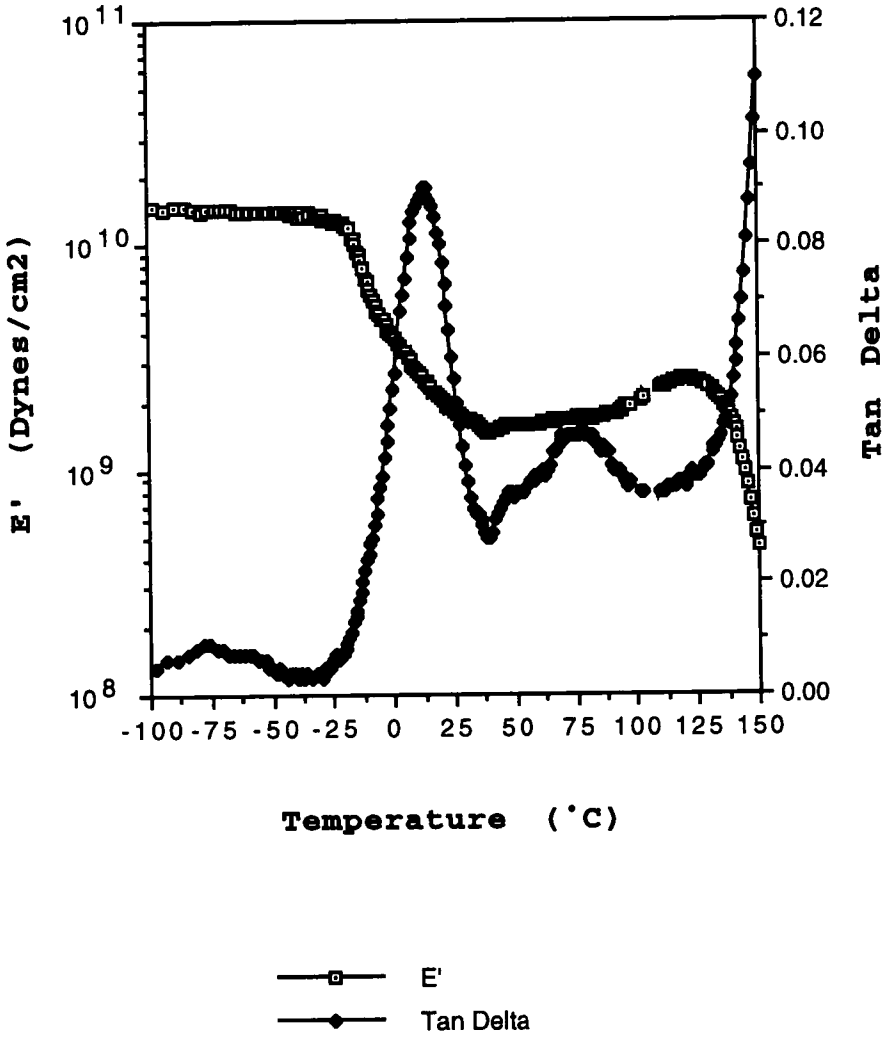


Figure 4.3 Tan delta and storage modulus as a function of temperature for water cooled PEA 6,2 unoriented film.

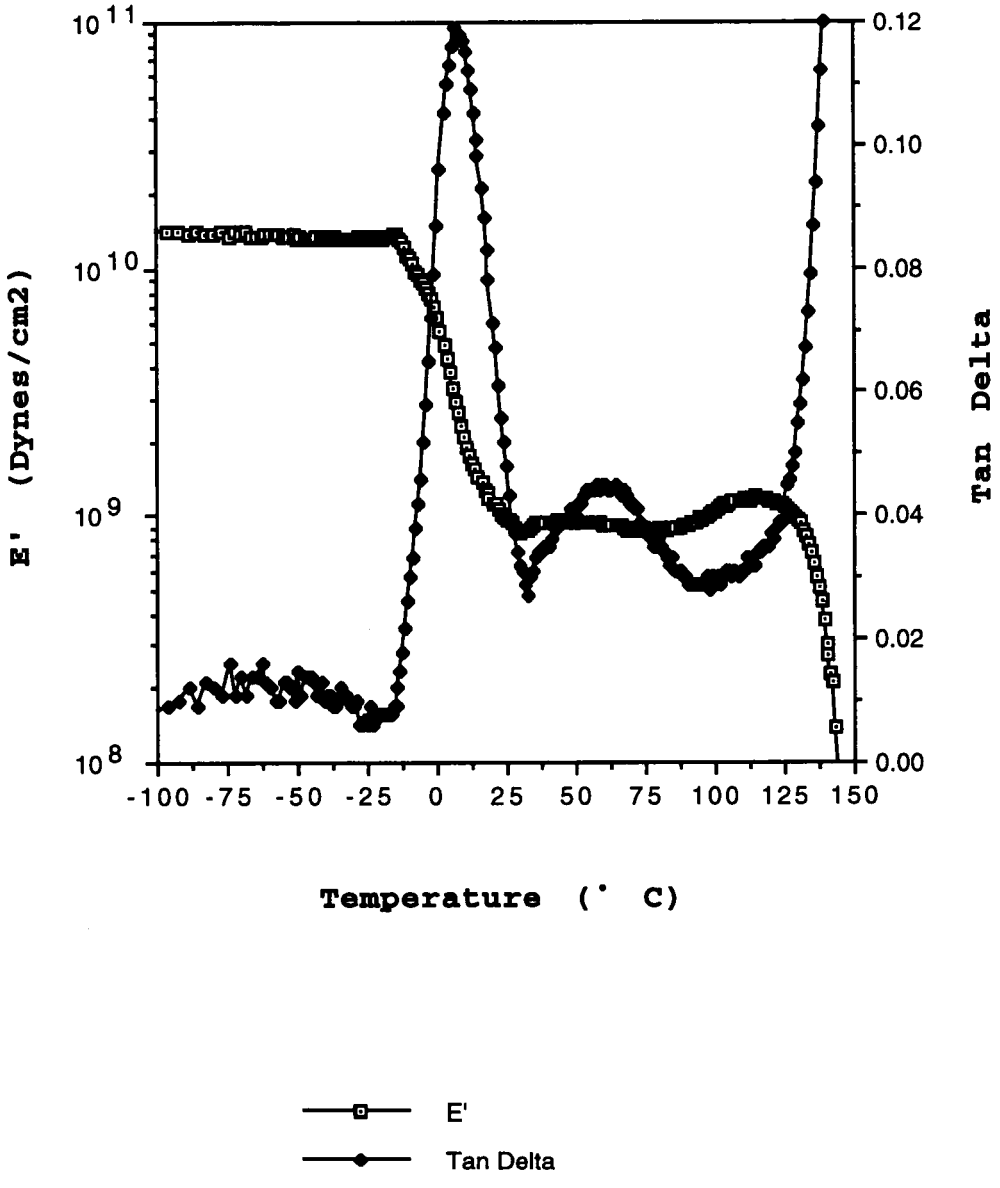


Figure 4.4 Tan delta and storage modulus as a function of temperature for air cooled PEA 6,2 copolymer unoriented film.

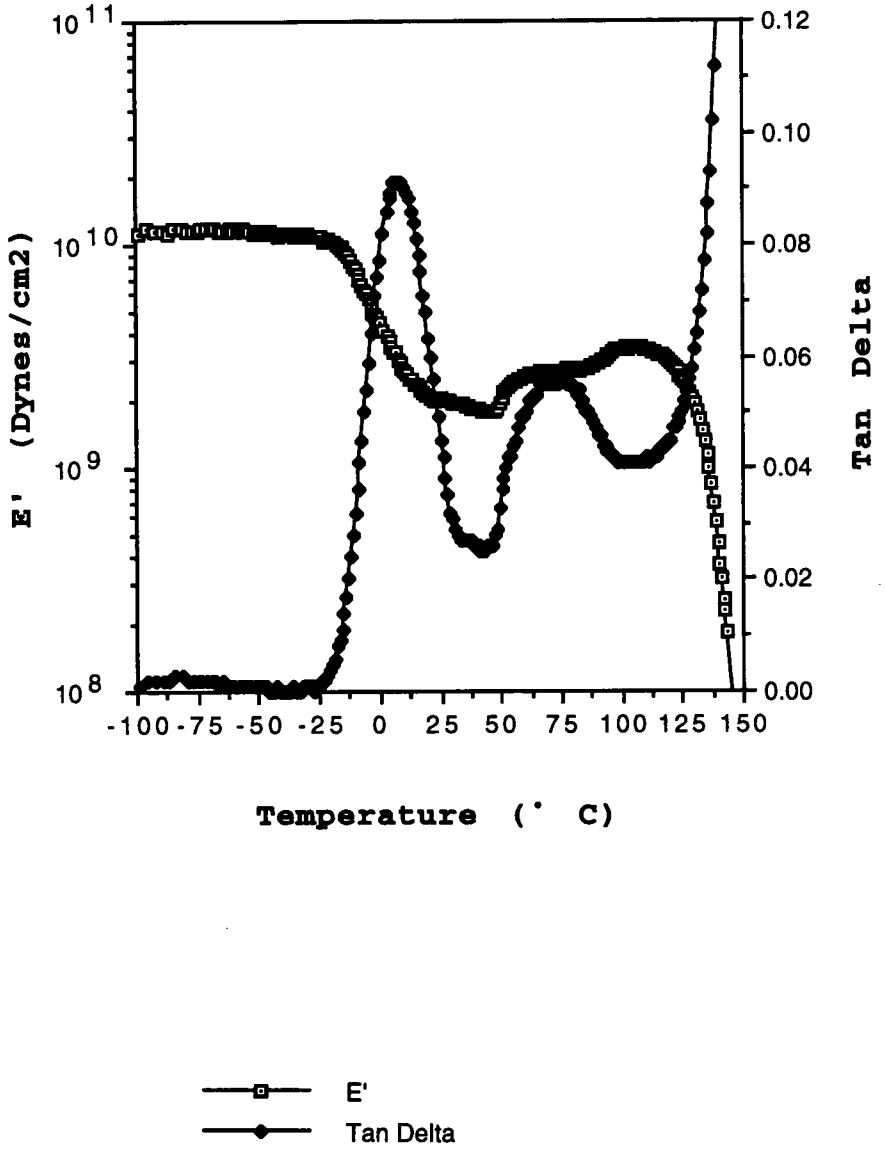


Figure 4.5 Tan delta and storage modulus as a function of temperature for water cooled PEA 6,2 copolymer unoriented film.

Table 4.1 Results of glass transition studies on PEA polymers using dynamic mechanical analysis.

Sample Description	Tg (°C)	Gamma Peak (°C)	Beta 1 Peak (°C)	Beta 2 Peak (°C)
PEA 10,2 fiber *	55			
PEA 6,2 fiber*	45			
PEA 6,2 air cooled film	23.3	-75.5	23.3	60.4
PEA 6,2 water cooled film	13.6	-78.3	13.6	77.4
PEA 6,2 copolymer air cooled film	8	-77.5	8	60.8
PEA 6,2 copolymer water cooled film	5.6	-84.1	5.6	75.3

* Source: D. D. Agrawal, "Processing and Characterization of Poly(ester-amide) Monofilaments." Master of Science Thesis in Polymer Engineering, The University of Tennessee, Knoxville, December, 1993.

modulus curve for all of the samples.

The T_g of PEA 10,2 oriented fiber is found to be about 10°C higher than PEA 6,2 oriented fiber. This change is of the same magnitude as the peak melting temperature measured using the DSC. Additionally, the T_g of unoriented PEA 6,2 films was found to be 23°C, nearly 20°C lower than the oriented fiber. This difference is believed to be associated with the orientation present in the fiber, which restricts the relaxation process of the amorphous regions, requiring more thermal energy input to cause the transition. A difference in T_g was also observed for the unoriented film samples cooled by the two techniques. The T_g of samples cooled in water were 10°C lower than similar air cooled films for PEA 6,2 and about 3°C lower for PEA 6,2 copolymer ones. This decrease is evidently due to the water, which acts as a plasticizer, increasing the mobility of the polymer chains and lowering the transition temperature.

4.1.2 Enhancement of Crystallinity

Two different annealing techniques were used to obtain improved resolution of the crystalline reflections and to obtain an idea of the maximum attainable crystallinity for PEA 6,2 and the PEA 6,2 copolymer. Amorphous films of these materials were annealed thermally in a vacuum oven and in water for three hours. The annealing temperature chosen

corresponds to the peak exotherm temperature obtained from the DSC cooling curves for the amorphous films. For PEA 6,2, this temperature is 92° C, but only a slight exotherm was observed for the copolymer, due to its sluggish crystallization kinetics mentioned previously. For the PEA 6,2 copolymer an annealing temperature of 82° C was chosen. Figure 4.6 displays the DSC cooling curves for the two materials. The dashed line corresponds to the PEA 6,2 film and the solid line represents the PEA 6,2 copolymer film.

WAXD scans and flat plate film patterns were taken of the amorphous and annealed films and are shown in Figures 4.7-4.12. WAXD scans were taken in the reflection mode over a 2θ range of 3° to 50°, while flat plate film patterns were obtained by transmission of x-rays through the sample using a Statton camera. Any x's that appear on the film plate patterns for the film or fiber specimens are marks used for measuring distances on the films.

4.1.2.1 Qualitative Interpretation of X-ray Data

The diffractometer scans display relatively low amounts of order for the amorphous structures of both polymers as seen by the single broad diffraction peak. With annealing, the intensity of the crystalline reflections increased, while more reflections were resolved and the breadth of these reflections decreased, as seen in the thermally annealed and

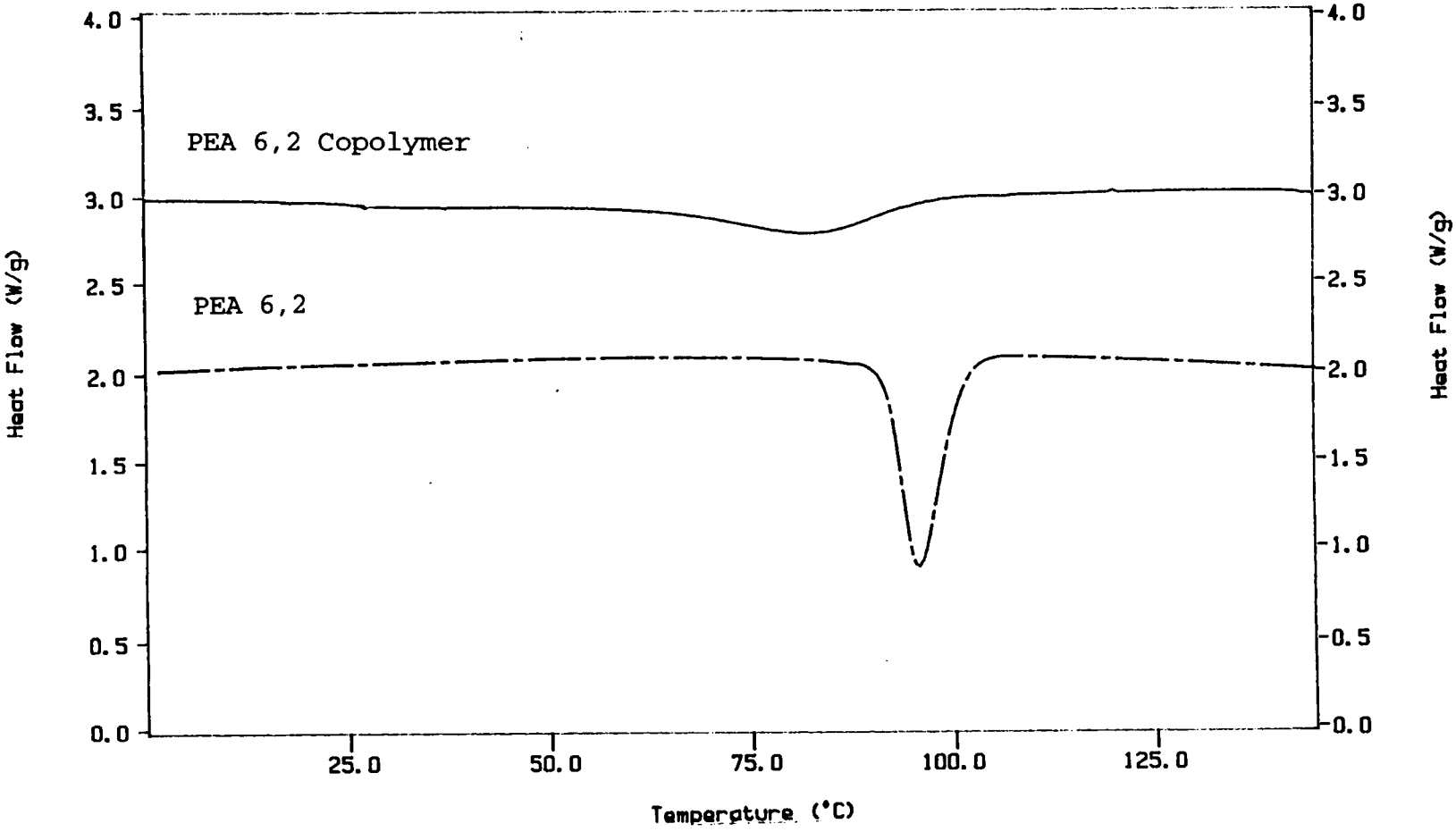
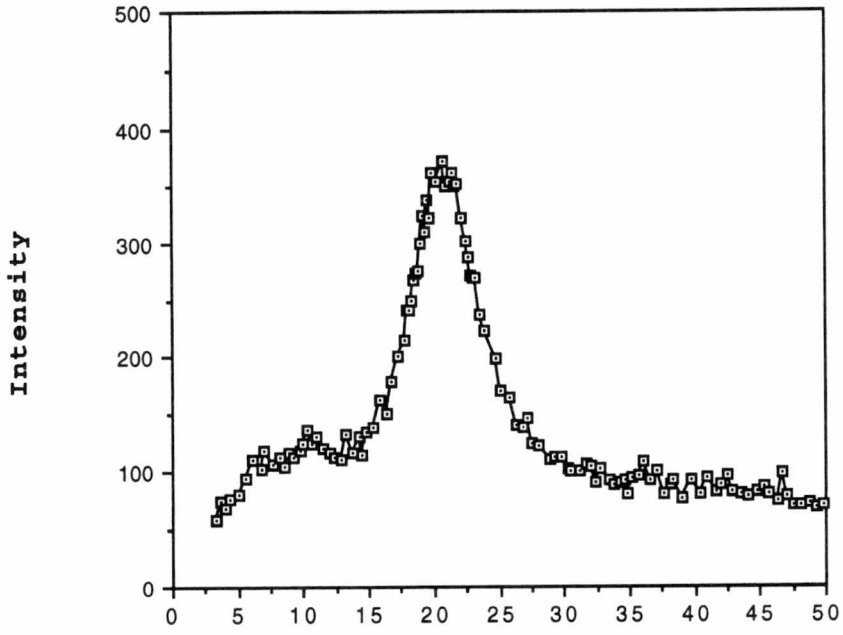
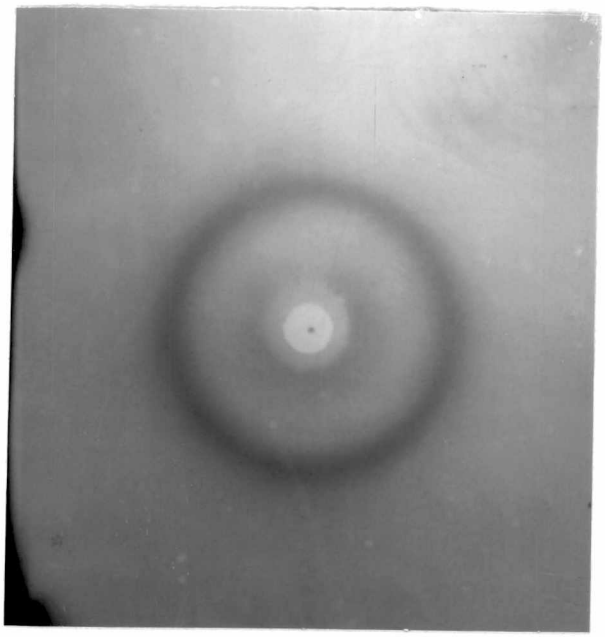


Figure 4.6 DSC cooling curves for PEA 6,2 and PEA 6,2 copolymer unoriented films.

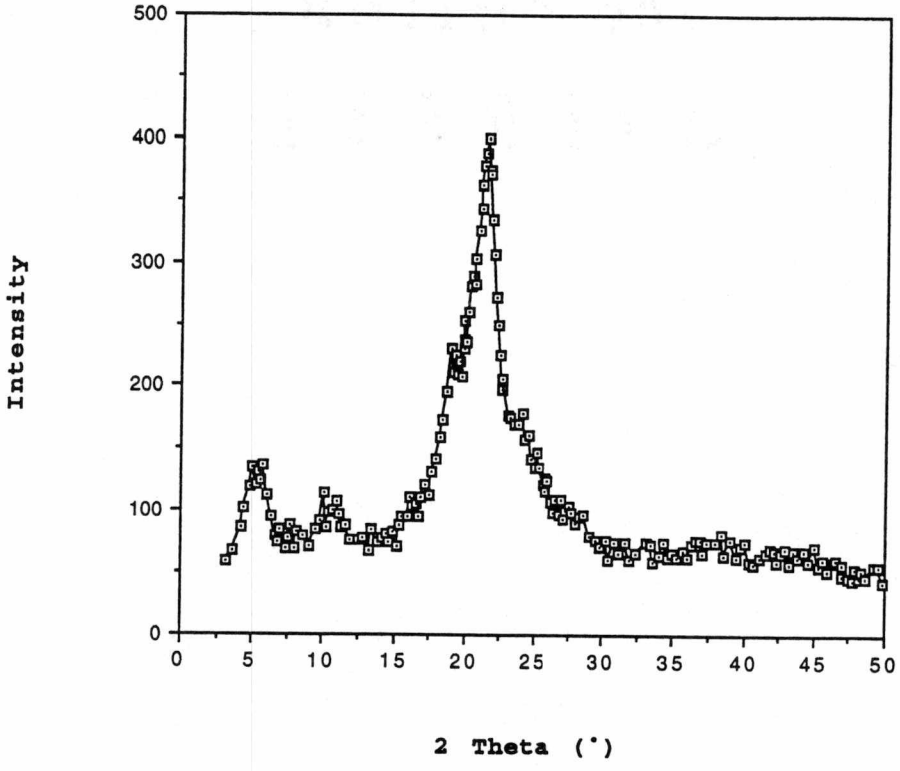


(a)

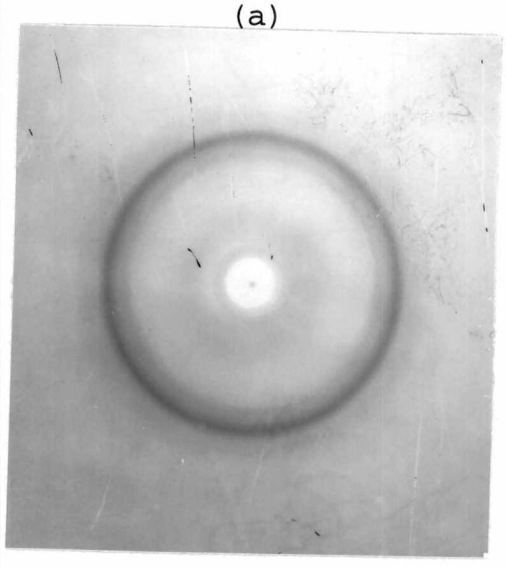


(b)

Figure 4.7 WAXD scan (a) and flat plate film pattern (b) of PEA 6,2 amorphous film.

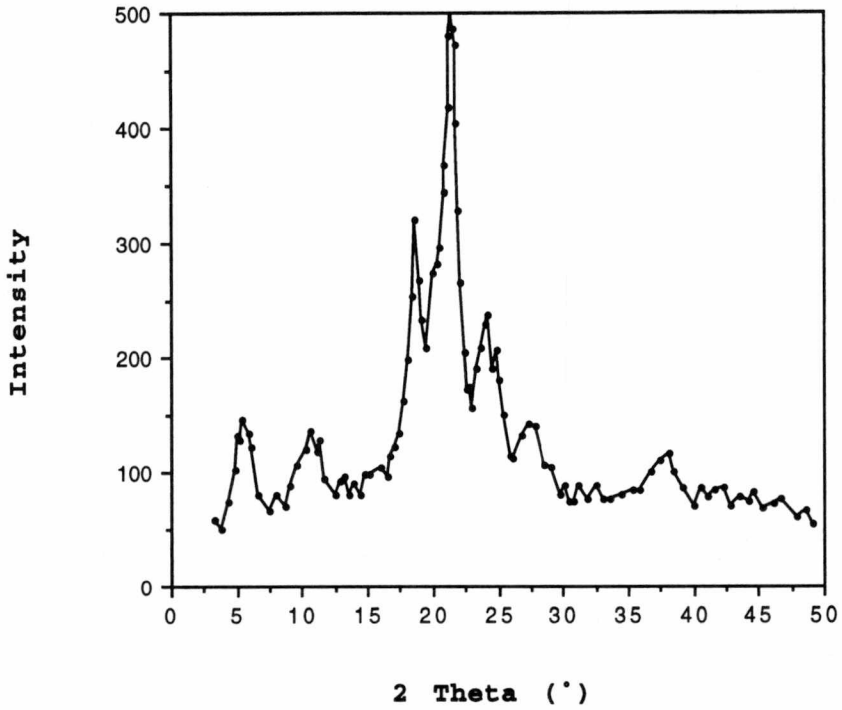


(a)

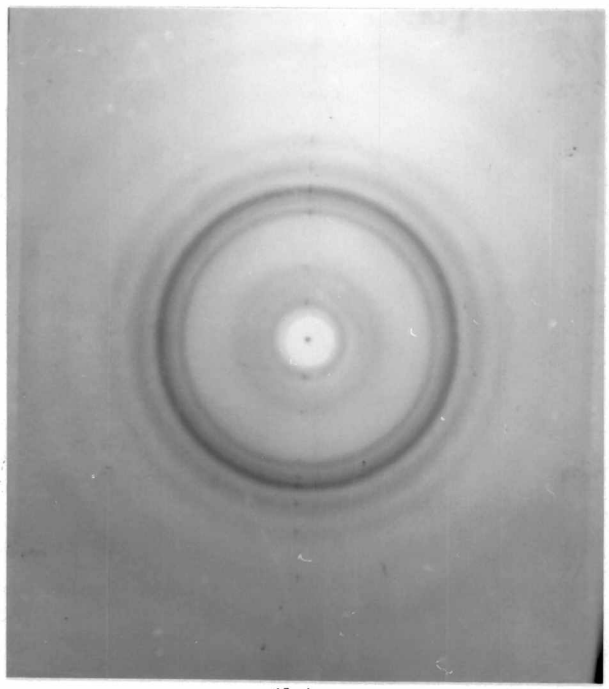


(b)

Figure 4.8 WAXD scan (a) and flat plate film pattern (b) of PEA 6,2 thermally annealed film.

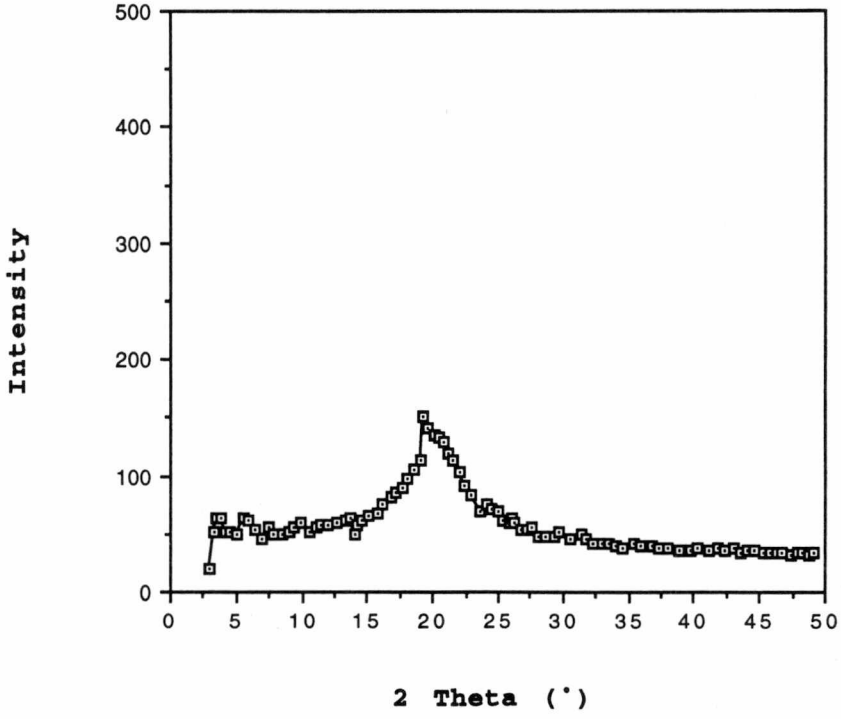


(a)

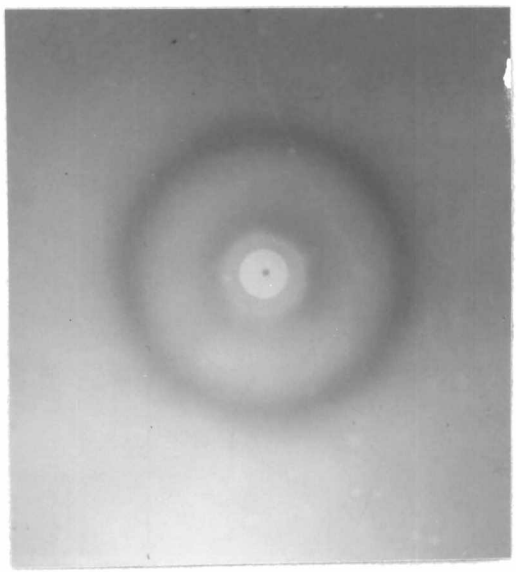


(b)

Figure 4.9 WAXD scan (a) and flat plate film pattern (b) of PEA 6,2 water annealed film.

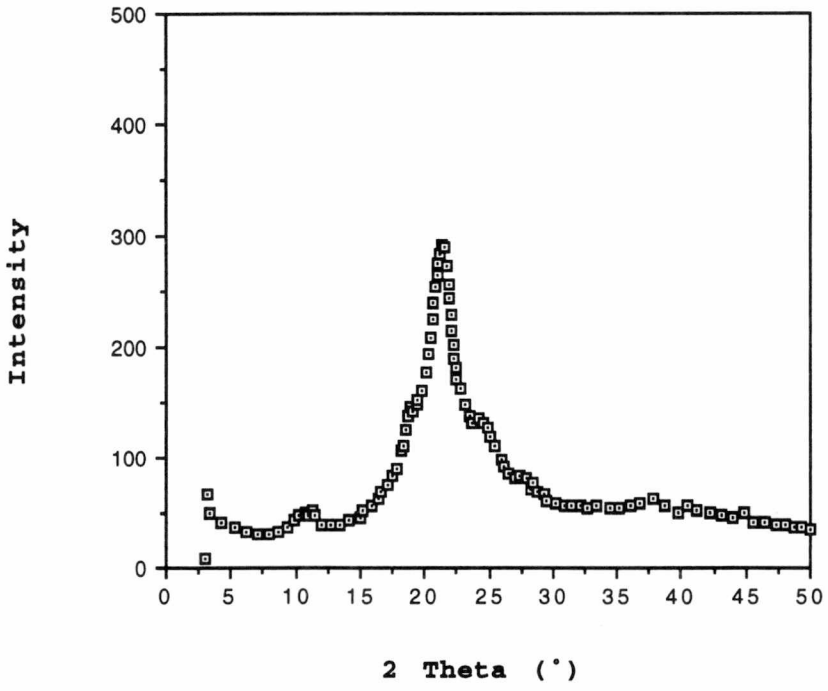


(a)

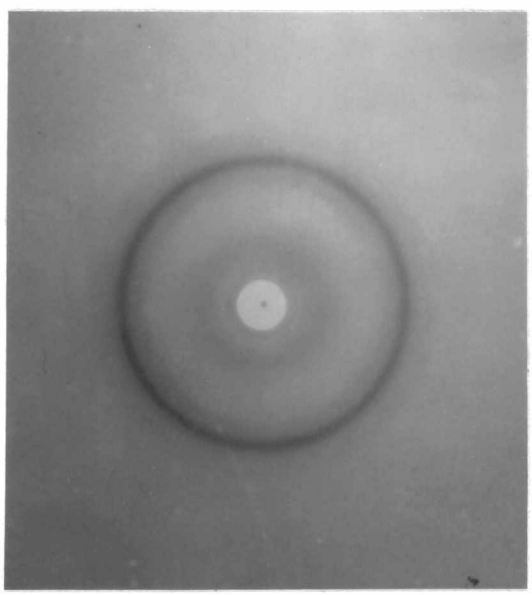


(b)

Figure 4.10 WAXD scan (a) and flat plate film pattern (b) of PEA 6,2 copolymer amorphous film.

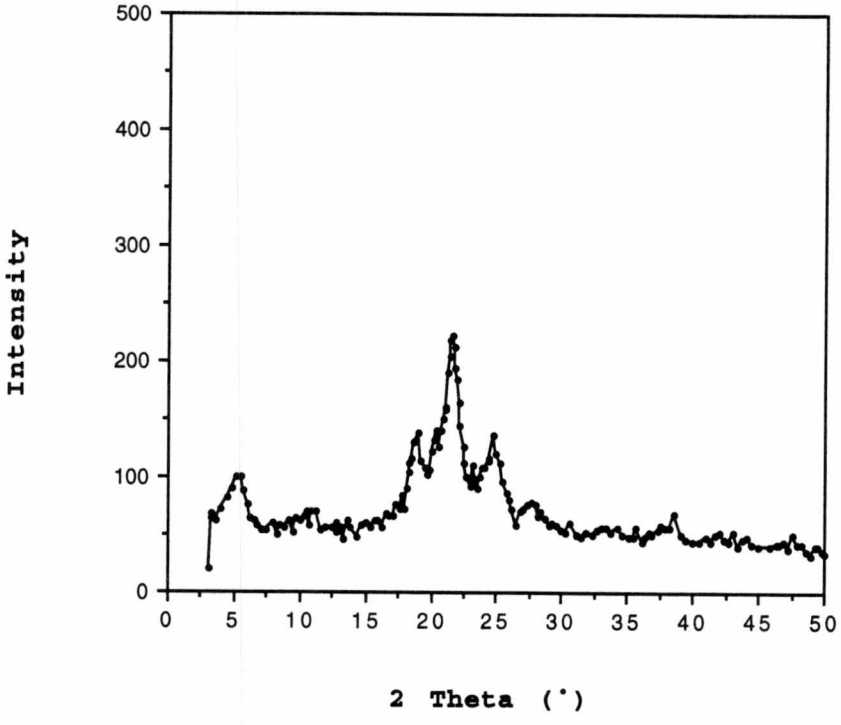


(a)

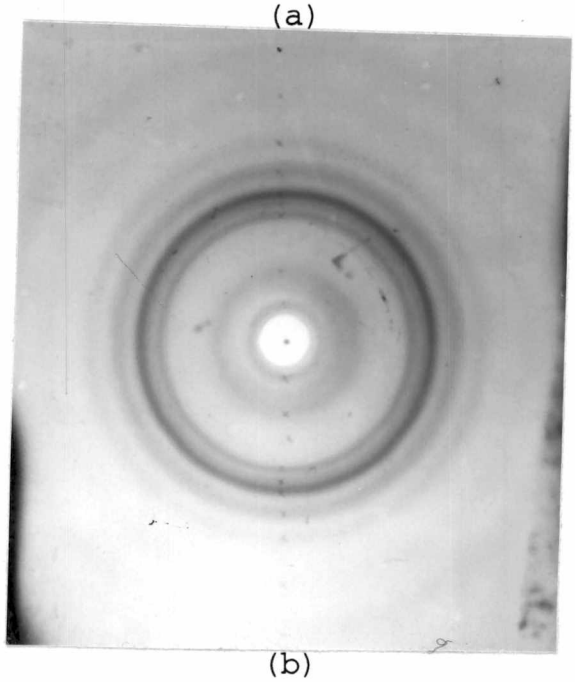


(b)

Figure 4.11 WAXD scan (a) and flat plate film pattern (b) of PEA 6,2 copolymer thermally annealed film.



(a)



(b)

Figure 4.12 WAXD scan (a) and flat plate film pattern (b) of PEA 6,2 copolymer water annealed film.

water annealed diffractometer scans. For both polymers, the crystallinity was enhanced using the two annealing techniques, although water annealing appears to be a more effective method.

Very diffuse rings, indicative of amorphous structures are observed for the flat plate film patterns of the unannealed polymers. The diffraction rings become more numerous, sharper and intense with annealing. The number of rings observed with annealing corresponds with the number of peaks distinguished in the diffractometer patterns, confirming their existence. In the case of the water annealed PEA 6,2 and PEA 6,2 copolymer, nine crystalline reflections were observed over the 2θ range measured using each technique. However, some of these reflections are very weak and difficult to distinguish. It is important to note the similarities observed in the PEA 6,2 and PEA 6,2 copolymer in both the diffractometer and flat plate film patterns. They both display the same number of crystalline reflections for essentially the same 2θ angles, which will be presented in the following section. This indicates that they possess essentially the same crystal structure.

A diffractometer scan of water annealed PEA 10,2 reported previously is shown in Figure 4.13 (54). It is important to note the similarities observed for the PEA 10,2, PEA 6,2 and PEA 6,2 copolymer diffractometer patterns. This data clearly indicates that they all go to one crystal

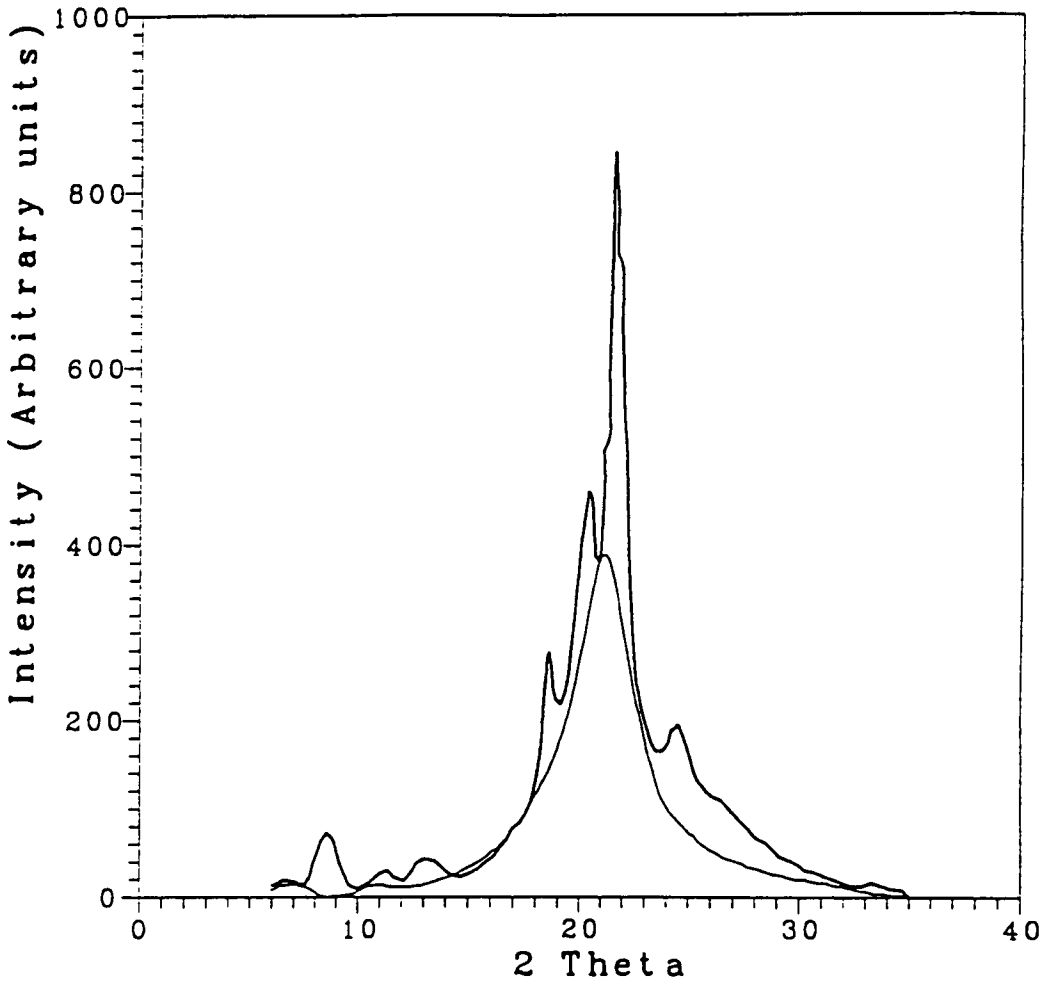


Figure 4.13 Scaled WAXD pattern of PEA 10,2 amorphous film overlaid on the WAXD pattern of PEA 10,2 slow crystallized film.

Source: D. D. Agrawal, "Processing and Characterization of Poly(ester-amide) Monofilaments." Master of Science Thesis in Polymer Engineering, The University of Tennessee, Knoxville, December 1993.

structure with annealing.

4.1.2.2 Quantitative Interpretation of X-ray Data

The d-spacings from the diffractometer scans were calculated using Bragg's Law. The Bragg angle was taken as one-half the angle corresponding to half the width at half the height for each reflection. In the case of the flat plate film patterns, the image produced is the specimen's reciprocal lattice. The diameter of the Debye rings were measured to determine the d-spacings of the crystalline reflections.

The d-spacings and corresponding 2θ angles of the crystalline reflections obtained from diffractometer scans and flat plate film patterns observed for water annealed PEA 6,2 and PEA 6,2 copolymer are listed in Tables 4.2 and 4.3, respectively. The 2θ angle values reported for the diffractometer scans are within ± 0.5° of the average value reported. For the flat plat film patterns, the 2θ values are within ± 0.6° of the reported values. The d-spacing values obtained using the two techniques are within experimental error of each other and therefore are essentially the same. For 2θ angles less than 6°, the d-spacings are within ± 1 Å for both techniques. At these low angles very small differences in where the reflection is measured lead to large variations in the d-spacings calculated for both techniques.

Table 4.2 PEA 6,2 water annealed film crystalline reflections obtained from diffractometer scan and flat plate film patterns.

Line Number	Diffractometer Scan		Flat Plate Film Pattern	
	2 Theta (deg)	d-spacing Å	2 Theta (deg)	d-spacing Å
1	M 5.60	15.8	M 5.25	16.8
2	W 11.10	7.97	W 10.90	8.12
3	M 19.30	4.60	M 18.25	4.86
4	S 20.45	4.34	W 20.20	4.40
5	VS 21.75	4.09	VS 21.20	4.19
6	S 24.75	3.60	S 24.25	3.67
7	M 28.25	3.16	M 27.50	3.24
8	VW 33.45	2.68	VW 33.55	2.67
9	W 38.00	2.37	VW 38.00	2.37

Table 4.3 Water annealed PEA 6,2 copolymer d-spacings obtained from diffractometer scan and flat plate film patterns.

Line Number	Diffractometer Scan		Flat Plate Film Pattern	
	2 Theta (deg)	d-spacing Å	2 Theta	d-spacing Å
1	M 5.2	17	M 5.10	17.3
2	M 10.7	8.27	W 10.6	8.35
3	S 18.75	4.73	M 18.4	4.82
4	S 20.55	4.32	W 20.1	4.42
5	VS 21.55	4.12	S 21.4	4.15
6	S 24.65	3.61	M 24.2	3.68
7	M 27.95	3.19	W 27.4	3.25
8	VW 32.75	2.73	VW 32.8	2.73
9	W 38.05	2.36	VW 37.6	2.39

At the low 2θ angles, the flat plate film pattern data is believed to be more accurate, because of a possible alignment problem with the diffractometer at these angles. At higher 2θ angles, the d-spacing range decreases to less than ± 0.1 Å, and better agreement is observed between the two techniques. Additionally, the crystal structure and accurate crystallographic repeat distance along the unit cell can not be obtained with the annealed film samples. Therefore, oriented fiber samples were examined to attempt to determine these parameters.

4.1.2.3 Oriented Fibers

By measuring the coordinates of the crystalline reflections in terms of x and y, the d-spacings of the crystalline reflections of fiber patterns can be calculated through a series of relations. A film reader manufactured by *Ernest F. Fullam Co.*, was used to read the coordinates of the center of the crystalline reflections, using the center of the film as the origin. The x and y coordinate values, as well as the specimen to film distance, D, were used to calculate the dimensionless cylindrical coordinates of a point *hkl* in reciprocal space, as shown in Figure 4.14.

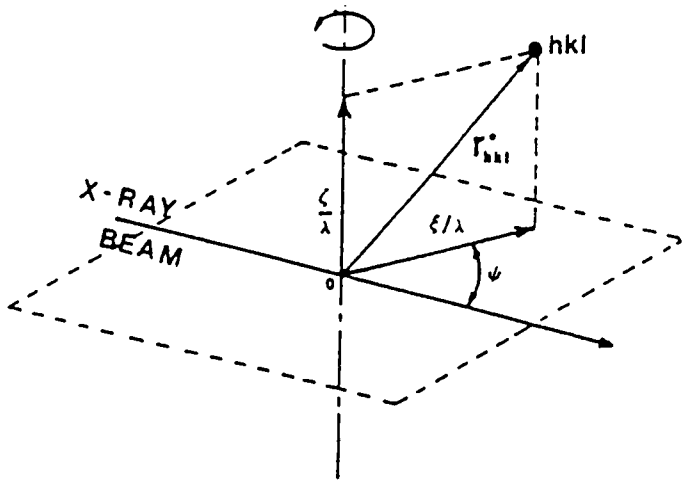


Figure 4.14 Cylindrical coordinates of the point hkl in reciprocal space.

Source: J. E. Spruiell, and E. S. Clark, in "Methods of Experimental Physics, Vol. 16B", Academic Press, 1980.

These dimensionless quantities, ζ and ξ are calculated from the following relations:

$$\zeta = y / (D^2 + x^2 + y^2)^{1/2}$$

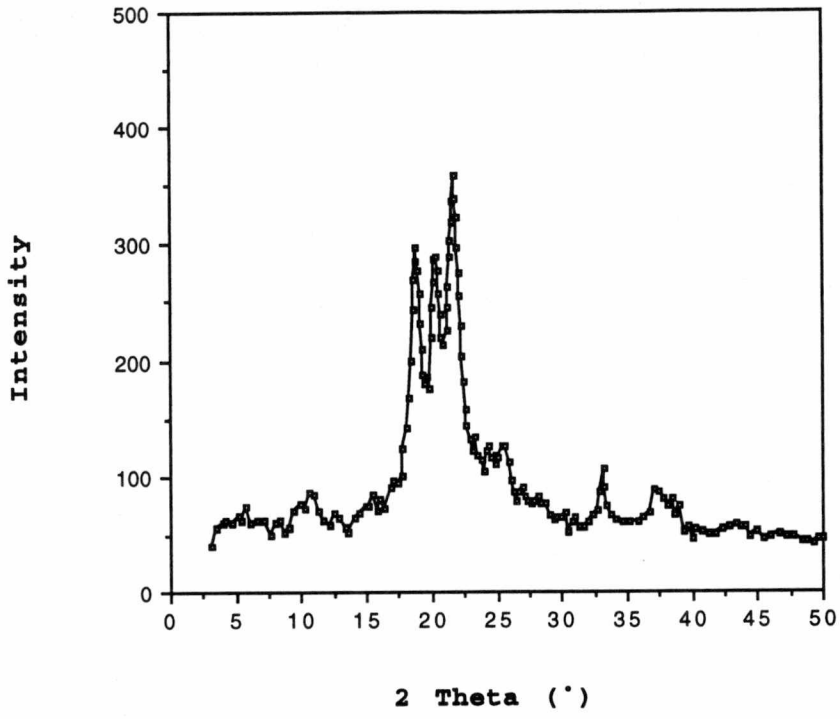
and

$$\xi = [2 - \zeta^2 - 2 (1 - \zeta^2)^{1/2}(D/(D^2 + x^2)^{1/2})]^{1/2}$$

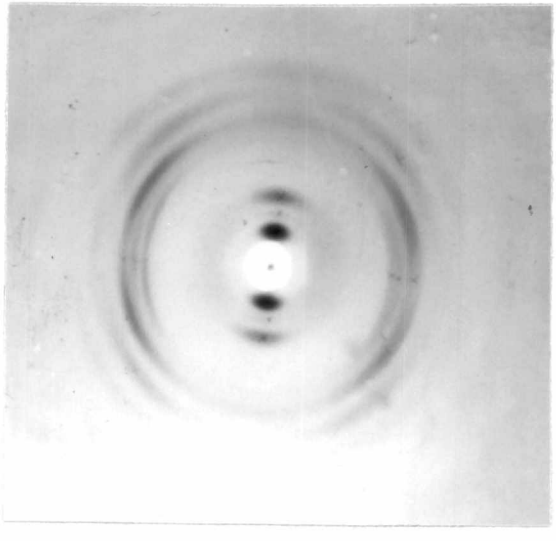
From ζ, ξ and λ, the wavelength of radiation, the interplanar spacing, d can be obtained using the equation below:

$$1/d^2 = | r^* |^2 = (\xi^2 + \zeta^2) / \lambda^2$$

A PEA 6,2 fiber drawn by hand was annealed in water at 92° C for 1.5 hours. The WAXD equatorial scan and the flat plate film pattern for this sample are displayed in Figure 4.15. This fiber pattern was used to categorize the crystalline reflections in terms of meridonal, equatorial or some other type of reflection in hopes of proposing a unit cell structure for the material. A summary of the classification of the reflections, as well as their d-spacings and corresponding 2θ angles is listed in Table 4.4. Nine reflections are observed on the diffractometer scan, but only eight are seen for the flat plate film pattern. It is possible that the other reflection exists, but is too faint to measure. The d-spacings calculated agree well with those presented for the water annealed PEA 6,2 film. Two equatorial reflections are observed. An attempt was made to



(a)



(b)

Figure 4.15 WAXD equatorial scan (a) and flat plate film pattern (b) of PEA 6,2 water annealed fiber.

Table 4.4 PEA 6,2 water annealed fiber d-spacings obtained from flat plate film patterns and equatorial diffractometer scans.

Line Number	Type of Reflection	Flat Plate Film Pattern 2 Theta (deg)	d-spacing Å	Diffractometer 2 Theta (deg)	Scan d-spacing Å
1	Meridonal	S 5.30	16.7	VW 5.25	16.8
2	Meridonal	W 10.50	8.42	W 10.40	8.50
3	Equatorial	M 18.20	4.87	S 18.90	4.70
4	Equatorial	M 19.40	4.58	S 20.60	4.31
5	Other	S 21.20	4.19	VS 21.65	4.10
6	Other	S 24.20	3.68	S 25.05	3.55
7	Other	VW 27.70	3.22	M 28.25	3.16
8	Other	VW 37.70	2.39	W 37.95	2.37

index the pattern on the basis of a pseudo-orthorhombic unit cell. On this basis, the two equatorial reflections could be indexed as (100) and (010), with $a \simeq 0.487$ nm and $b \simeq 0.458$ nm. A crystallographic repeat distance of approximately 1.67 nm was calculated for the water annealed fiber, which is consistent with the d-spacing reported for the first reflection of the PEA 6,2 unoriented film.

Flat plate film patterns were also made of several PEA 6,2 unannealed, drawn fiber specimens to obtain d-spacings for the crystalline reflections and observe the changes in the crystallographic repeat distance with orientation. These pattern were also used to get an idea of the overall orientation and crystallinity of these materials, which will be discussed further in the characterization section. Figure 4.16 displays 5 cm and 17 cm film patterns for fiber 71580, drawn 4.05X at 80°C and its as-spun precursor, 715. Two meridonal layer lines are shown for the as-spun and drawn fibers and were indexed as the (001) and (002). The first plane was used to calculate the chain axis crystallographic repeat distance of the polymer structure. Table 4.5 lists the values obtained for the two fibers at 5 cm and 17 cm. Since the values obtained for these two distances are within experimental error, only 5 cm patterns were obtained for samples.

An approximate chemical repeat distance 18.606 ± 0.018 nm was calculated for PEA 6,2 by subtracting the distance of

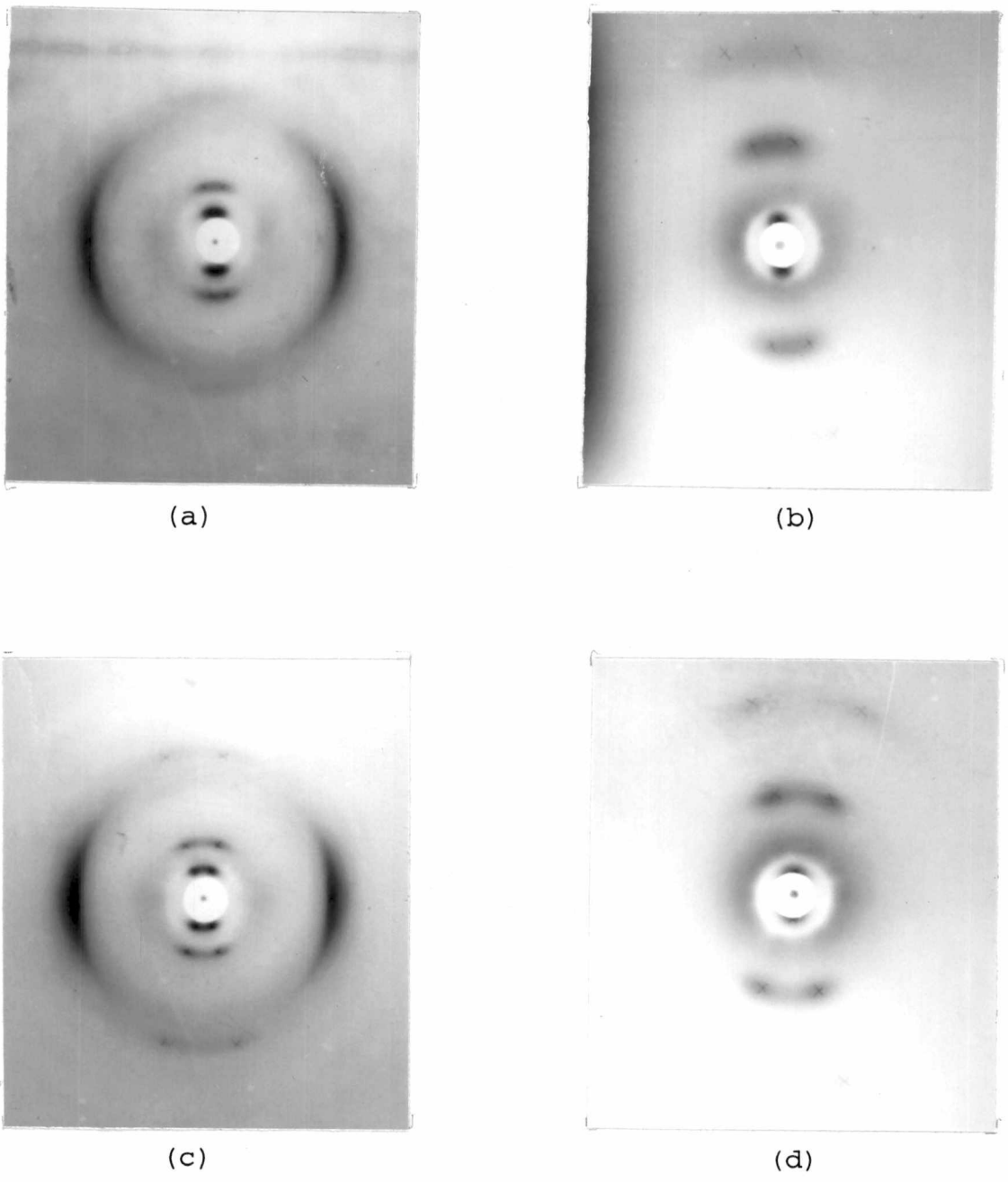


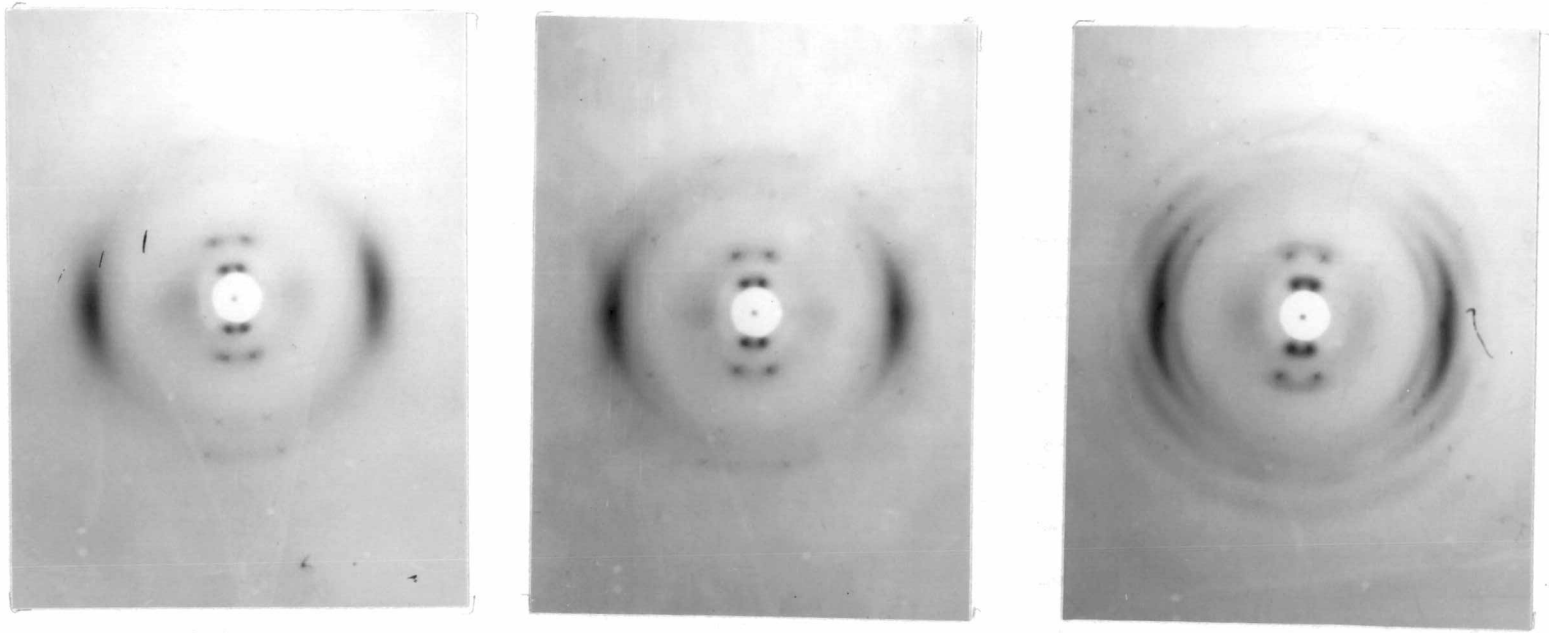
Figure 4.16 Flat plate film patterns of PEA 6,2 fibers. (a) 715 (5 cm) drawdown ratio 23.3, (b) 715 (17 cm), (c) 71580 (5 cm) fiber 715 drawn 4.05X at 80° C, (d) 71580 (17 cm).

Table 4.5 Crystallographic repeat distance for oriented PEA 6,2 fibers.

Fiber ID	5 cm Pattern	17 cm Pattern
715	17.9 nm	17.6 nm
71580	18.2 nm	17.8 nm

four methylene units from the chemical repeat distance estimated for PEA 10,2 reported in reference 54. This crystallographic repeat distance for PEA 6,2's unit cell agrees well with the chain axis crystallographic repeat distance of approximately 1.79 nm and 1.82 nm observed for the fiber 715 and 71580 fibers, respectively. An increase in the crystallographic repeat distance was observed with drawing, apparently due to the stretching of the polymer chain's axis with respect to the draw direction. The crystallographic repeat distance obtained for the annealed fiber and unoriented film specimens are lower than the estimated repeat distance estimated for the repeat structure. This is possibly due to a slight helical shape or "kink" in the chains caused by annealing the samples in water.

Figure 4.17 displays the 5 cm flat plate film patterns for the following PEA 6,2 copolymer fibers: Pro1255 (drawn 2.71X at 25° C), Pro1451 (drawn 2.71X at 45° C), and Pro1802 (drawn 2.63X at 80° C). The crystallographic repeat distance for the PEA 6,2 copolymer is only slightly higher than that of PEA 6,2. This indicates that the incorporation of the proprietary materials only slightly distorts the repeat distance. Additionally, an increase in crystallographic repeat distance is observed with orientation as seen in Table 4.6. It would be helpful to have a sample of the homopolymer made from the diamidediol and the proprietary diacid to see of the d-spacings of the copolymer relate to the two



(a) (b) (c)

Figure 4.17 Flat plate film patterns of PEA 6,2 copolymer fibers taken at 5 cm. (a) Pro1255, drawn 2.71X at 25° C, (b) Pro1451, drawn 2.71X at 45° C, (c) Pro1802, drawn 2.63X at 80° C.

Table 4.6 Crystallographic repeat distance for oriented PEA 6,2 copolymer fibers.

Fiber ID	Draw Ratio	Repeat Distance 5 cm
Pro1255	2.71	18.5 nm
Pro1451	2.71	19.1 nm
Pro1802	2.63	18.0 nm

homopolymers.

As seen in Figures 4.16 and 4.17, the meridonal reflections split into two symmetrical reflections with drawing for PEA 6,2 and PEA 6,2 copolymer fibers. This phenomena is also observed with drawing of fibers formed from PEA 10,2 (54). This type of pattern has been observed by other researchers for different polymer systems, and the split symmetrical reflections are still assumed to represent the respective layer lines (74). It has been proposed by Blackwell that the unit cell's c axis is tilted at an angle of φ with respect to the draw direction to produce this type of reflection. The tilt is rationalized by the asymmetry of the polymer chains that emerge from the top and bottom of the crystalline lamellae, resulting from staggering of the molecules to form a hydrogen bonded network (74). Other polymers reporting this behavior include poly(ethylene terephthalate) and other polymers with triclinic unit cells (74, 75).

4.1.3 Determination of Crystalline and Amorphous Densities

The crystalline and amorphous densities of the PEAs are needed to estimate the crystalline fraction of various film and fiber samples from density measurements. Therefore, it was necessary to get approximations for the amorphous and crystalline densities. This section discusses the

techniques, problems and results obtained in estimating these densities. It must be emphasized that the purpose of this research project was not to accurately determine the crystal structure of the PEAs. However, rough estimates of the amorphous and crystalline densities are needed to estimate relative crystallinity for various fibers and films.

4.1.3.1 Crystalline Density

The density of the crystalline phase of semi-crystalline materials can be theoretically calculated from the basic building block of the material, the unit cell. In order to determine the dimensions of the unit cell, fiber patterns of highly oriented, highly crystalline fibers are needed. We were not able to obtain x-ray patterns of the high quality necessary to determine the crystal structure accurately. Consequently, the results in this section are only rough estimates for the materials crystal structure and crystalline density.

Possible unit cell structures considered for the PEA polymers include pseudo-hexagonal, trigonal, pseudo-orthorhombic and triclinic. In previous work conducted on PEA 10,2, it was proposed that the PEAs formed a pseudo-hexagonal structure. This option, as well as a pseudo-orthorhombic interpretation were explored for PEA 6,2 and the PEA 6,2 copolymer.

4.1.3.1.1 Pseudo-hexagonal Interpretation

The theoretical crystalline density value for PEA 10,2 was approximated as $\rho_c \simeq 1.31$ g/cm^3, assuming a pseudo-hexagonal cell and one polymer repeat unit per unit cell (54). The estimated unit cell dimensions reported for PEA 10,2 are $a \simeq 0.491$ nm and $c \simeq 2.25$ nm.

The unit cell for PEA 6,2 was also presumed to be pseudo-hexagonal with one polymer repeat unit per unit cell. The flat plate film pattern for unannealed 71580 fiber (drawn 4.05X at 80° C) shown previously in Figure 4.16, was used for the interpretation. One broad equatorial reflection is present and was indexed as (100). The (100) reflection corresponds to a d-spacing of approximately 0.427 nm. The d-spacing of the first meridonal layer line was used for the chain axis crystallographic repeat distance. From these d-spacings, the approximate unit cell parameters of $a \simeq 0.493$ nm and $c \simeq 1.82$ nm were obtained, resulting in a crystalline density of approximately 1.36 g/cm^3.

A pseudo-hexagonal interpretation was also attempted for PEA 6,2 copolymer with one polymer repeat unit per unit cell. Unannealed Pro1802 (drawn 2.63X at 80° C) fiber pattern shown previously in Figure 4.17 was indexed. With the incorporation of the proprietary diacid into the polymer structure, the d-spacings changed to larger values and consequently the unit cell volume increased. The approximate unit cell parameters

are a $\simeq$ 0.513 nm and c $\simeq$ 1.80 nm, resulting in an approximate crystalline density of 1.27 g/cm^3. Although the a and c values estimated for the PEA 6,2 copolymer are within experimental error of those values estimated for PEA 6,2, the estimated crystalline density is considerably lower. The low value for crystalline density can be explained in terms of the changes in the unit cell volume, while the molecular weight of the crystal structure remains constant. The volume of the unit cell for a hexagonal structure is calculated by squaring the value for a and multiplying it by 0.866c. By increasing the value for a, the volume of the unit cell increases. Since the appropriate molecular unit for the PEA 6,2 copolymer is the same as for the PEA 6,2 cell, assuming the copolymer cannot participate in the crystal structure, and the volume of the unit cell increases, the calculated crystalline density decreases.

The density obtained from the DGC for fiber and film samples formed from the PEA 6,2 copolymer were between 1.2960 and 1.3142 g/cm^3 , considerably higher than for a 100 % crystalline material. In light of this data, the pseudo-hexagonal interpretation for the crystal structure of the PEAs is incorrect. A new interpretation of the crystal structure of PEA 6,2 and PEA 6,2 copolymer is proposed assuming a pseudo-orthorhombic structure.

4.1.3.1.2 Pseudo-orthorhombic Interpretation

The PEA 6,2 annealed fiber pattern shown previously in Figure 4.15 was used for the pseudo-orthorhombic interpretation. In this pattern, two equatorial reflections could be distinguished and were indexed as (100) and (010). The approximate unit cell parameters are $a \simeq 0.487$ nm , $b \simeq 0.458$ nm , and $c \simeq 1.67$ nm, resulting in a crystalline density of approximately 1.40 g/cm^3, which agrees well with the theoretical crystalline density of many polyesters.

Previously, the line numbers for the crystalline reflections were indexed in terms of meridonal, equatorial and some other type of reflection for PEA 6,2. Since the same reflections are observed for PEA 6,2 and the PEA 6,2 copolymer, the line numbers corresponding to the equatorial reflections and the crystallographic repeat distance from the unoriented water annealed films were used to estimate unit cell parameters for the copolymer. The approximate unit cell parameters for the PEA 6,2 copolymer are $a \simeq 0.482$ nm, $b \sim 0.442$ nm and $c \simeq 1.76$ nm, resulting in an approximate crystalline density of 1.41 g/cm^3. This value agrees well with that estimated for PEA 6,2, further indicating that the two structures are basically the same.

4.1.3.2 Amorphous Density

Accurate density measurements of quenched (amorphous) PEA 6,2 and PEA 6,2 copolymer films could not be obtained from the sodium bromide density gradient column. It was observed that the films continued to move downwards in the DGC over time, never reaching an equilibrium position. This phenomena was also observed for PEA 10,2 specimens in columns made of both sodium bromide and toluene-carbon tetrachloride solutions. The increase in density was probably due to hydrogen bonding, additional crystallization, and perfection in crystal structure resulting from depression of the T_g caused by the aqueous medium.

A mathematical relationship between the crystalline and amorphous density values has been proposed by Bessonov and Smirnova in 1971. They have observed that for a number of polymers, ρ_c/ρ_a is close to 1.09 ± 0.04. For some aliphatic polyamides and polyesters, this ratio is much larger, while some of the helical polymers have a much smaller ratio (55). Using this relation, an estimate of a material's crystallinity is possible knowing only the unit cell dimensions and the material's density. The ratio for PEA 10,2 was determined from previously reported data and calculated to be 1.086, assuming a pseudo-hexagonal unit cell. Using this value and the theoretical crystalline

density for pseudo-hexagonal PEA 6,2, the amorphous density was estimated to be 1.25 g/cm^3.

The pseudo-orthorhombic interpretation of the PEA 6,2's unit cell appears to give a better fit for the observed data. However, the ratio of crystalline to amorphous density calculated for PEA 10,2 can not be used in this case because it is a different unit cell interpretation. Consequently, a ratio of 1.13, the upper limit proposed by Bessonov and Smirnova was used, resulting in an amorphous density of approximately 1.24 g/cm^3. This is a reasonable approximation since the PEAs are composed of linear, aliphatic amide and ester linkages. These amorphous and crystalline density values were used to determine the relative percent crystallinity of PEA 6,2 samples, which will be addressed in the characterization section.

The amorphous density for the PEA 6,2 copolymer cannot be determined by the above procedure because two different monomer types are present, and we do not know how this affects the density of the amorphous phase. Generally, higher density values were observed for the PEA 6,2 copolymer samples than PEA 6,2 samples, although these materials are less crystalline than the homopolymer. It appear that the amorphous density of polymer produced from the proprietary diacid is much higher than the amorphous density of PEA 6,2, resulting in the higher density values observed.

Although the Bessonov and Smirnova approximation can be used to obtain a rough estimate of the amorphous density of the PEA materials, an experimental method should be developed to determine the density. A new technique for measuring the time dependent density changes in amorphous polymers has recently been published (76). This technique involves measurement of the descent of the sample in the DGC as a function of time, until the sample reaches an equilibrium position. An "aged" sample is first used as a calibration standard, and then it is reprocessed and rapidly cooled. Through a series of force balance equations, the density can be determined. It is also possible to extrapolate to the "time zero" position and estimate the sample's density at this position. It may be possible to use this technique with some slight modifications to determine the amorphous density of the PEAs. It would also be useful as a technique for measuring the density of PEA materials as a function of processing history.

4.2 PROCESSING OF POLY(ESTER-AMIDE)S

A great deal of work has been done in the area of establishing appropriate processing conditions for the PEAs. In the following sections, the effect of polymer characteristics, resulting from the chemical nature and synthesis of the polymer is discussed in relation to the

processing conditions. Discussion of the properties resulting from the different processing operations will be addressed in the characterization section.

4.2.1 Initial Processing of PEA 10,2

Initial work on the processing of the PEA family of polymers was conducted on the *Fourne* extruder with PEA 10,2. For a more detailed description of the processing and characterization of PEA 10,2 on the *Fourne* extruder refer to reference 54. Briefly, it was concluded from these studies that PEAs with an initial IV$\geq$1.0 were adequate for extrusion, A significant drop in molecular weight was observed with processing for these materials, which affected the fiber's drawing behavior and mechanical properties. The optimal draw temperature for PEA 10,2 was found to be in the range of 50°C to 70°C, and a maximum draw ratio of 6.0X was achieved at 70°C. Finally, the draw ratio was found to be dependent on the molecular weight and initial molecular orientation of the fiber. From these initial studies, it was decided to investigate the thermal behavior of this material and try to find ways to preserve its molecular weight during processing.

4.2.2 Thermal Degradation Studies

Thermal degradation studies were conducted on PEA 10,2 to get a better understanding of the factors contributing to the drop in molecular weight. The results of this study are shown in Figure 4.18. From this figure, it can be seen that the molecular weight decreases rapidly in the first few minutes at elevated temperatures. Additionally, the processing temperature contributes to the decrease in molecular weight, although the drop is more strongly associated with time. From these results, it is apparent that decreasing the residence time of the polymer at these elevated temperatures during melt spinning would aid in preserving the molecular weight. It is also important to process the polymer at the lowest possible temperature while still maintaining a stable continuous spinline.

Several possible options for reducing the polymer degradation problem include: improving the thermal stability of the polymer, decreasing the shearing and residence time during processing, or by reducing the processing temperature.

4.2.3 Gel Spinning

Solvent can be added to a polymer, which allows the polymer to flow at lower temperatures, resulting in lower extrusion temperatures. This technique is known as gel

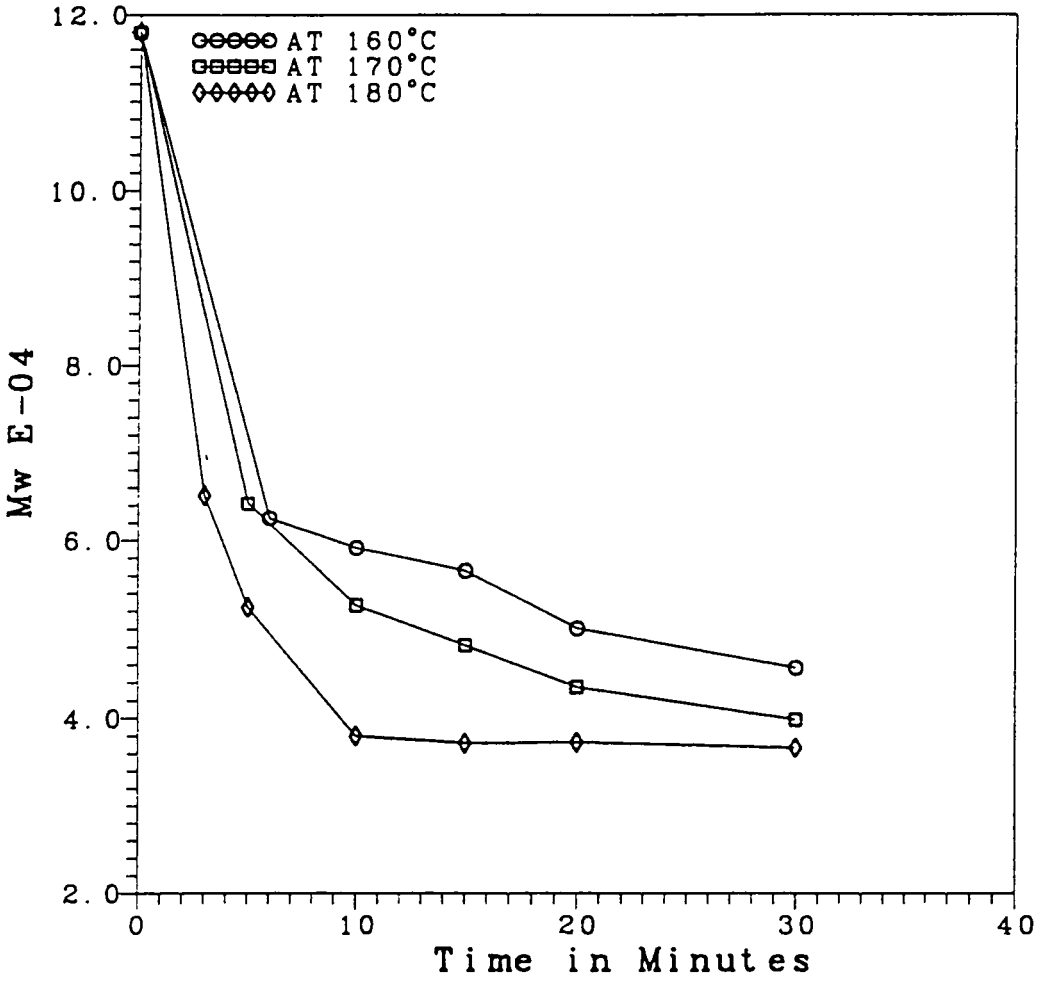


Figure 4.18 Plot showing the effect of residence time on the molecular weight degradation of PEA 10,2 polymer.

Source: D. D. Agrawal, "Processing and Characterization of Poly(ester-amide) Monofilaments." Master of Science Thesis in Polymer Engineering, The University of Tennessee, December 1993.

spinning. Preliminary studies on PEA 10,2 and PEA 6,2 containing various concentrations of NMP were conducted. The peak melting temperatures from DSC and extrusion temperatures for the Instron capillary rheometer are listed in Table 4.7. The peak melting temperatures and extrudate viscosities substantially decrease with increasing solvent concentration. In fact, extrusion of polymer filament with solvent concentration above 50% was not feasible. In order to produce continuous filament, the optimal solvent concentration appears to be approximately 20% or less.

Additional complications arise in gel spinning as opposed to melt spinning with the solvent removal step. While the monofilament is at the elevated temperature necessary to evaporate the solvent, changes in the fiber structure are possible. For example, it is possible for the polymer chains to relax and additional crystallization to occur at these elevated temperatures. Furthermore, residual solvent may remain in the fiber, which is not acceptable for the fiber's end use applications. Consequently, another method for fiber extrusion to aid in molecular weight retention was investigated.

4.2.4 Melt Spinning Using the Maxwell Extruder

Due to the limited amount of polymer available and in an attempt to reduce the residence time and shearing of the

Table 4.7 Effect of solvent content on the melting of PEA polymers.

Polymer	Solvent Concentration (%)	Peak Melting Temperature (°C)	Processing Temperature (°C)
PEA 10,2	0	161	175
PEA 10,2	14	150	158
PEA 10,2	40	118	137
PEA 10,2	44	117	131
PEA 10,2	53	99	-
PEA 10,2	60	95	-
PEA 6,2	0	147	170
PEA 6,2	15	140	-
PEA 6,2	19	135	140
PEA 6,2	34	125	134
PEA 6,2	57	92	-
PEA 6,2	67	71	-

Source: D. D. Agrawal, "Processing and Characterization of Poly(ester-amide Monofilaments." Master of Science Thesis in Polymer Engineering, The University of Tennessee, Knoxville, December, 1993.

polymer experienced during screw extrusion, the Maxwell extruder was employed. Extrusion of the PEAs using the Maxwell extruder aids in retaining the polymer's molecular weight, as seen in Table 4.8, which contains the extrusion temperatures and pre and post IV data for the PEAs.

4.2.4.1 PEA 10,2

Drawdown ratios in the range of 22 to 150 were achieved for PEA 10,2 as-spun fibers using the Maxwell extruder and draw bench. At drawdown ratios exceeding 150, the spinline breaks. In-line drawing was performed for the PEA 10,2 monofilaments at room temperature, 50° C and 60° C for several draw ratios. Second stage drawing was also performed on as-spun and in-line drawn (with and without snubbing pins) fibers to various draw ratios at 65° C.

The draw ratio achieved for the PEA 10,2 fibers was found to be dependent on the initial molecular orientation and will be discussed along the properties observed in the fiber characterization section. Finally, heat setting was performed on several monofilaments at 100° C and 105° C to reduce possible shrinkage of the highly oriented fibers. Fibers broke and curled up at heat setting temperatures greater than 105° C. The properties of all of these monofilaments will be discussed in the fiber characterization sections.

Table 4. 8 Extrusion conditions for PEAs.

Polymer and Initial IV	Rotor Temperature (°C)	Header Temperature (°C)	Cooling Technique	Post Extrusion IV
PEA 10,2 IV = 1.15*	156	176	-	0.82
PEA 6,2 IV = 1.18	155	168	Air blower	0.88
PEA 6,2 IV = 1.18	155	168	Water bath	0.90
			and air blower	
PEA 6,2 IV = 1.58	172	195	Air blower	0.67
PEA 6,2 copolymer	176	194	Water bath	0.98
IV = 1.00				

* Source: D. D. Agrawal, "Processing and Characterization of Poly(ester-amide) Monofilaments." Master of Science Thesis in Polymer Engineering, The University of Tennessee, Knoxville, December, 1993.

All of the fibers produced for the PEA polymers and copolymer exhibited an aging phenomena after being spun. Drawing became more difficult and lower draw ratios were achieved if the fiber was stored at room temperature for a few days. This phenomenon is not well understood, but it could be related to the influence of moisture absorption on crystallization kinetics.

4.2.4.2 PEA 6,2

A thermally stabilized PEA 6,2 (IV = 1.18 dl/g) prepared by an improved synthesis process was dried and sealed in containers by 3M. It was believed that an additional drying step prior to processing was not needed. Many differences were noted in the processing conditions and drawing behavior of the monofilaments produced from PEA 6,2 as compared to PEA 10,2 polymer. These differences are believed to be associated with the chemical structure of the polymers and artifacts of the synthesis.

Lower extrusion temperatures were used for processing PEA 6,2 as compared to PEA 10,2 (refer to Table 4.8). However, the fibers remained tacky when they reached the godet and required additional cooling devices. Initially, cooling was supplied from an air blower, blowing air countercurrent to the spinline, which helped to some extent but a combination of a water quench bath and the air blower

was more effective. Additionally, the post extrusion molecular weights of the fibers produced from the thermally stabilized PEA 6,2 showed better molecular weight retention than that obtained for PEA 10,2 fibers (refer to Table 4.8). This improvement may be associated with the thermally stabilized polymer, lower extrusion temperatures, cooling techniques, or combinations of these. It appears that there is little difference in the molecular weight retention of fibers produced from the combination of water and air cooling as opposed to air cooling alone as seen in Table 4.8.

Other differences observed in the processing of PEA 6,2 include the fiber's ability to draw both during spinning operations and in second stage operations. Draw down ratios in the range of 10.6 to 79 were achieved for PEA 6,2, a more narrow range than that for PEA 10,2. Additionally, PEA 6,2 could not be in-line drawn during melt spinning; therefore, only second stage drawing was performed.

Due to the limited amount of polymer supplied (200 grams) and consequently, small quantity of fiber produced, the effect of increasing draw ratios for all as-spun fibers could not be investigated. Instead, water quenched and air cooled fibers of the same drawdown ratio were drawn in a second stage, and the resulting properties were examined. In these experiments, fibers were drawn to their maximum attainable draw ratio at 25° C, 60° C and 80° C.

The maximum draw ratio achieved for the PEA 6,2 monofilaments was 4.05X at 80° C, considerably lower than the maximum of 7.0X for PEA 10,2. These differences in processing behavior are believed to be associated with the chemical structures and crystallinity of the two polymers, which will be discussed in greater detail in the fiber characterization section.

An attempt to process a second thermally stabilized PEA 6,2 with an initial IV of 1.56 dl/g was made. Unfortunately, the molecular weight was too high to be extruded with the Maxwell extruder, even at higher extrusion temperatures. The polymer was able to flow at these higher temperatures, but the extrudate was black, indicating thermal degradation. It was believed that this polymer may be crosslinked, which was confirmed by trying to dissolve the material in NMP at 60° C. The material dissolved to some extent, but particles remained in the solution.

4.2.4.3 PEA 6,2 Copolymer

This was the first attempt ever made to process the PEA 6,2 copolymer, synthesized with 20 mole % of a proprietary diacid. Prior to processing, the polymer was redried overnight in a vacuum oven set at 100° C. Many differences and similarities were noted in the processing behavior of the PEA 6,2 copolymer as compared with PEA 6,2. For example,

higher extrusion temperatures were required for this material to flow, even though the melting point of the copolymer is lower than PEA 6,2 and PEA 10,2 (refer to Table 4.8). Even though higher extrusion temperatures were used, this material had the best molecular weight retention of all of the PEAs processed on the Maxwell extruder (refer to Table 4.8). This phenomena is most likely due to redrying the polymer prior to processing, and it is recommended to redry any of the PEAs before attempting to process them.

The polymer exhibited very elastic behavior during spinning even at these higher extrusion temperatures, resulting in a low drawdown ratio. The maximum drawdown ratio achieved while maintaining a stable spinline with no breaks was 9.6, which resulted in large diameter filaments. It is possible that this material may have been crosslinked to some extent, which might explain the higher extrusion temperatures needed and drawing behavior observed. In addition to its elastic properties, fiber produced from the PEA 6,2 copolymer remained tacky before reaching the take-up device, and a water quench bath was required.

Problems with draw line breakage were encountered, resulting from the high rates of drawing and the presence of gel particles in the monofilaments. In order to obtain higher draw ratios, the fiber was drawn very slowly to low extension ratios in several stages. Fibers were drawn at 25° C, 45° C, 65° C, 70° C and 80°C. The drawing behavior of

the fibers formed from the PEA 6,2 copolymer improved at these elevated draw temperatures. The maximum draw ratio obtained for this material was 3.97X, slightly lower than that for PEA 6,2, and substantially lower than PEA 10,2's maximum draw ratio. The properties obtained for these fibers will be presented and discussed in the characterization section.

Due to the limited amount of polymer supplied and therefore small quantity of fiber produced, the optimal processing and drawing conditions could not be ascertained. Additional study is needed on this material, if it is to be considered for surgical suture applications.

4.3 CHARACTERIZATION OF PEA MONOFILAMENTS

The effect of different processing operations on the structure and properties of the PEA monofilaments was studied in an attempt to optimize the processing conditions and obtain the most desirable properties in the final fibers. Results of characterization studies on PEA 6,2 and PEA 6,2 copolymer monofilaments are presented and compared. A brief account of the properties observed for PEA 10,2 monofilaments is also included for comparison. For a more detailed account of PEA 10,2 refer to reference 54.

4.3.1 PEA 10,2 Fibers Extruded on Maxwell Extruder

The properties of as-spun PEA 10,2 fibers are listed in Table 4.9. Properties of fibers drawn at 65°C are listed in Table 4.10. The mechanical testing values are within plus or minus 10% of the average value reported for all fibers tested. As expected birefringence values increase with increasing drawdown and draw ratio, due to the increase in molecular orientation with respect to the fiber axis. Additionally, the orientation induced during drawdown influences the fiber's drawability. The maximum attainable draw ratio decreases for fibers with high drawdown ratios as in the case of fibers MA113 and MA117, refer to Table 4.9. From these studies, the optimal drawdown ratios for subsequent drawing are in the range of 20-50.

In addition to drawing at various temperatures, MA119 fiber exposed to moisture and steam was drawn. Table 4.11 lists the tensile strength and modulus values of these drawn fibers. Higher draw ratios are achieved at room temperature for fibers exposed to water, which acts as a plasticizing agent and increases mobility of the polymer chains. These fibers exhibited higher strengths and lower moduli than the same fiber drawn at 65° C. Additionally, fiber drawn under a jet of steam exhibited higher strength and lower modulus as compared with other fibers of similar draw ratio. These properties are desirable for the fiber's end use application,

Table 4.9 Properties of PEA 10,2 as-spun fibers.

Fiber ID	Drawdown Ratio	Birefringence	Maximum Draw Ratio	Maximum Strength, (MPa)	Density (g/cm3)
MA119	22	0.0225	5.15	291	1.2065
MA111	45	0.028	7.13	475	1.2074
MA113	95	0.0313	3.19	399	1.2075
MA117	138	0.0338	3.19	363	1.2077

Source: D. D. Agrawal, "Processing and Characterization of Poly(ester-amide) Monofilaments." Master of Science Thesis in Polymer Engineering, The University of Tennessee, Knoxville, December 1993.

Table 4.10 Strength and orientation of fibers drawn at 65° C.

Fiber ID	Draw Ratio	Birefringence	Tensile Strength, MPa	Modulus (GPa)	Percent Elongation
MA111-1	3.5	0.0491	222	0.71	130
MA111-2	5.02	0.0599	439	1.71	22
MA111-3	7.13	0.061	475	1.64	28
MA113-1	3.19	0.0428	399	1.5	47
MA117-1	3.19	0.0597	363	1.39	52
MA119-1	3.19	0.0494	244	0.69	114
MA119-2	4.44	0.0529	252	0.74	121
MA119-3	5.15	0.0584	291	0.8	99

Source: D. D. Agrawal, "Processing and Characterization of Poly(ester-amide) Monofilaments." Master of Science Thesis in Polymer Engineering, The University of Tennessee, Knoxville, December 1993.

Table 4.11 Comparison of tensile strength (<>) and Young's modulus ([]) of fiber MA119 after drawing under different conditions.

Drawing Conditions	Draw Ratio					
	3	3.19	3.66*	4.44	4.95*	5.15
Drawn at room temperature, 25°C.	<245> [0.75]	-	-	-	-	-
Drawn at 65°C.	-	<244> [0.69]	-	<252> [0.74]	-	<291> [0.80]
Drawn at room temperature, 25°C, after immersing in water.	-	<251> [0.65]	-	<375> [0.67]	-	-
Drawn under a jet of steam at the feeding pulley.	-	-	-	<416> [1.1]	-	-
Drawn at room temperature to 3X, and then redraw in second stage at 65°C.	-	-	<370> [1.39]	-	<439> [1.53]	-

<> Strength is in MPa. [] Modulus is in GPa. * Drawn in two stages.

Source: D. D. Agrawal, "Processing and Characterization of Poly(ester-amide) Monofilaments." Master of Science Thesis in Polymer Engineering, The University of Tennessee, Knoxville, December 1993.

but more study is needed on this processing operation.

In-line drawing of fibers was performed at several temperatures and with and without snubbing pins. The results of this study are summarized in Table 4.12, which also includes properties of some as-spun fibers. Fibers drawn in-line at room temperature could be drawn to higher extensions than fibers drawn in-line at elevated temperatures. Additionally, the use of either steel or Teflon snubbing pins did not seem to affect the final properties to a great extent. As expected, increases in tensile strength, birefringence and modulus were observed with increased drawing.

Several in-line drawn fibers were drawn in a second stage at 65° C, and the results are tabulated in Table 4.13. The first stage, second stage, and overall draw ratios are included in this table. By comparing the results obtained for as-spun and second stage drawn fibers with in-line and second stage drawn fibers, it appears that higher strengths are obtained from the later technique. From these results it appears that the best approach for obtaining the desired high strength properties is to draw the fibers in two stages, where the first stage consists of drawing the fiber in-line to the highest attainable draw ratio at room temperature.

The results of heat setting at 100° C and 105° C for several fibers are listed in Table 4.14. Heat setting appears to enhance the modulus, rather than improve the

Table 4.12 Strength and orientation in as-spun and in-line drawn fibers.

Fiber ID	Draw Ratio	Draw Temp. °C	Birefringence	Percent Elongation	Tensile Strength, MPa	Modulus GPa	Snubbing Pin
MI110	3.00	50	0.0487	89	236	0.84	-
MI112	3.00	60	0.0458	103	265	0.73	-
MI114	3.73	25	0.045	100	333	1.07	Steel
MI115	3.80	25	0.045	63	379	1.27	Steel
MI116	3.00	25	0.0454	105	273	0.73	Teflon
MI120	3.00	25	0.0452	74	284	0.85	-
MA111	45 (DDR)	-	0.028	355	90	-	-
MA113	95 (DDR)	-	0.0313	325	99	-	-
MA117	138 (DDR)	-	0.0338	346	96	-	-
MA119	22 (DDR)	-	0.0225	470	110	-	-

(DDR) = drawdown ratio

Adapted from D. D. Agrawal, "Processsing and Characterization of Poly(ester-amide) Monofilaments." Master of Science Thesis in Polymer Engineering, The University of Tennessee, Knoxville, December 1993.

Table 4.13 Strength and orientation in the in-line drawn fibers after redrawing at 65°C.

Fiber ID	In-line DR	Second Stage DR	Overall DR	Birefringence	Percent Elongation	Tensile Strength, MPa	Modulus GPa
MI110-1	3.00	2.28	5.28	0.0586	36	459	1.56
MI112-1	3.00	1.32	4.32	0.0464	112	289	0.79
MI112-2	3.00	1.42	4.42	0.0559	40	395	1.49
MI112-3	3.00	1.80	4.80	0.052	84	334	1.18
MI116-1	3.00	1.83	4.83	-	59	335	1.05
MI116-2	3.00	2.53	5.53	0.0602	71	323	1.19
MI116-3	3.00	2.80	5.80	0.0569	51	439	1.29
MI120-1	3.00	1.32	4.32	0.0551	96	291	0.88
MI120-2	3.00	1.80	4.80	0.0573	77	318	1.11
MI120-3	3.00	2.53	5.53	0.0557	79	366	1.16
MI120-4	3.00	2.80	5.80	0.058	69	360	1.14
MI120-5	3.00	3.20	6.20	0.0555	32	420	1.65
MI114-1	3.73	1.32	5.05	0.0458	62	380	1.39
MI114-2	3.73	1.80	5.53	0.0633	46	501	1.6
MI115-1	3.80	1.32	5.12	0.0701	34	557	2.08

Adapted from D. D. Agrawal, "Processing and Characterization of Poly(ester-amide) Monofilaments." Master of Science Thesis in Polymer Engineering, The University of Tennessee, Knoxville, December 1993.

Table 4.14 Comparison of strength and orientation after heat setting.

Fiber ID	Overall Draw Ratio	Birefringence	Percent Elongation	Tensile Strength, MPa	Modulus GPa	Percent Crystallinity
MI115-2.1	4.64	0.0528	34.7	458	1.56	-
MI115-2.1H1	4.73	0.0545	34.8	465	2.2	-
MI116-2.1	3.66	0.051	87.1	280	-	-
MI116-2.1H1	3.73	0.0546	66.9	271	-	-
MI116-2.2	6.99	0.0554	58.4	294	1.04	4.7
MI116-2.2H1	7.13	0.0605	45.6	369	1.48	7.3
MI116-2.2H2	7.13	0.0575	52.2	327	1.67	8.5
MI116-2.3	7.74	0.0573	35.5	426	-	-
MI116-2.3H1	7.89	0.062	42.1	372	-	-
MI116-2.3H2	7.89	0.0576	52.4	359	-	-
MI120-4	8.40	0.058	69	360	1.14	-
MI120-4H1	8.56	0.0605	60	363	1.51	-

H1- Heat set at 100°C.

H2- Heat set at 105°C.

Source: D. D. Agrawal, "Processing and Characterization of Poly(ester-amide) Monofilaments." Master of Science Thesis in Polymer Engineering, The University of Tennessee, Knoxville, December 1993.

tensile strength to a great extent. The increase in modulus may be explained by additional crystallization of the fibers at these elevated temperatures, as seen in column 7 of Table 4.14. Furthermore, it is possible for the polymer chains to relax at these higher temperatures as seen by the lower tensile strength values observed for MI116-2.2H2 as compared to MI116-2.2H1 (both having the same draw ratio).

In summary, PEA 10,2 fibers exhibit high strength with drawing, although the higher strengths are obtained in a two stage drawing operation, with the first stage consisting of in-line drawing at room temperature. These fibers also exhibit low crystallinity values with the highest values obtained from heat setting the material. It appears that the high strength values for 10,2 are due to the increase in molecular orientation, instead of crystallinity. This is further supported by the lower modulus values observed for drawn fibers, as compared with those reported for the heat set fibers.

4.3.2 PEA 6,2 Fibers Extruded on the Maxwell Extruder

As-spun fibers of various drawdown ratios and solidified by different cooling techniques were characterized. The results of tensile testing, birefringence, density, and crystallinity measurements are listed in Table 4.15. The mechanical testing values are within plus or minus 10% of the

Table 4.15 Properties of PEA 6,2 as-spun fibers.

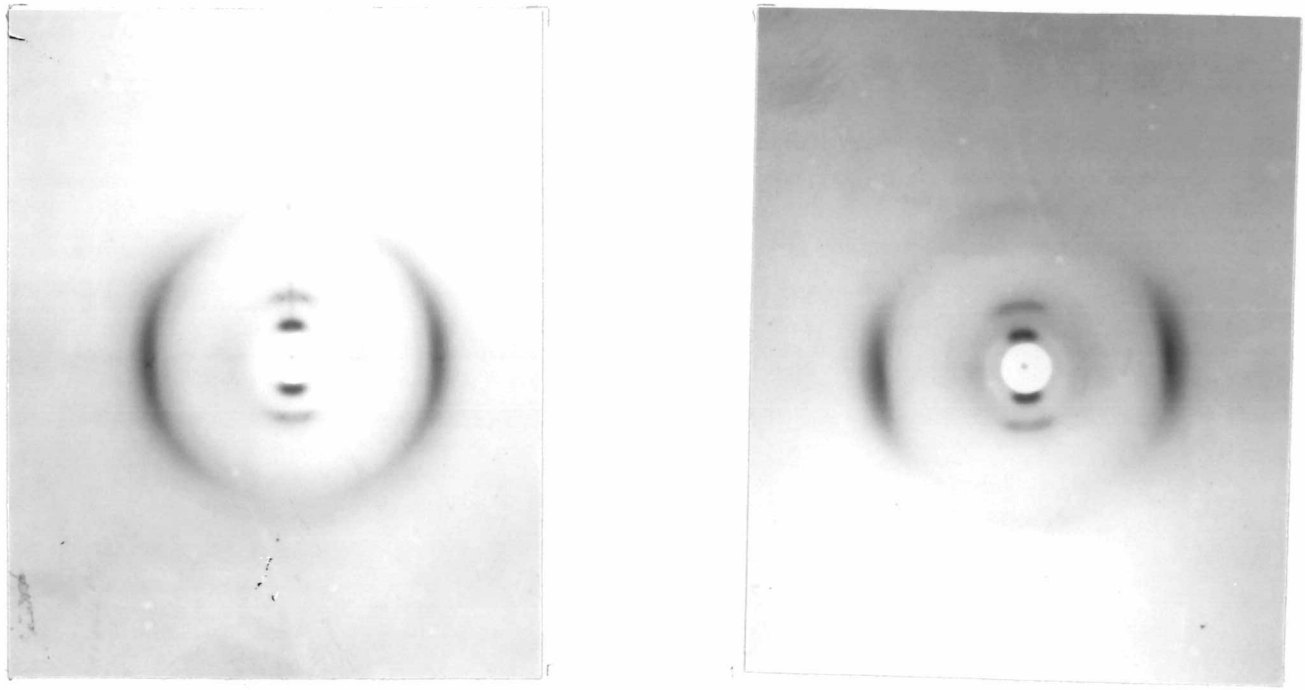
Fiber ID	Cooling Technique	Drawdown Ratio	Birefringence	Tensile Strength, MPa	Percent Elongation	Density g/cm3	Relative % Crystallinity
711	Air	78.8	0.0156	87	120	1.2805	29.5
712	Air	10.9	0.0024	53.9	567	1.276	26.3
713	Water/Air	24.4	0.0181	83.8	335	1.2799	29.1
714	Air	23.3	0.0149	64.8	222	1.2755	26
715	Water/Air	23.3	0.017	84.1	373	1.2761	26.4

average value reported for all fibers tested. The percent crystallinity, X for the fiber samples and annealed films was estimated using the following relation:

$$X = \rho_c (\rho - \rho_a) / \rho (\rho_c - \rho_a) \times 100$$

where ρ is the density of the fiber sample, and ρ_a and ρ_c are the densities of the amorphous and crystalline densities, respectively. In these calculations, ρ_a and ρ_c are 1.24 and 1.40 g/cm^3, respectively. The percent crystallinity values are only rough estimates to be used for comparison purposes with other fibers.

The tensile strength and birefringence increased with increasing drawdown ratio, while elongation decreased. By increasing the drawdown ratio, the polymer chains became more oriented with respect to the fiber axis. This can easily be seen by comparing the equatorial reflections of the 714 (drawdown ratio 23) and 711 (drawdown ratio 79) fiber patterns in Figure 4.19. With increasing drawdown ratio, the equatorial arcs become shorter, indicating higher orientation. Furthermore, stress induced crystallization may have resulted from the increased tension imparted by the take-up device. This idea is supported by the higher density and relative crystallinity values obtained for fibers of greater drawdown ratio as seen in columns 7 and 8 of Table 4.15.



(a) (b)

Figure 4.19 5 cm flat plate film patterns of PEA 6,2 as-spun fibers. (a) 714 drawdown ratio 23.3, (b) 711 drawdown ratio 79.

The results of tensile testing, birefringence and density measurements, and relative crystallinity values for the drawn fibers and their as-spun precursors are listed in Table 4.16. Increases in birefringence, tensile strength and modulus were observed with drawing for the air cooled fibers. Comparing the maximum draw ratio at the three drawing temperatures: fiber drawn to 2.97X at 60° C exhibited higher birefringence, tensile strength, and modulus than those achieved for fiber drawn 2.79X at 25° C, and fiber drawn to 2.74X at 80° C. Additional crystallization occurred during drawing at the elevated temperatures as indicated by the increased density. The x-ray fiber patterns shown in Figure 4.20 also display the increase in crystalline orientation and enhancement of crystallinity under the various conditions.

Fibers solidified by the combination of the water quench bath and air cooling achieved higher birefringence and tensile strength values than fibers of similar drawdown ratios cooled only by air. Lower draw ratios were achieved for these fibers at 25° C and 60° C as compared to the air cooled fibers, although there appears to be some ductility remaining in them as indicated by the large % elongation values. At 80° C, the highest draw ratio and strength were obtained for the water quench/air cooled fibers. Increases in birefringence, tensile strength, modulus, and density values were observed with increasing molecular orientation imparted by drawing, as seen in Table 4.16. The increase in

Table 4.16 Properties of as-spun and drawn PEA 6,2 fibers.

Sample ID	Draw Ratio	Birefringence	Tensile Strength (MPa)	% Elongation	Modulus (GPa)	Density g/cm3	Relative Crystallinity
711	78.8 (DDR)	0.0156	87.06	120	-	1.2805	29.5
712	10.9 (DDR)	0.0024	53.85	567	-	1.276	26.3
713	24.4 (DDR)	0.0181	83.82	335.1	-	1.2799	29.1
714	23.3 (DDR)	0.0149	64.83	222.3	-	1.2755	26
71425	2.79	0.0357	191.39	60.1	1.62	1.2771	27.1
71461	1.62	0.0377	138.89	108.4	1.54	1.2778	27.6
71462	2.97	0.0504	237.87	45.7	2.08	1.2781	27.8
71480	2.74	0.0459	168.69	40.8	1.7	1.2777	27.5
715	23.3 (DDR)	0.017	84.13	372.9	-	1.2761	26.4
71525	2.05	0.046	178.62	132	1.44	1.277	27
71561	1.84	0.0393	164.77	131	1.31	1.2768	26.9
71562	2.13	0.0455	147.28	100.5	0.92	1.2772	27.1
71580	4.05	0.0586	315.74	39	2.93	1.2796	28.9

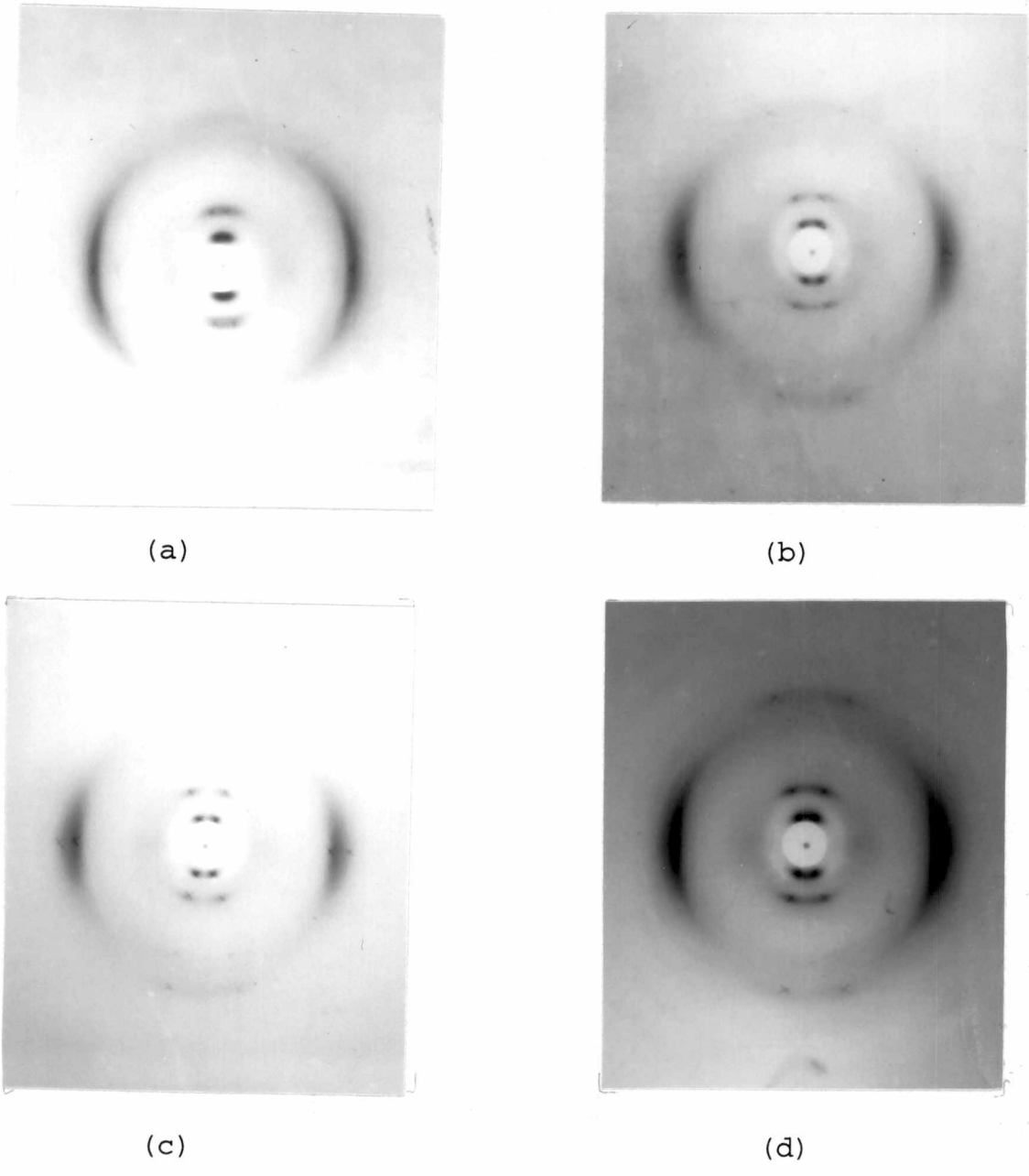


Figure 4.20 Flat plate film patterns of PEA 6,2 as-spun fibers and drawn PEA 6,2 fibers taken at 5 cm. (a) 715 drawdown ratio 23.3, (b) 71525 drawn 2.79X at 25° C, (c) 71562 drawn 2.13X at 60° C, (d) 71580 drawn 4.05X at 80° C.

orientation is further confirmed by comparing the WAXD fiber patterns for the as-spun fibers with those drawn under the various conditions.

This was the only successful extrusion of PEA 6,2 monofilaments on the Maxwell extruder. Additional study is needed to optimize the processing conditions for PEA 6,2. From this initial study, several observations were made in relation to fiber properties resulting from spinning and drawing operations. The spinning and drawing behavior and resulting properties of these fibers are quite different than those observed for PEA 10,2. Lower drawdown and second stage draw ratios were achieved for the PEA 6,2 fibers as compared with those attained for PEA 10,2 fibers. Additionally, the maximum tensile strength values achieved for the PEA 6,2 fibers are considerably lower than those observed for PEA 10,2 fibers. However, higher modulus values are reported for the PEA 6,2 than those observed for PEA 10,2 fibers of similar draw ratios. These differences are believed to be associated with the chemical structure and strengthening mechanism of the two polymers. It appears that the strength of PEA 6,2 fibers results from the inherent crystallinity of the material, as supported by the higher density and modulus values, while PEA 10,2's strength appears to be due to orientation.

4.3.3 PEA 6,2 Copolymer Extruded on the Maxwell Extruder

One as-spun sample, having a drawdown ratio of 9.6 was collected for the PEA 6,2 copolymer. Tables 4.17 and 4.18 list mechanical properties and birefringence and density measurements for these as-spun and drawn fibers drawn for the various temperatures. A column for the change in density relative to the density of the as-spun fiber is also included since relative crystallinity can not be calculated as explained earlier. In previous tensile testing experiments, a crosshead speed of 100 mm/min was used. All of these fibers were tested for a crosshead speed of 50 mm/min, and some fibers were also tested at 100 mm/min and are distinguished by the two tables. The mechanical testing values are within plus or minus 10% of the average value reported for all fibers tested.

Figures 4.21 and 4.22 show the correlation between birefringence and tensile strength (crosshead speed 50 mm/min) with increasing draw ratios at 25° C, 70° C, and 80° C. Higher tensile strength and modulus values were attained for fibers drawn at elevated temperatures to comparable draw ratios. The higher modulus is likely due to increase in crystallinity, but the increase in tensile strength is more likely due to orientation. Increases in density and change in density were observed with increased drawing and increased draw temperatures for these fibers, which is attributed to

Table 4.17 Properties of as-spun and drawn PEA 6,2 copolymer fibers using a crosshead speed of 50 mm/min.

Sample ID	Draw Ratio	Birefringence	Tensile Strength (MPa)	% Elongation	Modulus (MPa)	Density g/cm3	Change in Density
Pro1	9.6 (DDR)	0.0019	84.2	485	207	1.296	-
Pro1251	1.27	0.0141	99.2	207.8	218	1.3031	0.0071
Pro1252	1.56	0.0155	107	135.2	277	1.3036	0.0076
Pro1253	1.92	0.0184	129.2	117.6	342	1.3039	0.0079
Pro1254	2.39	0.0239	171.8	103.6	636	1.306	0.01
Pro1255	2.71	>0.0385	222.6	78.3	822	1.3042	0.0082
Pro1451	2.71	>0.0419	232.7	45.8	842	1.3055	0.0095
Pro1452	3.97	0.029	197.8	53.9	1128	1.3038	0.0078
Pro1651	2.74	0.035	213.4	42	975	1.3039	0.0079
Pro1701	2.26	0.0231	188	59.7	868	1.3061	0.0101
Pro1702	2.47	>0.0365	193	66.4	878	1.3062	0.0102
Pro1703	3.71	>0.0432	270.7	56.1	1317	1.3087	0.0127
Pro1801	1.67	0.0122	195.2	82.7	595	1.3084	0.0124
Pro1802	2.63	0.0217	202.6	44.6	624	1.3142	0.0182

Table 4.18 Properties of selected PEA 6,2 copolymer fibers using a crosshead speed of 100 mm/min.

Sample ID	Draw Ratio	Birefringence	Tensile Strength (MPa)	% Elongation	Modulus (MPa)	Density g/cm3	Change in Density
Pro1253	1.92	0.0184	79.4	71.4	243	1.3039	0.0079
Pro1254	2.39	0.0239	111	55.4	398	1.306	0.01
Pro1255	2.71	>0.0385	156	36.1	602	1.3042	0.0082
Pro1451	2.71	>0.0419	163	33.8	521	1.3055	0.0095
Pro1651	2.74	0.035	167.5	28.9	853	1.3039	0.0079
Pro1701	2.26	0.0231	117.8	55.1	459	1.3061	0.01
Pro1702	2.47	>0.0365	122.6	38.4	549	1.3062	0.0102
Pro1703	3.71	>0.0432	184	44.3	823	1.3087	0.0127

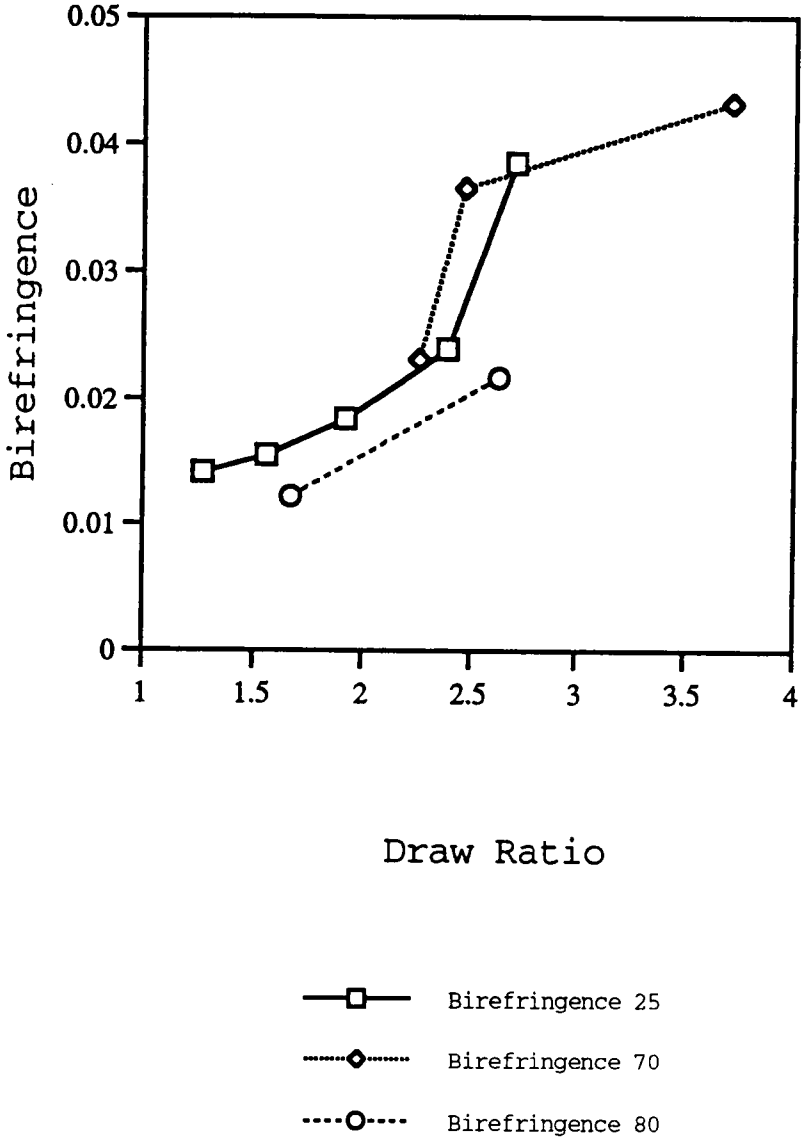


Figure 4.21 Birefringence as a function of draw ratio for PEA 6,2 copolymer fibers.

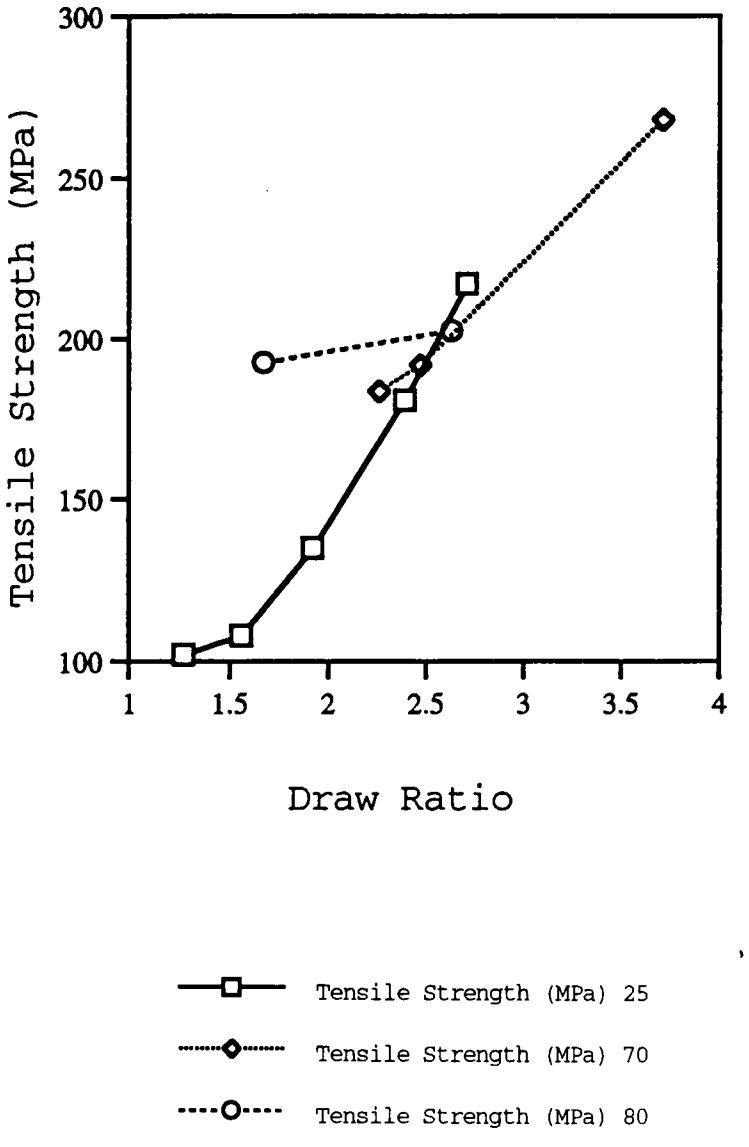
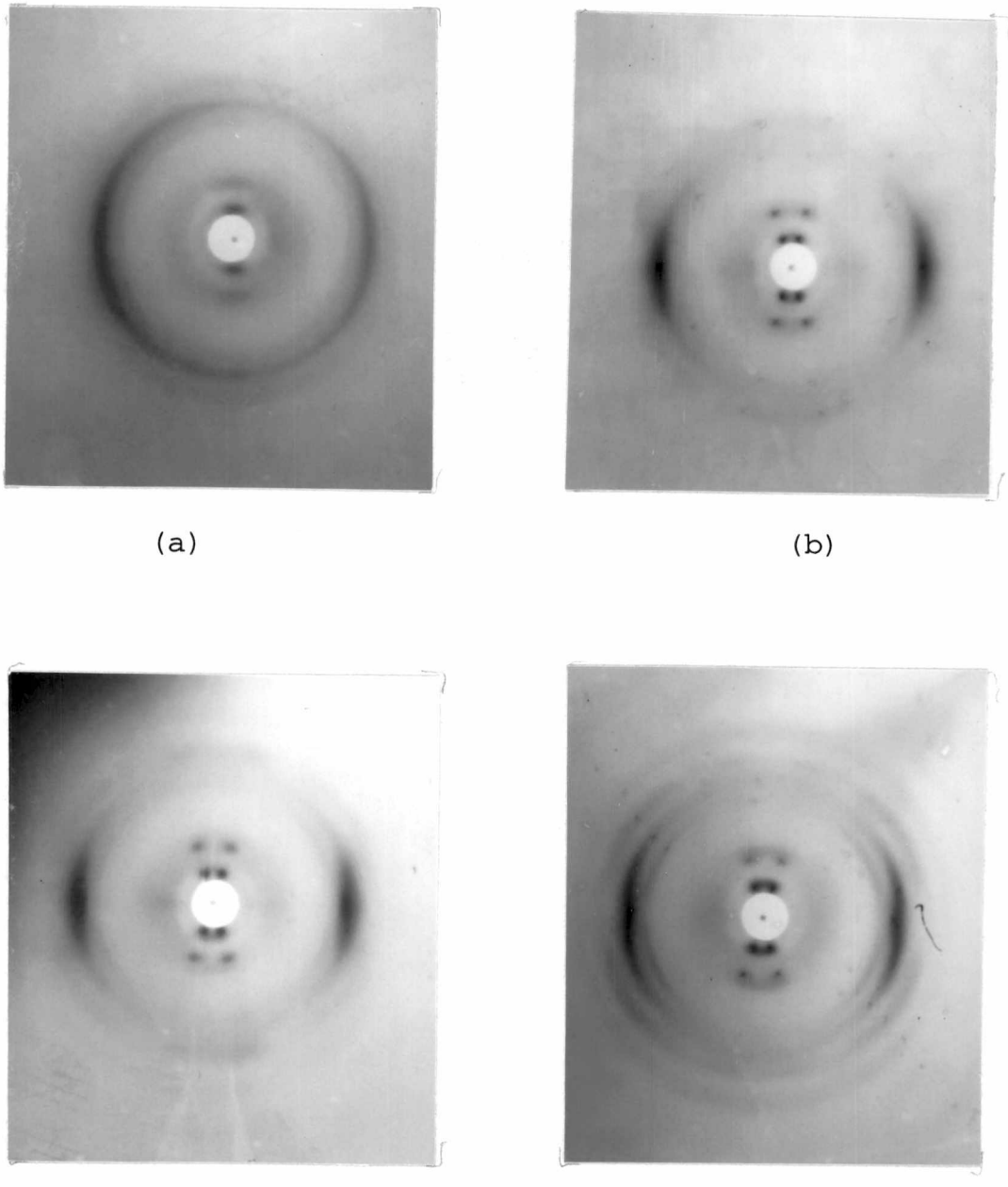


Figure 4.22 Tensile strength as a function of draw ratio for PEA 6,2 copolymer fibers.

increased crystallinity of the fiber. Additional crystalline reflections are observed in the WAXD fiber patterns of Pro1451 (drawn 2.71X at 45° C), Pro1703 (drawn 3.71X at 70° C) and Pro1802 (drawn 2.63X at 80° C), shown in Figure 4.23, corresponding with the higher density values recorded.

In general, birefringence increased with increased drawing; however, birefringence values were lower for some fibers drawn at higher temperatures. This may be due to relaxation of the polymer chains at the elevated temperatures. Lower strengths and elongations are observed for fibers tested at the higher extension rate. This is attributed to a lower degree of strain hardening and reorganization of polymer chains occurring at the higher extension rate. Additionally, lower strengths were observed for the copolymer as compared with the values reported for PEA 6,2 at the crosshead speed of 100 mm/min. Furthermore, considerably lower modulus values are observed for the copolymer than those obtained for PEA 6,2. The difference in strength and modulus is believed to be associated with incorporation of the second polymer repeat unit into the polymer chain. The crystalline order of the polymer structure is disrupted with the incorporation of the other repeat unit. As a result lower amounts of crystallinity are achieved as seen in the WAXD fiber patterns, as compared the amounts observed for PEA 6,2.



(a) (b)

(c) (d)

Figure 4.23 Flat plate film patterns of PEA 6,2 copolymer fibers taken at 5 cm. (a) Pro1 as-spun fiber drawdown ratio 9.6, (b) Pro1451 drawn 2.71X at 45° C, (c) Pro1703 drawn 3.71X at 70° C, (d) Pro1802 drawn 2.63X at 80° C.

Chapter 5

CONCLUSIONS AND RECOMMENDATIONS

The results obtained from the Fiber Spinning Group at the University of Tennessee are the first in the studies of processing and characterization of PEA and PEA copolymer monofilaments. Typically, a thorough understanding and careful investigation of all aspects is required to come to any conclusion from experimental results. Working with a new material in which little information is known makes this task even more difficult. The conclusions in this chapter follow from results obtained during the present study and previously reported results.

5.1 CONCLUSIONS

- The incorporation 20 mole % of a proprietary diacid into the synthesis of PEA 6,2 lowers the melting temperature and crystallinity of the homopolymer. Additionally, this copolymer is very slow to crystallize and exhibits small exotherms during cooling, relative to the homopolymer.

- It has been observed from WAXD scans and flat plate film patterns that PEA 10,2, PEA 6,2 and the PEA 6,2 copolymer films all form the same basic crystal structure with annealing. A crystallographic repeat distance of approximately 2.25 nm has been reported for PEA 10,2 fiber. For PEA 6,2 and the PEA 6,2 copolymer fibers, the approximate crystallographic repeat distances obtained are 1.79 nm and 1.85 nm, respectively. PEA 6,2 and the PEA 6,2 copolymer have four fewer methylene lingkages than PEA 10,2, resulting in the lower crystallographic repeat distance observed. Additionally, the repeat distance for PEA 6,2 and the PEA 6,2 copolymer are very close. From this data, we are uncertain as to what extent the crystals formed from these two materials differ.

- The crystalline density of PEA 6,2 is estimated to be 1.40 g/cm^3, assuming a pseudo-orthorhombic unit cell and one polymer repeat unit per unit cell. Using an approximation developed by Bessonov and Smirnova, an estimate of amorphous density of 1.24 g/cm^3 was obtained for PEA 6,2. These density values are only approximations and further evaluation is needed to obtain accurate values.

- Good monofilaments can be produced by melt spinning and drawing PEA polymers and copolymers having an initial IV$\geq$1.0 dl/g. However, if the molecular weight is too high

or the material is crosslinked, fiber cannot be produced. Consequently, steps need to be taken during synthesis and subsequent processing to obtain and retain the desired molecular weight, while preventing crosslinks to form in the process.

- Little crystallization was observed during the extrusion of PEA 6,2 and the PEA 6,2 copolymer. Resulting monofilaments were tacky and difficult to handle if not cooled. In our experiments, the best way to eliminate this problem was to run the monofilaments through a water quench bath to expedite solidification, although it does not appear to adversely affect the molecular weight of the fibers. This tackiness phenomena is believed to be related to the polymers' glass transition temperature, which is near room temperature and its crystallization kinetics. It has been reported previously that PEA 10,2 has a T_g 10° C higher than that observed for PEA 6,2, which may possibly explain why the tackiness problem was not observed for this material.

- The molecular weight of the PEA polymers drops significantly during melt spinning due to instability of the polymer at high temperatures, and the residence time and shearing the polymer undergoes during extrusion. The decrease in molecular weight tends to adversely affect the

drawability and tensile strength of PEA 10,2 fibers, in the range of molecular weights studies. Better molecular weight retention has been observed for PEA 10,2 and thermally stabilized PEA 6,2 processed on the Maxwell extruder. Additional improvement in molecular weight retention has been observed for the PEA 6,2 copolymer, which was redried overnight in a vacuum oven. A careful drying stage prior to processing any of the PEAs is recommended.

- The initial orientation and molecular weight have been shown to influence the drawability of the PEA fibers. The optimal drawdown ratio for subsequent drawing of PEA 10,2 is in the range of 20-50. It appears that the optimal drawdown ratio for PEA 6,2 and the PEA 6,2 copolymer are considerably lower. Drawdown ratios of 10-25 exhibit better drawability for fiber formed from the PEA 6,2 and PEA 6,2 copolymer provided. These low drawdown ratios may be related to the crystallinity of the material or artifacts of the synthesis, such as crosslinking.

- PEA 10,2 fibers exhibit higher tensile strengths than those obtained for PEA 6,2 and PEA 6,2 copolymer fibers. However, PEA 6,2 monofilaments exhibit higher modulus, crystallinity and density than PEA 10,2. Furthermore, with the incorporation of the proprietary repeat unit into PEA

6,2, lower tensile strengths and modulus values are obtained.

- The best approach to achieving higher strengths for PEA 10,2 fibers is to draw the fibers in two stages, with the first stage drawing performed in-line to the maximum draw ratio at room temperature. Additionally, elevated temperatures tend to adversely affect the in-line drawing process. The differences in strength observed may be related to the chemical structure of the materials, or they may have different strengthening mechanisms.

- Heat setting tends to increase the crystallinity and modulus of the fibers and has little affect on the tensile strength. This is not a desirable property for surgical suture applications.

5.2 RECOMMENDATIONS

It is crucial to resolve issues with regard to the synthesis of the PEAs in order to optimize the processing conditions and properties of resulting fibers. The current method of synthesis in which intermediate molecular weight materials must be heated as a solid to advance the molecular weight is not reliable. If this heating stage proceeds too long excessively crosslinked or "gelled" material is formed,

which cannot be extruded. If the heating process is not carried out long enough, the polymer lacks storage and thermal stability, resulting from the presence of unreacted acid chloride functionality (5).

Crystallization kinetic studies should be performed on the PEA polymers to get a better understanding of the rates these materials crystallize at different temperatures. Additionally, occurrence of multiple melting peaks for the PEA 6,2 and PEA 6,2 copolymer need to be explored further to determine whether it is due to a rate effect, formation of more than one crystal structure, the presence of crosslinks, or if it results from two different thicknesses of lamellae.

Issues with regard to the unit cell the PEAs form also need to be resolved. It has been proposed that PEA 6,2 and PEA 6,2 copolymer for a pseudo-orthorhombic unit cell. Based on the diffractometer scans previously reported, it appears that PEA 10,2 also forms this crystal structure. This information is necessary to obtain accurate values for crystalline densities. Additionally, a method needs to be developed to determine the amorphous density of the PEAs.

Further studies should be performed on PEA 6,2 and PEA 6,2 copolymer to determine the optimal processing conditions necessary to obtain the desired end use properties.

REFERENCES

1. F. Rodriguez, "Principles of Polymer Systems", 3rd ed., Hemisphere Publishing Corp., N. Y. (1989).
2. F. W. Billmeyer, Jr., "Textbook of Polymer Science", 3rd ed., Wiley-Interscience, N. Y. (1984).
3. H. Strathmann, Trends in Biotechnology, 13, 112 (1985).
4. C. C. Chu, in Szycher, ed. "Biocompatible Polymers, Metals, and Composites", 477-524, Technomic, (1985).
5. T. H. Barrows, U. S. Patent 5,286,837, February, 1994.
6. J. E. Spruiell, Private communication.
7. T. Hayashi in "Biomedical Applications of Polymeric Materials", CRC Press, 1993, edited by T. Tsuruta, et al.
8. H. Tanzawa in "Biomedical Applications of Polymeric Materials", CRC Press, 1993, edited by T. Tsuruta,et al.
9. D. J. Lyman, Poly. Sci. Tech, 8, 29 (1975).
10. J. B. Park, "Biomaterials: An Introduction", Plenum Press, N. Y. 1979.
11. D. J. Lyman, Poly. Sci. Tech, 23, 215 (1983).
12. J. Paul, Ph. D. dissertation, I.I.T. Delhi, April (1991).
13. P. K. Gita, Ph. D. dissertation, I.I.T. Delhi, July (1992).
14. R. T. Darby, and A. M. Kaplan, Appli. Microbiol., 16, 900 (1068).
15. X. Li, M. S. Thesis, The University of Tennessee at Knoxville, May (1993).

16. D. Waitzovå, et al., Polimery w Medycynie, 16, 93 (1986).

17. Y. Kimura in "Biomedical Applications of Polymeric Materials", CRC Press, 1993, edited by T. Tsuruta, et al.

18. R. Narayan in "Degradable Materials: First International Scientific Consensus Workshop", ed. by S. A. Barenberg, et al., CRC Press (1990).

19. S. Vainionpåå, P. Rokkanen, and P. Tormålå, Prog. Polym. Sci., 14, 679, (1989).

20. J. E. Potts, et al., Polymer Preprints, 13,629 (1972).

21. R. D. Fields, F. Rodrigues, and R. K. Finn, J. Appl. Poly. Sci., 18, 3571 (1974).

22. J. H. Harrison, Am. J. Surg., 95, 16 (1980).

23. R. I. Leininger, et al., Trans. Am. Soc. Artif. Int. Org., 10, 320 (1964).

24. R. W. Postlethwart, Ann. Surgery, 17, 892 (1970).

25. A. Yamanaka, et al., Trans. Opthal. Soc., 104, 517 (1985).

26. D. P. Vanderbilt, et al., U. S. Patent 4,950,735, August (1990).

27. D. P. Vanderbilt, et al., in "Progress in Biomedical Polymers", edited by C. G. Gebelein, and Richard L. Dunn.

28. T. H. Barrows, D. M. Grussing, and D. W. Hegdahl, Trans. Soc. Biomater., 6, 109, (1983).

29. T. H. Barrows, et al., "The Design and Synthesis of Poly(ester-amides)".

30. T. H. Barrows, U. S. Patent 4,529,792, July (1985).

31. S. W. Shalaby, and D. D. Jamiokowski, U. S. Patent 4,209,607, June (1980).

32. Bezwada, D. D. Jamiokowski, S. W. Shalaby, U. S. Patent 5,133,739.

33. Bezwada and Jamiolkowski, in "19th Annual Meeting of the Society for Biomaterials".

34. Gonsalves, Chen and Cameron, Macromolecules, 25, 3309 (1992).

35. Gonsalves, Chen and Cameron, J. of Applied Poly. Sci., 50, 1999, (1993).

36. R. T. Ingwall, et al, Macromolecules, 15, 25, (1982).

37. W. J. Becktel, L. J. Mattais, and M. Goodman, Macromolecules, 14, 203 (1981).

38. R. Kakatai and M. Goodman, Macromolecules, 15, 25, (1982).

39. G. Wouters, et al., Macromolecules, 15, 31 (1982).

40. Y. Tokiwa, et al., in "Degradable Materials: First International Scientific consensus Workshop", ed. S. A. Barenber, et al., CRC Press (1990).

41. Y. Tokiwa, T. Suzuki, and T. Ando, J. of Appl. Polym. Sci., 24, 1701 (1979).

42. Bera and Jedlinski, Polymer vol.33, no.20 4337 (1992).

43. P. J. A. in't Veld, P. J. Dijkstra, and J. Feijen, Makromol. Chem., 193, no 11, 2713 (1992).

44. T. H. Barrows, Clin. Mater., 1, 233 (1986).

45. T. H. Barrows, U. S. Patent 4,343,931, August (1982).

46. A. Ziabicki, "Fundamentals of Fibre Formation", Wiley-Interscience, N.Y. (1976).

47. H. F. Mark, S. M. Atlas, and E. Cernia, editors, "Man-Made Fibers, Vol. 1", 1967.

48. R. G. Griskey, in J. J. McKetta, ed. "Encyclopedia of Chemical Processing and Design", Marcel Dekker, N.Y. (1984).

49. U. S. Patent 3,046,603.

50. B. Maxwell and A. J. Scalora, Mod. Plast., 37, 107 (1959).

51. B. Maxwell, Plast. Eng., 40 (1974).

52. H. L. Davis, et al., U. S. Patent 4,195,052. March (1980).

53. A. N. Good, U. S. Patent 3,311,691, March (1967).

54. D. D. Agrawal, M.S. Thesis, The University of Tennessee at Knoxville, December (1993).

55. B. Wunderlich, "Macromolecular Physics, Vol. I", Academic Press, N. Y. (1973).

56. A. P. Gray, Thermochim. Acta, 1, 563 (1970).

57. S. Kavesh, and J. M. Schultz, Polym. Eng. Sci., 9, (1969).

58. G. L. Wilkes, Adv. Polym. Sci., 8, 91 (1971).

59. H. H. Yang, M. P.. Chovinard, and W. L. Lingg, J. Polym. Sci, 20, 981 (1982).

60. R. S. Stein, J. Polym. Sci., 31, 327, (1958).

61. B. E. Read, and R. S. Stein, Macromolecules, 1, 116, (1968).

62. E. Collins, J. Bares, and F. Billmeyer, "Experiments in Polymer Science", Wiley-Interscience, N. Y., 1973.

63. D. Hemsley, in G. Allen and J. C. Bevington, ed. "Comprehensive Polymer Science, Vol. 1", Pergamon Press, N. Y. (1989).

64. B. E. Read et al., Polymer, 13, 485 (1972).

65. G. Kampf, "Characterization of Plastics by Physical Methods", Hanser, N. Y. (1986).

66. ASTM D76.

67. ASTM D2256.

68. ASTM D1505-68.

69. B. Wunderlich, J. Polym. Sci., A-2 vol 6, 833, (1968).

70. J. H. Magill, J. Polym. Sci., A-2 vol 4, 243, (1966).

71. C. G. Cannon, F. P. Chappel, and J. I. Tidmarch, J. Text. Inst., 54, T210 (1963).

72. M. I. Kohan, ed. "Nylon Plastics." John Wiley & Sons, N. Y. 1973.

73. J. P. Bell and T. Murayama, J. Polym. Sci., A-2 vol 7, 1059, (1969).

74. J. R. Quay, Z. Sun, J. Blackwell, R. M. Briber, and E. L. Thomas, Polymer, 31, 1003 (1990).

75. R. Caubeny, C. W. Bunn, and C. J. Brown, Proc. Roy. Soc. Lond., A226, 531 (1954).

76. He, C. Ph.D. Dissertation, The University of Tennessee, August (1994).

VITA

Martha Anne Jones was born in Wilmington, North Carolina on September 3, 1969. She graduated from John T. Hoggard High School in June, 1987. The following August, she entered North Carolina State University and in December, 1991 received a Bachelor of Science degree in Materials Science and Engineering. After working in industry briefly, she returned to school to pursue a graduate degree in polymer engineering. In August, 1992, she entered The University of Tennessee, Knoxville as a graduate student in Polymer Engineering. She received a Master of Science degree in Polymer Engineering in December, 1994.

She is presently employed as a Research Associate in the Packaging Materials Engineering Group at International Paper.